

# Mechanical properties and structure of gel systems

Dissertation  
zur Erlangung des Grades  
"Doktor der Naturwissenschaften"  
im Promotionsfach Chemie

Fachbereich Chemie, Pharmazie und Geowissenschaften  
der Johannes Gutenberg-Universität  
in Mainz

Miao Wang  
geboren in Shanghai, China

Mainz, den 27.05.2013



Die vorliegende Arbeit wurde in der Zeit von März 2010 bis Mai 2013 unter der Betreuung von Dr. Günter K. Auernhammer und Prof. Dr. Hans-Jürgen Butt am Max-Planck-Institut für Polymerforschung in Mainz durchgeführt.

Tag der mündlichen Prüfung: 3. Juli 2013

Dekan: Prof. Dr. Holger Frey

1. Berichterstatter: Prof. Dr. H.-J. Butt
2. Berichterstatter: Prof. Dr. A. Kühnle
3. Berichterstatter: Prof. Dr. W. Tremel

---



# Abstract

Understanding the origins of the mechanical properties and its correlation with the microstructure of gel systems is of great scientific and industrial interest. In general, colloidal gels can be classified into chemical and physical gels, according to the life time of the network bonds. The characteristic differences in gelation dynamics can be observed with rheological measurements.

As a model system, a mixture of sodium silicate and low concentration sulfuric acid was used. Nano-sized silica particles grow and aggregate to a system-spanning network. The influence of the finite solubility of silica at high pH on the gelation was studied with classical and piezo rheometer. The storage modulus of the gel grew logarithmically with time with two distinct growth laws. A relaxation at low frequency was observed in the frequency dependent measurements. I attribute these two behaviors as a sign of structural rearrangements due to the finite solubility of silica at high pH. The reaction equilibrium between formation and dissolution of bonds leads to a finite life time of the bonds and behavior similar to physical gel. The frequency dependence was more pronounced for lower water concentrations, higher temperatures and shorter reaction times. With two relaxation models, I deduced characteristic relaxation times from the experimental data. Besides rheology, the evolution of silica gels at high pH on different length scales was studied by NMR and dynamic light scattering. The results revealed that the primary particles existed already in sodium silicate and aggregated after the mixing of reactants due to a chemical reaction. Throughout the aggregation process the system was in its chemical reaction equilibrium. Applying large oscillatory shear strain to the gel allowed for modifying the gel modulus. The effect of shear and shear history on the rheological properties of the gel were investigated. The storage modulus of the final gel increased with increasing strain. This behavior can

---

be explained with (i) shear-induced aggregate compaction and (ii) combination of breakage and new formation of bonds.

In comparison with the physical gel-like behavior of the silica gel at high pH, typical chemical gel features were exhibited by other gels formed from various chemical reactions. Influences of the chemical structure modification on the gelation were investigated with the piezo-rheometer. The external stimuli can be applied to tune the mechanical properties of the gel systems.

# Contents

<b>Abstract</b>	<b>v</b>
<b>1 Fundamentals and motivation</b>	<b>1</b>
1.1 Colloidal gel . . . . .	2
1.1.1 Chemical and physical gel . . . . .	2
1.1.2 Precipitated silica gel . . . . .	3
1.2 Rheology of the sol-gel process . . . . .	5
1.2.1 Rheology of the sol state: modification of the aggregation . .	6
1.2.2 Rheology of the gel state: determination of gel point, kinetics and yielding . . . . .	7
1.3 Objectives of the present work . . . . .	11
<b>2 Experimental methods</b>	<b>13</b>
2.1 Rheometry . . . . .	13
2.1.1 Dynamic mechanical measurement . . . . .	13
2.1.2 Classical rheometer . . . . .	18
2.1.3 Piezo-rheometer . . . . .	20
2.1.4 Relaxation spectrum . . . . .	22
2.1.4.1 Modified Cole-Cole equation . . . . .	27
2.1.4.2 BSW function . . . . .	27
2.2 Structural analysis . . . . .	28
2.2.1 Dynamic light scattering . . . . .	28
2.2.2 Nuclear magnetic resonance spectroscopy . . . . .	30
2.2.3 Scanning electron microscopy . . . . .	31

<b>3</b>	<b>Gelation of reactive silica gel</b>	<b>33</b>
3.1	Time and frequency dependent rheology . . . . .	34
3.1.1	Material and methods . . . . .	34
3.1.1.1	Material . . . . .	34
3.1.1.2	Experimental method . . . . .	36
3.1.2	Results . . . . .	37
3.1.2.1	Time dependence . . . . .	38
3.1.2.2	Frequency dependence . . . . .	41
3.1.3	Discussion . . . . .	44
3.1.3.1	Logarithmic time dependence of the storage modulus	44
3.1.3.2	Structure relaxation and fit of relaxation time . . .	47
3.1.4	Conclusion . . . . .	52
3.2	Structural analysis . . . . .	53
3.2.1	Material and methods . . . . .	53
3.2.1.1	Material . . . . .	53
3.2.1.2	Experimental method . . . . .	54
3.2.2	Results . . . . .	55
3.2.2.1	Nuclear magnetic resonance spectroscopy . . . . .	55
3.2.2.2	Dynamic light scattering . . . . .	56
3.2.3	Discussion . . . . .	58
3.2.4	Conclusion . . . . .	61
3.3	Modifying the gel modulus using shear strain . . . . .	61
3.3.1	Material and methods . . . . .	62
3.3.1.1	Material . . . . .	62
3.3.1.2	Experimental method . . . . .	62
3.3.2	Results . . . . .	62
3.3.3	Discussion . . . . .	66
3.3.4	Conclusion . . . . .	69
<b>4</b>	<b>Gelation of various systems</b>	<b>71</b>
4.1	Antibacterial Cl-dopamine gel . . . . .	72
4.1.1	Materials and methods . . . . .	73
4.1.2	Gelation kinetics and mechanical properties . . . . .	74
4.1.3	Conclusion . . . . .	77

4.2	Light-triggered gelation of alginates with caged $\text{Ca}^{2+}$ . . . . .	77
4.2.1	Materials and methods . . . . .	78
4.2.2	Gel behavior of ALG/nitr-T- $\text{Ca}^{2+}$ . . . . .	81
4.2.3	Conclusion . . . . .	84
4.3	Supramolecular gel via host-guest complexation . . . . .	85
4.3.1	Materials and methods . . . . .	85
4.3.2	Influence of host guest concentration on the moduli . . . . .	87
4.3.3	Conclusion . . . . .	89
<b>5</b>	<b>Conclusion</b>	<b>91</b>
	<b>Appendix</b>	<b>93</b>
	<b>List of abbreviations</b>	<b>95</b>
	<b>Bibliography</b>	<b>99</b>
	<b>Acknowledgments</b>	<b>111</b>
	<b>Curriculum Vitae and Publications</b>	<b>113</b>



# 1 Fundamentals and motivation

Gelation is the transition of a liquid to a disordered solid by formation of a network of chemical or physical bonds between the molecules or particles.<sup>1</sup> The liquid precursor is called sol and the solid network is the gel. Chemical gels can be produced by various chemical reactions: condensation, addition and cross-linking, also called vulcanization reaction<sup>2</sup>, while in physical gels the strong attraction amongst the colloidal particles results in the formation of space-filling networks from fractal clusters<sup>3,4</sup>.

Generally speaking, rheology is the study of the flow behavior of material systems. The pioneering work on gel rheology by Winter in 1986 presented the theoretical illustration of the dependence of steady shear viscosity  $\eta_0$  and equilibrium modulus  $G_0$  with the reaction time. The conversion from the sol to the gel is defined by a singular behavior (Fig. 1.1), which is not accessible to the experiments except by extrapolation.<sup>5</sup>

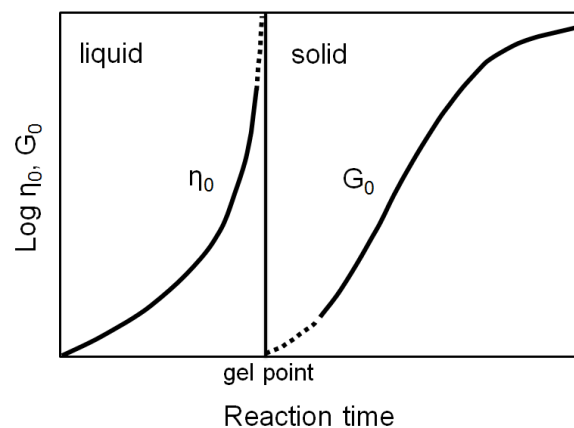


**Figure 1.1:** Illustration of steady shear viscosity and equilibrium modulus of a cross linking system.<sup>5</sup>

As presented in Fig. 1.1, the viscosity of the sol diverges to infinity and the equilibrium modulus increases from zero at the gel point. Here, the steady state viscosity  $\eta_0$  is the ratio of steady state shear stress  $\sigma$  to the shear rate  $\dot{\gamma}$ , which is the rate of change of shear strain  $\gamma$  with time. Details are explained in section 2.1.1.

$$\eta_0 = \frac{\sigma(\dot{\gamma})}{\dot{\gamma}} = \frac{\sigma(\dot{\gamma})}{d\gamma/dt} \quad (1.1)$$

The equilibrium modulus of the fully cured elastic solid can be calculated<sup>1,6,7</sup>:

$$G_0 = vR_gT_A \quad (1.2)$$

where  $v$  is the number of moles of network strand per unit volume.  $R_g$  is the gas constant and  $T_A$  is the absolute temperature.

In the present work, the relation between the mechanical properties of the model gel systems and its structural evolution was investigated with rheological measurements and structural analysis. The time- and frequency- dependence of rheological characteristics were used for understanding the influence of different variables, e.g., reactant concentration, temperature, reaction time, on the gelation process. However, it is necessary first to provide a brief overview on the fundamentals in the field of colloidal gel and gel rheology.

## 1.1 Colloidal gel

### 1.1.1 Chemical and physical gel

Aggregated colloids are of great importance for fundamental research and a typical sample is colloidal gel. The gel consists of colloids, in which the solute is much larger than the molecule of the solvent.<sup>8</sup> The tunability of the colloids and the analogy to atomic systems have motivated a strong scientific interest in the dynamic behavior of colloidal gels.<sup>9–13</sup> The particle properties, the interaction of particles and the structural characteristics can be modified with the chemical composition and the sample preparation in the experiments.



The gelation of colloidal and molecular systems is introduced by attractive interactions between the constituents, e.g., molecules, colloids or even more complex hierarchical structures like crystallites. The detailed mechanism may differ significantly from system to system. According to the reversibility of the bond between the constituents, gels can be classified as either chemical<sup>14,15</sup> or physical gels<sup>2,16–18</sup> as mentioned above. While chemical gels are assumed to have bonds of an infinite life time, e.g., covalent bonds, physical gels have bonds of a finite life time, e.g., physical association.<sup>19</sup> In both cases, the constituents aggregate and the growth of clusters eventually lead to the formation of a system-spanning network. Often the state of a gel depends on its history, i.e., the system is non-ergodic. Because of their irreversible bonds formed in the chemical reactions, chemical gels typically approach and then stay in a final state. And physical gels tend to age, resulted from their reversible bonds and the corresponding structural reorganization in the systems.

Despite the differences in bond life time, the common features between physical and chemical gels have been demonstrated in many studies. With the percolation model, the behavior of cluster formation is well understood and its application can be found in many fields, e.g., electrical resistance and gelation formation. Gelation is described as the development of the network by random filling of bonds on a lattice until an infinite, volume-spanning cluster appears.<sup>1,20</sup> In the aspect of rheology, the gel point is reached at the time, when the ratio between the real and imaginary part of the shear modulus is independent of frequency.<sup>21</sup> And theoretically the viscosity reaches infinity as illustrated in Fig. 1.1. The time from the beginning of reaction to the gel point is defined as gelation time. This behavior has been found in both polymer (chemical) gels<sup>21,22</sup> and physical gels<sup>23–25</sup>. In addition, the physical gel, e.g., PVC plastisols, exhibits the same power law relaxation as chemically cross-linked system at the gelation point.<sup>23</sup>

### 1.1.2 Precipitated silica gel

Besides scientific interest, further understanding of gel system has considerable impact in industry. Inorganic particles, which are widely used as filler particles in many fields, can be produced by fragmentation of the colloidal gel, e.g., silica gel.

Applications include coatings, pharmaceuticals and food products. A prominent example is precipitated silica gel, also called silicic acid gel. During the gelation, the mechanical properties of the gel can be tuned with processing parameters. Afterwards, the gel is milled and silica particles with desired size are produced.<sup>26</sup> Almost spherical silica particles, formed with this procedure are often added to paints, cosmetics and polymers as filler particles.<sup>26,27</sup>

Because of its wide industrial utilization, the characterization of precipitated silica gel has gained attention already since the 1920's.<sup>28</sup> In a series of the studies, Hurd et al. discussed the influence of reaction variables, e.g., pH-value<sup>29,30</sup> and temperature<sup>30,31</sup> on the gelation time. The chemical process and the gelation phenomenon were detailed by Iler and Brinker.<sup>27,32</sup> By acidifying a soluble silicate, the silicic acid is firstly formed, which reacts further to form primary particles by condensation. The suspended particles grow further and aggregate with each other. At the end, a particle network extends throughout the system and forms a gel.<sup>27,33</sup> Despite the good understanding of the gelation process of precipitated silica gel, questions remain unsolved: What is the particularity of the precipitated silica gel at high pH-value? Since the solubility of silica in water increases significantly with the pH-value when it is above 9<sup>34</sup>, how does it influence the gelation process? What is the effect of external shear on the gelation process and its mechanical properties?

The time-dependence of the viscosity was investigated for the precipitated silica gel before its gel point, i.e., in the sol state. Two phases were noted: a slow increase of viscosity during the preliminary stages, which was attributed to the formation of colloidal particles, and then a rapid increase of viscosity, in which the particle size determines the growth rate of the gel.<sup>34</sup>

The relaxation of silica gels, by which the material returns from the deformed state to a new equilibrium state (details see section 2.1.4) were studied theoretically<sup>35</sup> and experimentally by the 3-point bending method<sup>36,37</sup>. Wet gel bar samples were immersed in a bath of their medium liquid and the modulus was measured as the load required to produce a constant deflection (Fig. 1.2).<sup>38</sup> When a constant strain was imposed on the gel bar, the load decreased with time. This load relaxation is described as a sum of hydrodynamic and viscoelastic relaxation.<sup>38</sup> The hydrodynamic relaxation is caused by flow of the liquid medium in the nano-porous

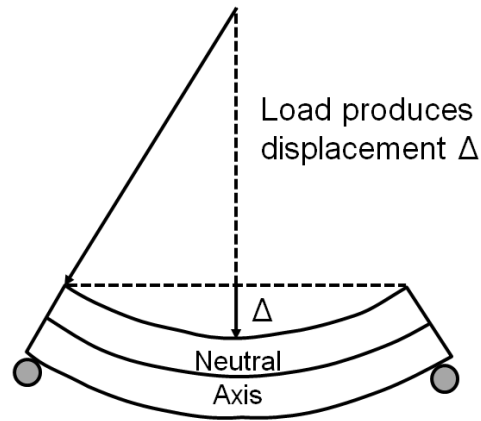


**Figure 1.2:** Schematic illustration of gel bar on three-point bending fixture.<sup>38</sup> A fixed deflection  $\Delta$  is imposed and the load is measured as a function of time.

structure of the system and the viscoelastic relaxation results from irreversible deformation of the network under load. At high pH-value, when there is water in the medium, the silica bonds dissociate in the water and break.<sup>36</sup> This hydrolysis of the medium liquid on the gel is believed to be the reason of the irreversible deformation.

## 1.2 Rheology of the sol-gel process

Sol-gel process is the gelation process from a liquid suspension of colloidal particles, such as  $\text{SiO}_2$ ,  $\text{ZrO}_2$ , or  $\text{Al}_2\text{O}_3$ , into a gel network by addition of a chemical agent.<sup>32</sup> The rheological behavior is of direct interest in the sol-gel processing because it is closely related to the energy consumption of the gel proceeding and the mechanical properties of the end products. Besides, the rheological characteristics can also be used to analyze the structural evolution of the gel systems.

The point when the aggregates of colloids spans the whole volume is defined as the gel point. The state before and after the gel point are called sol and gel state. In the following, the rheology of the sol-gel process is discussed separately: in sol and gel state.

### 1.2.1 Rheology of the sol state: modification of the aggregation

Since a sol is a colloidal suspension of solid particle in the liquid<sup>32</sup>, many studies of colloids can help for a better understanding of the correlation between macroscopic flow behavior and microscopic structure of the system. Recent examples are studies by Vermant et al.<sup>39,40</sup> and Mewis et al.<sup>41</sup>. Fruitful investigations were performed by combining rheological measurements with various structural analysis methods, like confocal microscopy<sup>42–47</sup>, light scattering<sup>12,48,49</sup>, x-ray scattering<sup>50</sup>, small angle neutron scattering<sup>51</sup> and optical tweezer<sup>52</sup>. The combination of methods aims at a understanding of the rheological behaviour through micro-structural changes in the samples. Shear thinning and thickening are typical examples of rheological changes that have been related to shear induced modifications in the micro-structure. For example, for highly concentrated (volume fraction  $\phi = 64\%$ ) silica dispersions (diameter  $d \leq 400$  nm), layering of the particles and formation of hydroclusters were demonstrated as the reason for the shear thinning and thickening.<sup>53</sup> More recently, study of the microscopic single-particle dynamics indicated that the shear thinning and thickening are the consequences of decreased entropic forces and clustering induced by hydrodynamic lubrication forces for the moderately concentrated ( $30 \leq \phi \leq 40\%$ ) silica dispersion ( $d=960$  nm).<sup>46</sup>

When a gelling system is in its sol state, shear influences the formation of the aggregates. The micro-structure of the aggregates can be modified by shear deformation. In a study with in situ small-angle neutron scattering, the gelation of colloidal silica in  $H_2O$ - $D_2O$  is induced by adjusting the pH with HCl.<sup>54</sup> It noted that shear induces an apparent fractal domain into the dense gels and increases the particle contact in colloidal silica suspensions. This compaction effect was also confirmed in a simulation works.<sup>55,56</sup> In a similar system, shear-induced restructuring of colloidal silica gel, formed from lowering the pH of a aqueous suspension of silica particles, was reported.<sup>57</sup> Constant shear changed the structure of the initial clusters to an extent that gelation could be suppressed and the system was held in its fluid state. In such a case the viscosity went through a maximum and then decreased. When the shear was removed, the system gelled again. The suppression of the gelation was then explained by the shear-induced densification of the clusters.

With static and dynamic light scattering, the shear-induced microstructural changes of the gel of adhesive hard spheres, i.e., colloidal silica with functional chains on the surface in hexadecane, was studied.<sup>58</sup> A complex phenomenology of cluster densification, expansion and anisotropy by the gelation under shear was demonstrated.

### 1.2.2 Rheology of the gel state: determination of gel point, kinetics and yielding

To define the gel point and to describe the gelation process after the sol-gel transition, theories have been developed by Flory and Stockmayer.<sup>59–61</sup> The theories can be used to describe infinitely three-dimensional network with statistical calculations and predict the gelation time of a system. Experimentally, rheological measurements have been widely applied to examine the gel point, investigate the gelation kinetics and characterize the influence of various parameters, e.g., reactant concentration and reaction temperature, on the mechanical properties of the gel.

One of the most important rheological characteristics shear modulus  $G^*$  is defined as the ratio of shear stress to the shear strain. It can be separated into two parts: storage modulus  $G'$  for the elasticity of the material system and loss modulus  $G''$  for the viscosity (details in section 2.1.1). The typical frequency dependency of the storage and loss modulus for gel system before, during and after the gel-point are shown in Fig. 1.3. Before the gel-point, the system is in its sol state. At low frequencies, the storage modulus is lower than the loss modulus. And the storage modulus is proportional to the frequency squared and the loss modulus is proportional to frequency. This frequency range is called terminal regime, where the rheological behavior obey these power laws. At the gel-point, the storage and loss modulus are parallel to each other. After the gel-point, the storage modulus is much higher than the loss modulus. At low frequencies, the storage modulus is independent of the frequency and the loss modulus is proportional to frequency.

When the storage modulus is plotted against the frequency, a plateau at low frequencies can be observed in chemical gels.<sup>62</sup> This behavior results from the infinite relaxation time of these gels, which exceeds the measurement time window.<sup>63,64</sup>

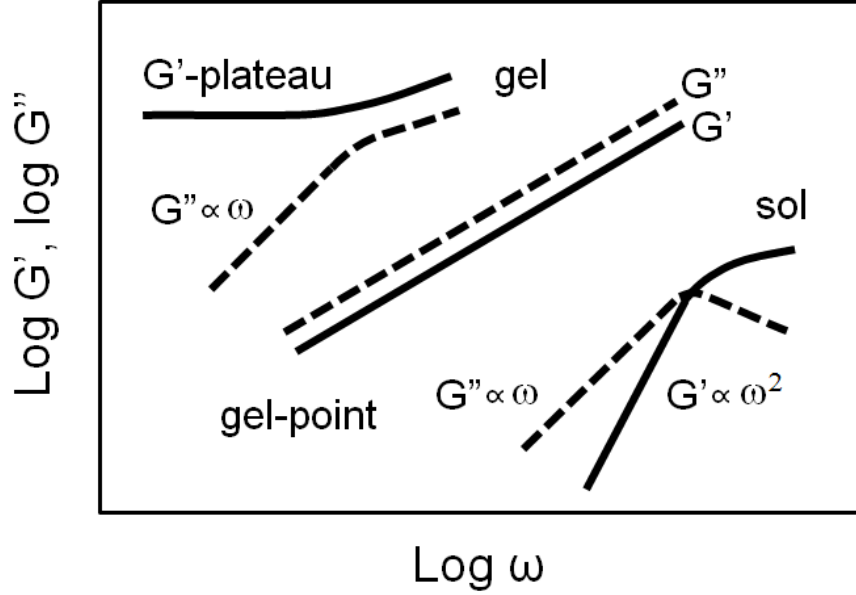


**Figure 1.3:** Typical frequency spectrum of the storage and loss modulus  $G'$  (solid line) and  $G''$  (dash line) for gel systems before, during and after the gel-point. Before the gel-point, the sample system is in its sol state. While after the gel-point, the sample system is in its gel state. The corresponding experimental data was reported by Winter et al. and the curves are shifted sideways to avoid overlap.<sup>5</sup>

The relaxation time describes the time that the sample systems goes back to a new equilibrium state after shear deformation. Details are presented in section 2.1.4. The development of the relaxation time with the time is demonstrated in Fig. 1.4. The cross-over of the extrapolation of storage and loss modulus  $\omega_C$  is a simple measure for the relaxation time. In the sol state, the frequency of the cross-over decreases with the time (Fig. 1.4 A) and it corresponds to an increase of the relaxation time. Contrary to this, the relaxation time decreases with the time when the sample system is in the gel state (Fig. 1.4 B).

With oscillatory shear measurements, the linear rheology of gel systems can be investigated. Here, the linearity means that the rheological properties of the material are independent on the external loadings, like applied stress and strain (details see section 2.1.1). The gel point and the corresponding gelation time can be well determined experimentally. By stopping the cross-linking reaction of Poly-

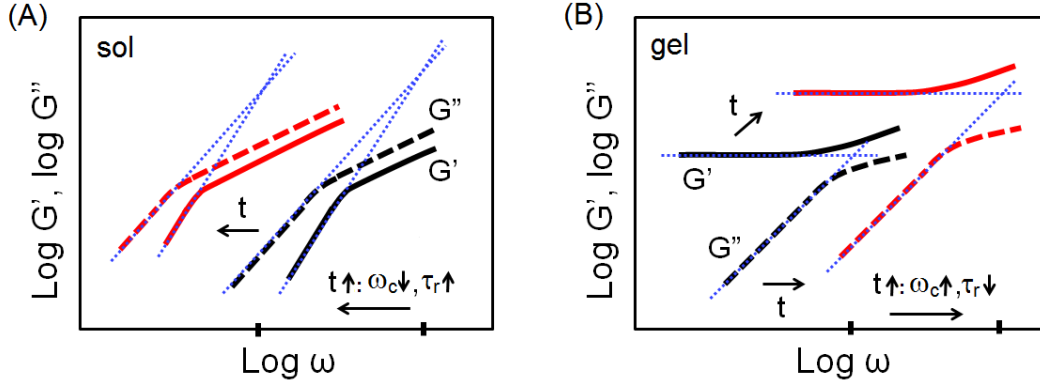


**Figure 1.4:** The development of the frequency spectrum with time for gelling systems before (A) and after (B) the gel-point. The black curves show the storage and loss modulus  $G'$  (solid line) and  $G''$  (dash line) at its original state. The red curves show the spectrum after a period of time. Blue dotted lines depict the cross-over of the extrapolation of storage and loss modulus  $\omega_C$ , which corresponds with the relaxation time  $\tau_r$  (details see section 2.1.4).

dimethylsiloxane (PDMS) at different reaction times, the direct analysis of the gel point was firstly achieved in 1985 by Chambon et al..<sup>65</sup> One method for the detection of the gel point has been often applied, because of its intuitiveness. The gel point was suggested to be the time, at which the storage and loss modulus are equal.<sup>66</sup> However, the validity of this method must be discussed in detail. Winter demonstrated that only for specific polymer gel system the gel point coincides with this cross-over of storage and loss modulus.<sup>67</sup> Generally, the gel point occurs when the ratio between the storage and loss modulus is independent of frequency.<sup>67</sup> This criterion, called the Winter-Chambon criterion, was validated by various experimental studies of chemical gels<sup>21,22</sup> and physical gels<sup>23,24</sup>.

However, the measurement signal can only be detected, when the responding stress of the gel is large enough to reach the measurable range of the rheometer, which is related to the amplitude, geometry and detection threshold of the device. Depending on the nature of the material, some gels are still relatively weak at the gel point, i.e., the moduli are low. Thus, the moduli can not be measured by the rheometer at the gel point. With time the moduli increase and the rheological properties can be investigated as soon as the moduli are large enough for the detection.

The temporal development of the moduli can also be studied with rheological measurements, from which an insight into the gelation kinetics is gained.<sup>23,34,68</sup> In the sol state, the sample behaves as a liquid-like system. The loss modulus is larger than the storage modulus and both increase with time (Fig. 1.3). However the storage modulus grows faster than the loss modulus and both eventually cross each other. For chemical gels, the storage modulus reaches a plateau when it is plotted as a function of time, which results from the complete conversion of the system, i.e., no ageing. For physical gels, the storage modulus exhibits a linear relation with the logarithmic time.<sup>23,68</sup> This structural aging behavior results mainly from the increase of the number of cross-links at early times, while the cross-link growth and internal rearrangements controls the development of the storage modulus in the log regime.<sup>68</sup>

By variation of the experimental conditions, the influence of gelation parameters on the gel point and gelation kinetics has been investigated. Examples include temperature<sup>69–71</sup>, pH-value<sup>69,72,73</sup>, colloid concentration<sup>17,24,74,75</sup>, attractive or repulsive force between colloids<sup>75</sup>.

Furthermore, under large shear strains, the linear range is exceeded and the gel structure can be modified or even destroyed. The yielding point is reached, when the sample system begins to deform plastically, i.e., irreversible. This yielding phenomenon has been observed in various systems.<sup>12,17,42,49,76,77</sup> For example, the microstructure during yielding of a 2D planar monolayer of model aggregated suspension was investigated by video microscopy.<sup>78</sup> The authors of this study suggest that the break-up and subsequent reaggregation lead to a local compaction and a more heterogeneous gel structure.

However under shear strain applied from classical rheometers, the network breakage can be a problem of the gel characterization. Also, if the material amount is limited, the availability of the measurements with classical rheometers is uncertain. For these reasons, other methods have been used to study the gel rheological properties. Via tracking the motion of tracer particles, the local response of the sample systems can be measured, from which the frequency spectrum of the storage and loss modulus of the medium can also be derived. Thereby the rheological study of small volume sample without applying external strain becomes possible. Also, advantages are gained at measuring spacial inhomogeneities in the soft net-



work. Based on this working principle, a number of techniques have been applied for gel analysis, including diffusing wave spectroscopy (DWS)<sup>79,80</sup>, trajectory of magnetic tweezer<sup>81,82</sup>, laser deflection particle tracking (LDPT)<sup>83,84</sup> and detection of thermal fluctuation<sup>85</sup>. The application details and limitations of microrheology are discussed in section 2.1.3.

Besides the method of microrheology, the piezo-rheometer can also be used to avoid these two problems mentioned above. In literature, the piezo-rheometer was applied to investigate liquid crystal systems<sup>86–88</sup> and liquid-crystalline network<sup>89</sup>, but not for gel systems yet. Several methods with comparable piezo-rheometric measuring units have been utilized to understand the rheological properties of complex fluids<sup>90–94</sup>. Compared to classical rheometers, piezo-rheometers use a very small strain (lower than  $10^{-2}$ ), need only very little sample (in microliter range) and can measure at higher frequencies up to  $10^3$  Hz (details see section 2.1.3). These advantages make piezo-rheometer suitable for the study of various gel systems, even for samples in limited amount.

## 1.3 Objectives of the present work

As introduced above, understanding the sol-gel process with respect to the correlation between mechanical properties and microstructure remains a challenging and open problem. Through experimental study of the rheological behaviors combined with the structural analysis on model gel systems, I concentrated in the present work on the following points:

1. Features of chemical and physical gels were investigated and studied with rheological measurements and their relation with the microstructure was analyzed (section 3.1 and 3.2). A model gel system, which was formed from a chemical reaction and connected with covalent bonds, was confirmed to behave like a physical gel. Experimental observation of the time and frequency dependence of the shear moduli aroused attention of this untypical behavior. The evolution of the gelation was characterized with rheological and structural measurements. Besides the discussion about the reversibility of the bonds and the reaction equilibrium, the structural relaxation during the gelation was studied with two models.

2. Rather than the studies mentioned in section 1.2, in which the shear influence on the sol-gel process was investigated in either the sol or gel state, the shear deformation is performed continuously on the sample system from its sol to gel state in this work (section 3.3). Because of the chemical reaction going on in the system and external shear deformation, competition between the formation and breakage of the network bonds exist. With this method, success was achieved to modify the final gel modulus at long times by varying the strain amplitude. Moreover the effect of shear history on the mechanical properties of the gel was studied by applying various shear strains for different periods of time.

3. The utilization of a piezo-rheometer was extended to the study of gel systems, which had not been done previously. The consistency of the results from classical Couette rheometer and piezo-rheometer confirmed the applicability of the piezo-rheometer on the gelation characterization. The influence of different variables, e.g., addition of functional groups, reaction conditions, on the mechanical properties of specific gel samples was investigated.

## 2 Experimental methods

The experimental methods applied in the present work are separated into two parts and introduced here. In the section of rheometry (section 2.1), definitions of shear strain, stress and their interactions are presented. The time- and frequency dependent experiments are described in detail. Also, the working principles of two measurement devices: classical Couette rheometer and piezo-rheometer are explained. In section 2.2, I give a comprehensive overview of the structural analysis and other methods utilized for additional characterization of gel samples.

### 2.1 Rheometry

#### 2.1.1 Dynamic mechanical measurement

Rheology is the study of the deformation that occurs when a sample is subjected to a stress (force per unit area).<sup>95</sup> Depending on the direction of stress, the study of rheology can be separated into extensional and shear rheology.

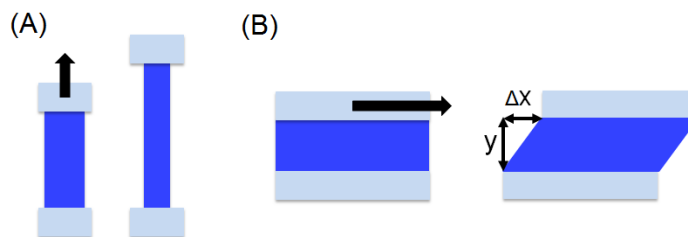


**Figure 2.1:** In a rheological experiment the sample is placed between two plates and deformed under extensional (A) and shear (B) stress.

When the stress is in normal direction, it is called extensional rheology (Fig. 2.1 A). It means that the stress is perpendicular to the plate, where the sample is placed. When the stress is in tangential direction, that is parallel to the plate, it is then shear rheology (Fig. 2.1 B). In the present work, I concentrate on the shear rheology.

Fig. 2.1 B illustrates the shear deformation of the sample system confined between two plates. The lower plate is stationary and the upper plate is moved. Shear strain  $\gamma$ , also called deformation, is then the response to the shear stress  $\tau$ . It can be expressed as:

$$\gamma = \frac{\Delta x}{y} \quad (2.1)$$

where  $\Delta x$  is the displacement in the direction of the shear and  $y$  is the thickness of the sample system.

The rheological properties of the samples were investigated with the dynamic-mechanical measurement, which can be separated into three modes: frequency-, strain- and time-sweep. Furthermore, the shear deformation can be applied either oscillatorily or continuously in one direction. In this work oscillatory shear experiments were performed.

At small strains, no rearrangement and interruption of the sample structure occurs. When the response of the sample system, i.e., the mechanical properties, is independent of the applied strain, the material is then in its linear range. For linear rheology, the strain-amplitude  $\hat{\gamma}$  must be chosen in the way that the linearity of the sample is confirmed. The method, which is used to determine the linear range of the samples, is described below.

A frequency-sweep is performed to study the frequency dependence of the rheological properties at constant temperature and strain-amplitude. The sinusoidal strain  $\gamma(\omega)$  is applied on the sample, following the equation:

$$\gamma(\omega) = \hat{\gamma} \sin(\omega t) \quad (2.2)$$

$\omega$  is the frequency and  $t$  is the time. The complex strain  $\gamma^*$  can then be written as:

$$\gamma^*(\omega) = \hat{\gamma} e^{i\omega t} \quad (2.3)$$

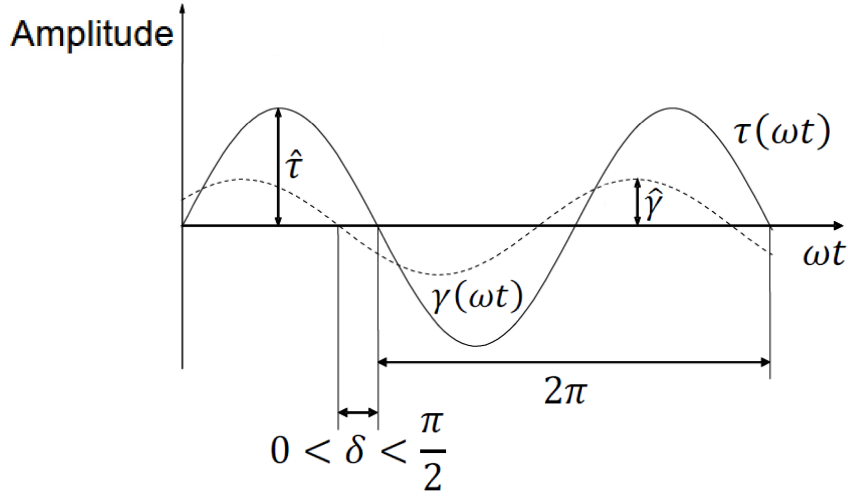


**Figure 2.2:** Oscillation of an applied strain and the resulting stress in a dynamic-mechanical experiment.<sup>96</sup>

where  $i$  is the imaginary unit. The strain propagates through the material and the resulting stress is then detected and recorded. In the linear range of the material, the resulting stress has also a sinusoidal form. The stress-amplitude is expressed as  $\hat{\tau}$ . However it is shifted by a phase angle  $\delta$  in comparison with the applied strain, as shown in Fig. 2.2.

$$\tau(\omega) = \hat{\tau} \sin(\omega t - \delta) \quad (2.4)$$

$$\tau^*(\omega) = \hat{\tau} e^{i\omega t - \delta} \quad (2.5)$$

The complex modulus  $G^*$  is defined as the stress divided with the strain and its absolute value is the ratio of stress- to strain-amplitude.

$$G^*(\omega) = \frac{\tau^*(\omega)}{\gamma^*(\omega)} = \frac{\hat{\tau} e^{i\omega t}}{\hat{\gamma} e^{i\omega t - \delta}} \quad (2.6)$$

$$|G^*(\omega)| = \frac{\hat{\tau}}{\hat{\gamma}} \quad (2.7)$$

Since the complex modulus  $G^*$  is a complex function, it can be separated to two parts, the real part: the storage modulus  $G'$ . And the imaginary part: the loss modulus  $G''$ . The storage modulus  $G'$  is correlated to the stored energy, representing the elasticity of the system, and the loss modulus  $G''$  is correlated with the

dissipated energy, representing the viscosity of the system.

$$G^* = G' + iG'' \quad (2.8)$$

$$|G^*| = \sqrt{G'^2 + G''^2} \quad (2.9)$$

$$G' = |G^*| \cos \delta \quad (2.10)$$

$$G'' = |G^*| \sin \delta \quad (2.11)$$

$$\tan \delta = \frac{G''}{G'} \quad (2.12)$$

The real and imaginary part are dependent on each other, which can be described with the Kramers-Kronig relations:

$$G' = \frac{1}{\pi} P \int_{-\infty}^{\infty} \frac{G''(\omega')}{\omega' - \omega} d\omega' \quad (2.13)$$

$$G'' = -\frac{1}{\pi} P \int_{-\infty}^{\infty} \frac{G'(\omega')}{\omega' - \omega} d\omega' \quad (2.14)$$

where  $P$  is the Cauchy principal value, which is defined by:

$$P \int_{-\infty}^{\infty} \frac{G''(\omega')}{\omega' - \omega} d\omega' = \lim_{\delta \rightarrow 0} \left[ \int_{-\infty}^{\omega - \delta} \frac{G''}{\omega' - \omega} d\omega' + \int_{\omega + \delta}^{\infty} \frac{G''}{\omega' - \omega} d\omega' \right] \quad (2.15)$$

$\omega$  is approached in a synchronized manner from both sides and the singularity is eliminated.<sup>97</sup>

The test of continuous frequency-sweep<sup>98</sup> was applied in the present study. The moduli were measured from low to high frequency and the cycle was repeated continuously. The frequency dependence of the moduli was studied with each single frequency-sweep measurement. Moreover, the time dependence of the moduli can be analyzed by collecting all the moduli at a certain frequency, measured at different times.

With strain-sweep, also called amplitude-sweep, the sample is sheared with increasing strain at a certain temperature and frequency. From the applied strain and the measured stress, the rheological properties can be derived as mentioned above. In order to determine the linear range, the storage modulus  $G'$  is usually

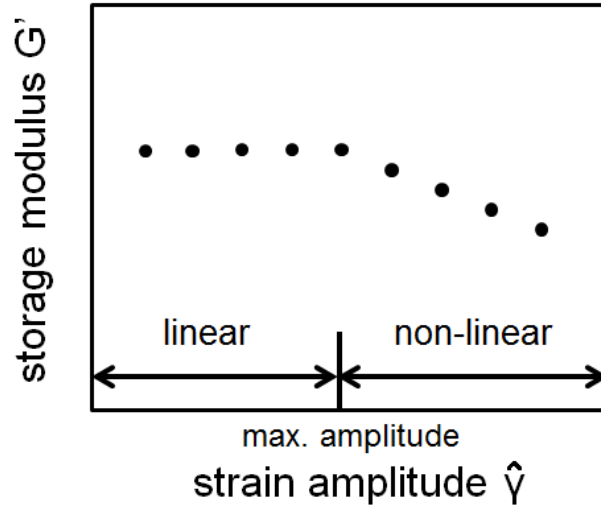


**Figure 2.3:** Illustration of strain-sweep data for the determination of the linear range of the sample systems. When the applied strain amplitude is smaller than the maximum amplitude, the linear rheological properties can be investigated.

plotted against the strain amplitude  $\hat{\gamma}$  (Fig. 2.3). It can be observed that under low strains, the moduli are independent of the strain. This means that the external loading doesn't influence the mechanical properties and the system is in its linear range. Over a certain strain amplitude, the storage modulus is dependent on the strain, which corresponds to structural change of the sample systems, e.g., breakage of the gel network under shear. And this certain strain amplitude is called maximum amplitude. In the frequency-sweep, when the applied strain-amplitude is smaller than maximum amplitude, the linear rheological behavior of the sample can be studied.

The temporal evolution of the moduli can be investigated with time-sweep, in which the temperature, strain and frequency are set. The data can be used to analyze the time-dependence of the mechanical properties, e.g., kinetics of the gelation process. Since both time-sweep and continuous frequency-sweep provide the information about the development of moduli with the time, the consistency of the results of these two modes are used to check the reproducibility of the measurements. In comparison with the continuous frequency-sweep, the time-sweep test has the advantage that more data points at the given frequency can be

recorded in a certain time range, because in time-sweep the moduli are measured at only one frequency. In continuous frequency-sweep, the time interval between data points are larger. In each frequency-sweep, the moduli are measured at several frequencies and only one data point from each frequency-sweep is taken out for the analysis of the time dependence.

### 2.1.2 Classical rheometer

In the current work, classical and piezo-rheometer are used for the rheological experiments. The working principles of these two methods are introduced and compared here. According to the origin of the shear, the shear rheometers can be divided into two groups. The first group relies on drag flows, e.g., Couette, cone-plate and plate-plate apparatus (Fig. 2.4), in which the shear arises from a moving and a stationary surface. The shear rate in cone-plate and Couette rheometer are assumed to be independent of the sample position, while for the plate-plate rheometer it depends on the radius, i.e., the distance from a certain position to the center of the plate. The second group relies on pressure-driven flows, e.g. the capillary rheometer, in which the shear is generated by a pressure difference over a closed channel.<sup>99</sup> The choice of the appropriate rheometer geometry depends on the sample and the question, which is to be studied.

For the gelling systems, which are sol at the beginning of the measurement, the Couette rheometer is chosen (Fig. 2.4 A). In other geometries, e.g. cone-plate and plate-plate rheometer, the average gap between two plates is around 2 mm. The capillary force is not large enough to hold the fluid sample between these plates. Therefore the cone-plate and plate-plate rheometer are usually used for measuring polymer melt, but not for fluid sample systems.

The first rotational rheometer was developed by Maurice Couette in 1890.<sup>100</sup> It consists of two coaxial cylinders. The outer stationary one is the rheometer cell and the inner one rotates (Fig. 2.4 A). Under the given shear stress  $\tau$ , the torque  $\tau_T$  is measured with the inner cylinder, which is needed to overcome the resistance



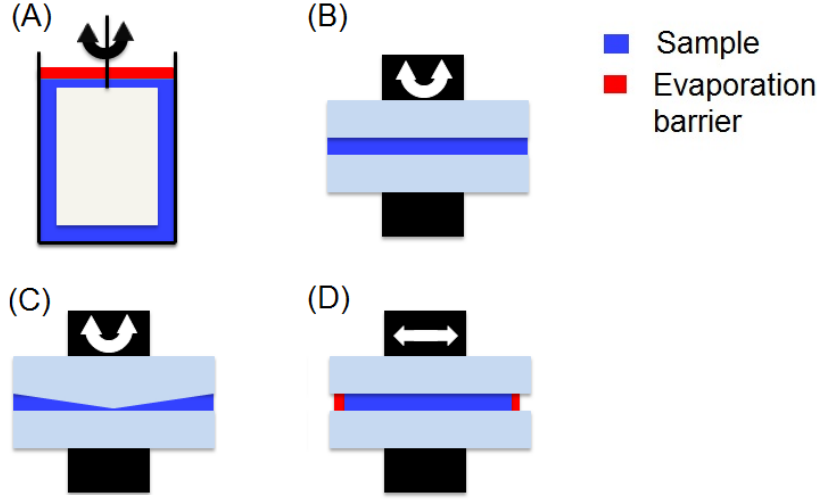


**Figure 2.4:** Setup of Couette (A), plate-plate (B), cone-plate (C) and piezo-rheometer (D). The Couette and piezo-rheometer are used in the present work. Technical information for the comparison between them are listed in Table 2.1.

from the sample. The stress can be calculated:

$$\begin{aligned}\tau_T &= rF = r\tau A = 2\pi r^2 l \tau \\ \tau &= \frac{\tau_T}{2\pi r^2 l}\end{aligned}\tag{2.16}$$

where  $r$  and  $F$  denote the radius of the inner cylinder and force, respectively.  $A$  is the contact area between cylinder and sample.  $l$  is the length of the inner cylinder. With the given strain and measured stress, the complex modulus can be determined (Eq. 2.7).

The Couette rheometer used in this study is a strain controlled rheometer (ARES-LS, Rheometric Scientific Inc., Piscataway, NJ, USA) equipped with a Couette cell. The diameter of the Couette cell and the inner cylinder was 27.0 mm and 25.0 mm respectively, and the length of the cylinder was 32.0 mm. The sample volume was 2.6 ml. The experiments were performed under the strain-controlled oscillatory shear in the frequency range of 0.62 to  $1.26 \times 10^4$  rad/s. The resolution limit of the transducer is 0.02 g · cm.

Sealing of the sample systems in the Couette cell was achieved with an evaporation barrier on the top of the sample (Fig. 2.4 A). With this method, the evaporation of water was avoided. Since the oil was immiscible with the water-based solution, it stayed only on the top of the sample and did not affect the measurement results.

### 2.1.3 Piezo-rheometer

Alternative rheological measurements were performed with a homemade piezo-rheometer with a plate-plate geometry (Fig. 2.4 D). The piezo-rheometer was first introduced by Durand et al.<sup>86</sup> and then further developed in other works<sup>88,101</sup>. Similar to classical rheometers, the stress propagated through the sample is measured under a given strain. The difference is only that the shear deformation in classical plate-plate rheometer is rotational, while it is translational in piezo-rheometer. Therefore the shear rate is overall the same in a piezo-rheometer. Details about the homemade piezo-rheometer were reported by Roth et al.<sup>94,102</sup>.

A comparison of technical informations between the Couette and piezo-rheometer is given in Table 2.1. The home-made piezo-rheometer is suitable for measurements at a higher frequency range up to  $10^3$  Hz and lower strain down to  $10^{-5}$ . Also, the small area of glass substrate ( $12 \times 20$  mm<sup>2</sup>) combined with the extremely small gap size (down to 50  $\mu$ m) offers an opportunity for measuring samples, which are available only in a limited amount. For the systems of Cl-dopamine gel (section 4.1), light-triggered alginate gel (section 4.2), self-healing supramolecular

---

	Couette rheometer	piezo-rheometer
Frequency range [Hz]	$1.6 \times 10^{-2} \dots 1.6 \times 10^2$	$10^{-1} \dots 10^3$
Shear strain [-]	$3 \times 10^{-3} \dots 3 \times 10^2$	$10^{-5} \dots 10^{-2}$
Sample volume [mm <sup>3</sup> ]	$2.6 \times 10^3$	1.2...12

---

**Table 2.1:** Comparison of technical informations between Couette and piezo-rheometer, which were used in the current study.

gel (section 4.3), the total sample amount was less than 2.6 ml, which is needed for one experiment with the Couette rheometer. Also, the disadvantage of gel sample preparation in the plate-plate and cone-plate rheometer, discussed above (section 2.1.2), were considered. Therefore, the mechanical properties of these systems with small sample amount were studied only with the piezo-rheometer in the present work.

The gap between two parallel plates in the piezo-rheometer cell was varied between 50 and 100  $\mu\text{m}$ , depending on the system. To avoid the evaporation of the solution in the sample system, e.g., water, PDMS (molecular weight approx. 8000 g/mol) was filled around the sample, which worked as an evaporation blockage layer. Since the blockage layer is measured together with the sample in the piezo-rheometer cell, the possible contribution of the PDMS was studied at first (Fig. 2.5). In comparison, the evaporation barrier of the sample in Couette rheometer is on the top of the sample and therefore has no influence on the experimental results (section 2.1.2).

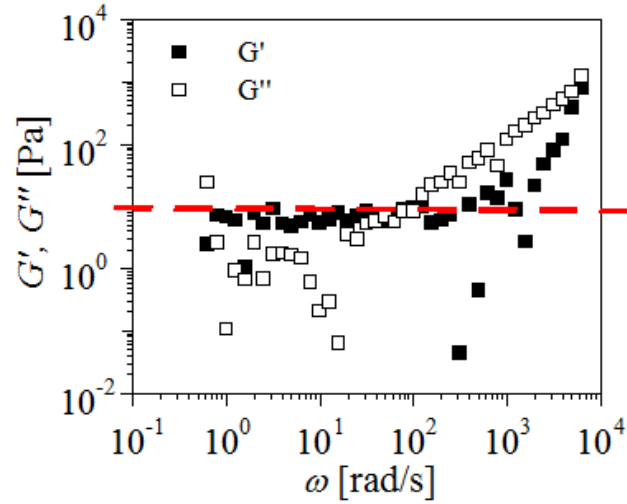


**Figure 2.5:** The frequency dependence of moduli of PDMS with molecular weight approx. 8000 g/mol. The data was measured with frequency sweep, under  $\gamma = 0.0032$ , at  $T = 23^\circ\text{C}$  with piezo-rheometer. The line demonstrates the resolution limit (10 Pa) of the piezo-rheometer.

The moduli of the pure PDMS was studied and they are at the resolution limit of the piezo-rheometer (10...100 Pa), far lower than the moduli of the sample systems (over  $10^3$  Pa). In addition, the cell was fully filled with the PDMS sample in this measurement of the moduli of pure PDMS. In other experiments, only part of the cell was filled with PDMS and the other part with gel samples. Therefore the measured moduli (10...100 Pa) are the maximum contribution from the evaporation barrier PDMS. For this reason, it can be concluded that the signals of the evaporation barrier PDMS doesn't contribute to the experimental results.

Another experimental technique for measuring the rheological properties of a small amount of sample is micro-rheology, discussed in section 1.2.2. The motion of a tracer particle is tracked, from which the calculated mean-square displacement can be transformed into the linear viscoelastic modulus.<sup>103</sup> Despite its various advantages, e.g., possibility of direct measurements at high frequencies (over  $6 \times 10^3$  rad/s)<sup>104</sup>, this method was not applicable in the current work. Because the movement of the tracer particle in the system can only be detected in soft systems (moduli around or below 10 Pa). However the moduli of the present samples are all in and above the order of  $10^3$  Pa. Therefore the application of micro-rheology is limited by the sensitivity of the detection. Another problem can be the interaction between tracer particle and the medium, i.e., sample system, which have significant influences on the rheological results.<sup>105</sup> Because of these arguments, the micro-rheology was not applied in this study.

### 2.1.4 Relaxation spectrum

By the imposition of an external field, e.g., strain, a thermodynamic system transits from a weak non-equilibrium state to a new equilibrium state. Here, in the weak non-equilibrium state, the sample system is globally in a non-equilibrium state but locally, at molecular scales, in a thermodynamic equilibrium state. This retarded transition into a new equilibrium state is addressed as relaxation process.<sup>97</sup> This process can be described with either a discrete spectrum, i.e., as a sum of single relaxation modes, or a continuous relaxation time spectrum.

For describing the mechanical properties and relaxation processes of a viscoelastic system, e.g., polymer melt, the Maxwell element is often applied (Fig. 2.6 A). It

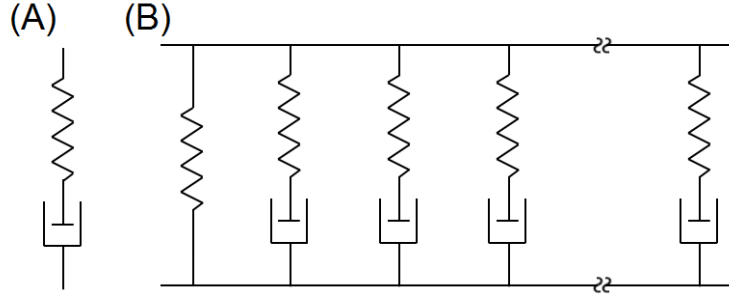


**Figure 2.6:** (A): The Maxwell element contains one spring and one dashpot in series. (B): The generalized Maxwell model consists of one spring and several Maxwell elements in parallel and is applied to describe a discrete spectrum of relaxation times. Here, the single spring represents the contribution of equilibrium modulus  $G_e$ .

contains one spring and one dashpot in series. While the spring corresponds to the elasticity, the dashpot represents the viscosity of the system. A group of Maxwell elements in parallel can be used to describe a discrete spectrum of relaxation times (Fig. 2.6 B). For each element, a relaxation time  $\tau_i$  can be associated with a spectral relaxation strength  $G_i$ .<sup>95</sup>

The relaxation modulus of the system is the sum of the  $n$  elements:

$$G(t) = G_e + \sum_{i=1}^n G_i e^{-\frac{t}{\tau_i}} \quad (2.17)$$

where equilibrium modulus  $G_e$  is finite for solids ( $G_e > 0$ ) and zero for liquids ( $G_e = 0$ ). Each element represents one relaxation mode. Therefore the relaxation of the whole system is the sum of  $n$  relaxation processes.

Using Fourier transform, this function of time can be transformed into a new function of frequency. According to the discrete spectrum, the storage  $G'$  can be expressed as<sup>106</sup>:

$$G'(\omega) = G_e + \sum_{i=1}^n G_i \frac{(\omega\tau_i)^2}{1 + (\omega\tau_i)^2} \quad (2.18)$$

When the relaxation time of the sample system is infinite, e.g., in chemical gels, the storage modulus is constant and therefore independent of the frequency.

$$\begin{aligned} \frac{(\omega\tau_i)^2}{1 + (\omega\tau_i)^2} &\approx 1, \tau_i \rightarrow \infty \\ G'(\omega) &\approx G_e + \sum_{i=1}^n G_i = \text{constant}, \tau_i \rightarrow \infty \end{aligned} \quad (2.19)$$

This explains for the storage modulus plateau of the chemical gel systems at low frequencies. At higher frequencies, the storage modulus is dependent on the frequency, because of other factors, e.g., polymer dynamics.

And the loss modulus  $G''$  can be expressed as<sup>106</sup>:

$$G''(\omega) = \sum_{i=1}^n G_i \frac{\omega\tau_i}{1 + (\omega\tau_i)^2} \quad (2.20)$$

For systems with finite relaxation time, the frequency spectrum of single element (Eq. 2.18 and 2.20) is presented in Fig. 2.7 A. The discrete relaxation spectrum can be determined by measuring the storage and loss modulus in experiments. Baumgaertel et al. showed that the measured storage and loss modulus can be separated to modulus from each element (Fig. 2.7 B, C).<sup>106</sup>

Besides the sum of single relaxation modes, in which the storage and loss modulus are represented as function of frequency, the relaxation process can also be mathematically described with a continuous relaxation time spectrum  $H(\tau)$ . Here, the moduli can be demonstrated as function of relaxation time.

$$G(t) = G_e + \int_0^\infty \frac{H(\tau)}{\tau} e^{-\frac{t}{\tau}} d\tau \quad (2.21)$$

The spectrum presents the distribution and different weights of the relaxation times.<sup>107</sup> In the present work, two models are applied to fit the experimental data and to calculate the relaxation time spectrum  $H(\tau)$ , from which a more quantitative description of the relaxation process can be obtained. One is the Cole-Cole model, which is usually used for the analysis of relaxation in dielectric spectroscopy. The modified Cole-Cole ansatz was adjusted for rheological applications.<sup>107</sup> Another is the empirical Baumgaertel-Schausberger-Winter (BSW) function.<sup>108</sup>

Both models describe well the linear viscoelastic behavior of polymer samples and their predictions are in good agreement with the experimental data from dynamical

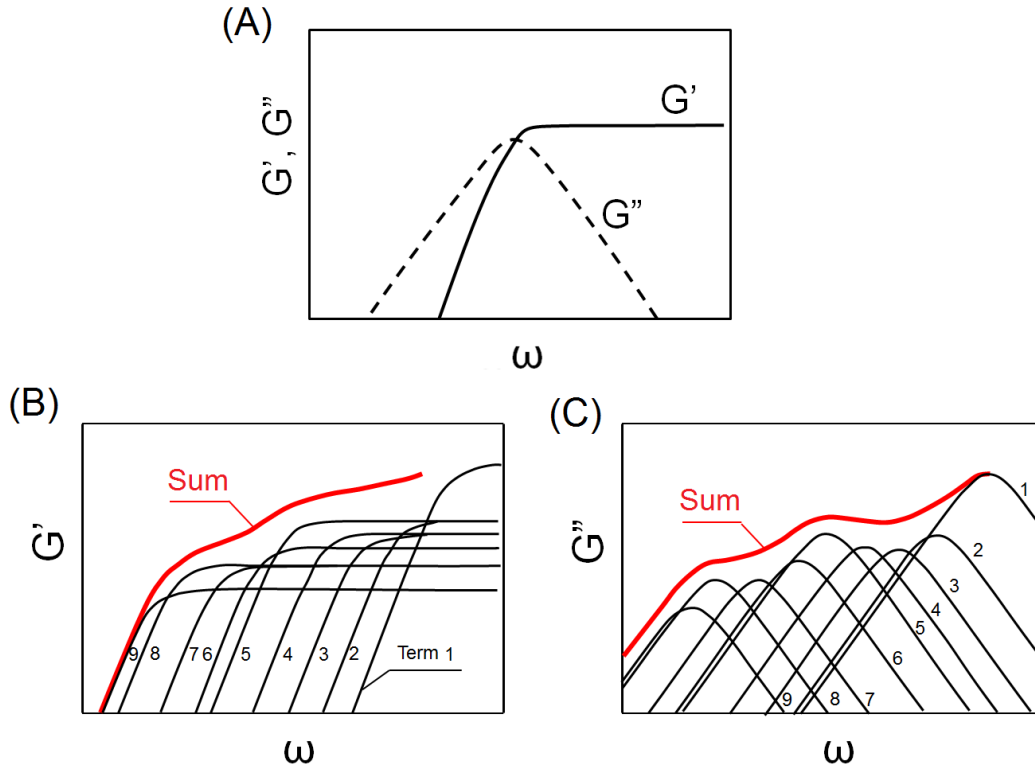


**Figure 2.7:** (A): According to the discrete spectrum of relaxation modulus, the frequency spectrum of storage and loss modulus  $G'$  (solid line) and  $G''$  (dash line) by single Maxwell element can be described with Eq. 2.18 and 2.20. The measured data is the sum of storage modulus  $G'$  (B) and loss modulus  $G''$  (C) of each element.<sup>106</sup>

mechanical measurement.<sup>98,107–109</sup> In addition, both of them are consistent with the Kramers-Konig relation (section 2.1.1), the fundamental relation between the real and imaginary part of complex modulus. Therefore the application of these two models allows for a simultaneous fit of the storage and loss modulus. Consequently, the fit is a consistency check for the measurement results.

However, the two models assume a different distribution of relaxation times in the sample (Fig. 2.8 A). In the modified Cole-Cole function the distribution of relaxation times is centered around a characteristic relaxation time, which results the curve of the storage and loss modulus as presented in Fig. 2.8 B. At low frequencies, a slope of two and one cannot be observed by the curve of storage

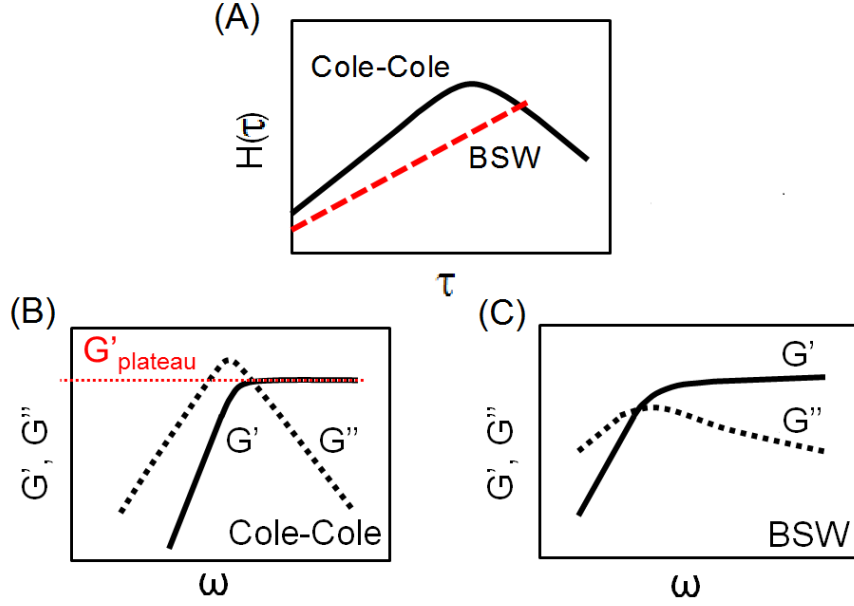


**Figure 2.8:** (A): Difference of the distribution of relaxation times between modified Cole-Cole (solid line) and BSW function (dash line). While the relaxation time spectrum  $H(\tau)$  is centered around a characteristic relaxation time in the modified Cole-Cole function, it increases monotonically with the increase of relaxation time in the BSW function. According to the relaxation time distribution, the spectrum of the storage and loss modulus  $G'$  (solid line) and  $G''$  (dash line) can be derived by the modified Cole-Cole (B) and BSW function (C).

and loss modulus plotted against frequency ( $G'$ - $\omega$  and  $G''$ - $\omega$ ) on the logarithmic scale. Since the polymer melt systems obey the power law: storage modulus is proportional to the frequency quadrat and loss modulus is proportional to the frequency in the terminal regime, as described in section 1.2.2, the modified Cole-Cole function cannot directly be used to describe the behavior of polymer samples in the terminal regime, and modifications have to be applied.<sup>107</sup> In the present work, the terminal behavior of the sample system was not observable because it was outside the frequency range of the measurement. Therefore, the application limit of the modified Cole-Cole equation does not influence the analysis in the current study.

In comparison, the BSW function is constructed such that it can be applied for describing the terminal behavior at low frequency. In the BSW model, the density



of the relaxation mode drops to 0 when the time is longer than a certain value, above which the distribution of relaxation time is cut. The spectrum of the storage and loss modulus  $G'$  and  $G''$ , derived by modified Cole-Cole and BSW function, have then a different form (Fig. 2.8 B,C).

#### 2.1.4.1 Modified Cole-Cole equation

The modified Cole-Cole equation<sup>107,110</sup> was applied to fit the experimental data and to calculate the high frequency plateau of the storage modulus  $G'_{plateau}$  (Fig. 2.8 B) and the relaxation time  $\tau_{CC}$ .

$$G^* = \frac{G'_{plateau}(i\omega\tau_{CC})^\alpha}{1 + (i\omega\tau_{CC})^\alpha} \quad 0 < \alpha \leq 1 \quad (2.22)$$

$$H(\tau) = \frac{G'_{plateau}}{\pi} \cdot \frac{(\frac{\tau}{\tau_{CC}})^\alpha \cdot \sin(\alpha\pi)}{1 + 2(\frac{\tau}{\tau_{CC}})^\alpha \cdot \cos(\alpha\pi) + (\frac{\tau}{\tau_{CC}})^{2\alpha}} \quad (2.23)$$

$G^*$  is the complex modulus, which is measured with the rheometer.  $\tau_{CC}$  is the characteristic relaxation time by modified Cole-Cole function.  $\alpha$  describes the broadness of the corresponding distribution of relaxation times. With smaller  $\alpha$ , the distribution becomes broader.<sup>107</sup> Using this equation, it is implicitly assumed that the distribution of relaxation time is centered around  $\tau_{CC}$ , as showed in Fig. 2.8 A.

#### 2.1.4.2 BSW function

In the literature, the BSW function was used to describe the relaxation properties of mono-disperse linear polymers<sup>98,108,109</sup> and near-glass colloidal suspension<sup>111</sup>.

$$H(\tau) = n_e G_N^0 \left( \left( \frac{\tau}{\tau_{max}} \right)^{n_e} + \left( \frac{\tau}{\tau_0} \right)^{-n_g} \right) \quad \tau \leq \tau_{max} \quad (2.24)$$

$$H(\tau) = 0 \quad \tau > \tau_{max} \quad (2.25)$$

$n_e$ : slope of the spectrum for the  $\alpha$ -relaxation region

$G_N^0$ : plateau modulus

$\tau_{max}$ : longest relaxation time

$\tau_0$ : relaxation time for  $\beta$  -relaxation state

$n_g$ : slope of the spectrum for the  $\beta$  -relaxation state

In the equation, the relaxation process is expressed as the sum of  $\beta$  - and  $\alpha$  - relaxation, which for polymer melt systems originate from flow behavior of polymer melt and entanglement at short time scales, i.e., high frequencies, and transition to the terminal regime at long time scales, i.e., low frequencies.

Since in this work the data at high frequency (over 30 rad/s) was not measured, I concentrated on the behavior at frequencies lower than 30 rad/s. As the  $\beta$  - relaxation part, i.e., the high-frequency term  $(\tau/\tau_0)^{-n_g}$ , could be ignored, I use a simplified version of equation 2.24 and 2.25 in the fitting of experimental data and calculation of relaxation time spectrum  $H(\tau)$ . The decreased number of parameters (three instead of six) also reduced the uncertainties in the fits.

$$H(\tau) = n_e G_N^0 \left( \frac{\tau}{\tau_{max}} \right)^{n_e} \quad \tau \leq \tau_{max} \quad (2.26)$$

$$H(\tau) = 0 \quad \tau > \tau_{max} \quad (2.27)$$

## 2.2 Structural analysis

### 2.2.1 Dynamic light scattering

In dynamic light scattering (DLS), the information about the movement of the scatterers, can be obtained by measuring the time-dependent fluctuation in the scattering intensity. The magnitude of the scattering vector  $q$  is defined as:

$$q = \frac{4\pi n_{solv}}{\lambda_0} \sin(\theta/2) \quad (2.28)$$

here  $n_{solv}$  is the refractive index of the used solvent and  $\theta$  denotes the scattering angle, at which the detector is located with respect to the sample cell.  $\lambda_0$  is the wavelength of the incident laser beam. The sketch of the instrument is showed in Fig. 2.9.

The scattered light contains a part which originates from the interference between the light emanating from the neighboring particle. In order to exploit this phenomenon, auto-correlation function of the scattered light is calculated. Here, the

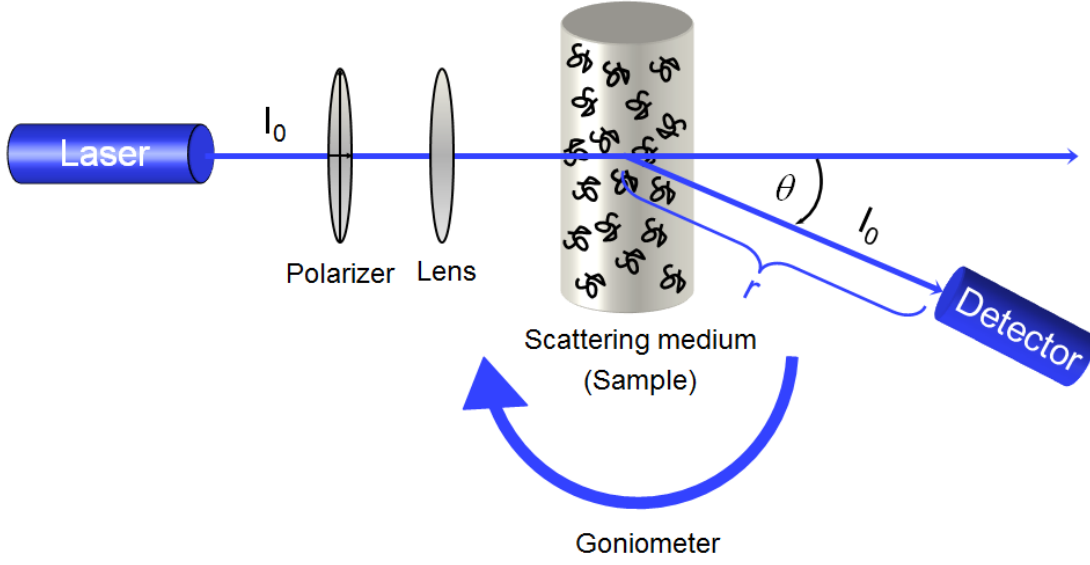


**Figure 2.9:** The light scattering setup of ALV instrument.

auto-correlation function  $K(q, t)$  measures the correlation of the scattered light intensity  $I(q, 0)$  at time  $t=0$  with itself  $I(q, t)$  at later time  $t$  and can be defined as<sup>112</sup>:

$$K(q, t) = \frac{I(q, 0)I(q, t)}{I(q, 0)^2} \quad (2.29)$$

also  $K(q, t)$  is related to the scattering vector  $q$ . In the following equation the diffusion coefficient  $D$  for the monodisperse nano-particle can be obtained.

$$K(q, t) = 1 + e^{-2q^2 Dt} \quad (2.30)$$

For the polydisperse systems, the auto-correlation function is the sum of single modes. Each single mode corresponds to the contribution of one particle size. Similar to the Maxwell-model for the relaxation process (Eq. 2.17), the separation of the auto-correlation function to different elements is performed by CONTIN-analyse.<sup>113</sup> With Stokes-Einstein equation the mean hydrodynamic radius of particles  $r_H$  can be calculated from the diffusion coefficient  $D$ :

$$D = \frac{k_B T_A}{6\pi\eta r_H} \quad (2.31)$$

$k_B$  is the Boltzmann's constant,  $T_A$  for the absolute temperature and  $\eta$  for the viscosity. In the calculation it is assumed that the particles are spherical and the

particles scatter independently. For this reason, this equation can only be used for low concentrated colloidal systems, in which no multiple scattering occurs.

In the present work, DLS experiments were performed in the group of Anja Kroeger-Brinkmann in Max-Planck Institute for Polymer Research (MPIP) on a ALV instrument. It consists of a goniometer and an ALV 5004 multiple-tau full-digital correlator (320 channels) and allows measurements over a time range  $10^{-7} \leq t \leq 10^3$  s and an angular range from  $30^\circ$  to  $150^\circ$  corresponding to a scattering vector  $q = 6.85 \times 10^{-3}$ - $2.56 \times 10^{-2}$  nm $^{-1}$ . A He-Ne laser (Uniphase with a single mode intensity of 25 mW operating at a laser wavelength of  $\lambda_0 = 632.8$  nm) was used as light source.

The datas were analyzed by the group of Anja Kroeger-Brinkmann. CONTIN method<sup>113</sup> was applied to study the relaxation function and the distribution of relaxation time. Further theoretical details and data evaluation procedure are give in the appendix and literature<sup>114–116</sup>.

(This chapter is written by Anja Kroeger-Brinkmann.)

### 2.2.2 Nuclear magnetic resonance spectroscopy

Nuclear magnetic resonance spectroscopy (NMR) is an essential technique for the chemical structural analysis at a molecular level. In the magnetic field, the NMR active nuclei, e.g.,  $^{29}\text{S}$  in the present work, has two spin states under an external magnetic field, which are aligned parallel and antiparallel to the external field. The applied magnetic field induces an electronic current in the molecule and results a local magnetic field. Its strength depends on the electronic structure around the magnetic nuclei of interest.<sup>117</sup> The total local field, i.e., addition of applied and local magnetic field, determines the frequency required to achieve resonance. The difference between the measured and standard resonance frequency is then defined as chemical shift, from which the local chemical structure of molecules can be studied. The amount of magnetic nuclei is related to the integral of the signal.

In the solid-state NMR, magic angle spinning (MAS) technology is applied. The sample is spun at the magic angle  $\theta_m = 54.74^\circ$ , where  $\cos^2 \theta_m = 1/3$ , with respect to the magnetic field direction. The dipole-dipole interaction and chemical

shift anisotropy, which cause the broadening of the spectral lines, can be averaged out with MAS. So a better resolution and identification of the spectrum can be achieved.

The  $^{29}\text{Si}$  MAS NMR measurements in this work have been performed in the group of Robert Graf in MPIP on a Bruker Avance III console operating at 139.11MHz  $^{29}\text{Si}$  Larmor frequency. From  $^{29}\text{Si}$  MAS NMR spectra the statistical chemical structure of a silica network (Fig. 2.10) can be quantified by the distribution of  $Q^n$  sites, where  $n$  denotes the number of Si atoms attached to the oxygen atoms of a  $\text{SiO}_4$  tetrahedron, typically seen as resolved signals in the  $^{29}\text{Si}$  MAS NMR spectra of silicates.  $Q^2$ ,  $Q^3$  and  $Q^4$  sites are observed in the range from -85 to -90 ppm, around -100 ppm and around -110 ppm.<sup>118,119</sup> The data was interpreted in the group of Robert Graf.

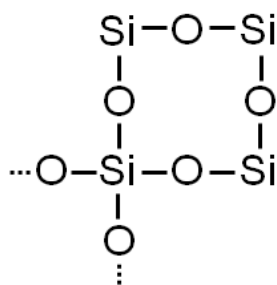


**Figure 2.10:** The chemical structure of silica network. One silicium atom can attach to maximum four oxygen atoms.

(This chapter is written by Robert Graf.)

### 2.2.3 Scanning electron microscopy

Scanning electron microscopy (SEM) is a type of conventional electron microscopy, which is widely used to record a microscopic image of an object with a resolution below 2 nm. Usually, the image of the material surface structure can be constructed, from which the information about the particle size, shape and dispersity is obtained. In SEM, a focused beam of electrons scans across the specimen surface. The signals are emitted by the interaction between electrons and atoms near

surface. One of the main types of the signal comes from low energy secondary electrons, which are loosely bound conduction electrons near the sample surface (within about 10 nm of surface). By collecting the signals, a synchronised scanning pattern is recorded. This mode was applied in the present work. Other imaging modes record the elastical back-scattered electrons, which are ejected from atoms of high atomic weight (or if the incident electron has low energy).<sup>120</sup> Therefore these signals are widely used to determine the chemical composition of the material.

For the present work, a LEO Gemini 1530 with a In-Lens SE detection system (Carl Zeiss NTS GmbH, Germany) at an electron energy of 0.5-5 keV was applied for SEM images.

### 3 Gelation of reactive silica gel

In a mixture of sodium silicate and low concentrated sulfuric acid, nano-sized silica particles grow and aggregate to a system-spanning gel network. Direct preparation of the sample in the Couette rheometer cell avoided any pre-shear of the gel structure due to the filling of the rheometer. The gelation of the silica gel model system was investigated on three aspects:

1. The influences of the finite solubility of silica at high pH on the mechanical properties and structural development of the gel were studied with a Couette rheometer. The time and frequency dependence of shear moduli were characterized by varying different parameters: reactant concentration, temperature and reaction time (section 3.1). The similarity between this silica gel system and physical gel was demonstrated with experimental results. This study was written in the paper “Time and frequency dependent rheology of reactive silica gels”<sup>121</sup>, which is ready for submission.
2. Besides the rheology, the evolution of the silica gel system was measured on different length scales with NMR and DLS. The structural analysis provided information about the gel formation, which can be correlated with the rheological data (section 3.2).
3. The effect of strain and strain-history were studied and explained by shear induced structural reorganization (section 3.3). The modification of final gel shear modulus can be achieved by applying oscillatory shear under large strain amplitude. Including the work from section 3.2 and 3.3, the paper “Reactive silica gels: formation and strain-history dependence”<sup>122</sup> is in preparation.

## 3.1 Time and frequency dependent rheology

The focus of this section is the time and frequency dependent dynamic moduli of precipitated silica gel. It was found that the rheological properties of the silica gel at high pH (pH=11.0) exhibit a number of similarities to physical gels. A logarithmic growth of the storage modulus with time as previously found with physical gels<sup>23,68</sup> was observed. This logarithmic time dependence is usually attributed to bond reversibility which can lead to a structural change, different from a chemical gel. The dynamic similarity between precipitated silica gels at high pH and physical gels was also found in the frequency sweep measurement. A frequency dependence behavior of the silica gel will be demonstrated below. In comparison, a gel of chemically bound hard particles is expected to show a constant, frequency independent storage modulus, since the relaxation time exceeds the experimental time window.<sup>63,64</sup> The silica gel samples I used were at concentrations close to the percolation threshold, i.e., close to the minimal concentration of reactants, which is necessary to form a system-spanning network. The rheological behavior of the system was sensitive to external parameters. The influence of water concentration, temperature and time on the frequency dependence was then studied. To understand the frequency dependence further, I applied two relaxation models: the modified Cole-Cole and BSW model to analyze the experimental data. The introduction of these two models was given in section 2.1.4.

In the discussion, I concentrate on the following points:

1. Is the precipitated silica gel of high pH-value a real chemical gel?
2. Can the relaxation models developed for polymer systems describe the relaxation behavior of silica gel?
3. Are there any unifying relaxation features for the silica gel and physical gel?

### 3.1.1 Material and methods

#### 3.1.1.1 Material

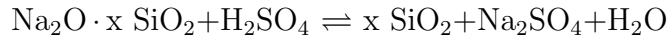
The reactants are sodium silicate solution (Natronwasserglas 37/40°, 40 wt.%, kindly provided by KRUSE-GROUP, Hanau, Germany) and sulfuric acid (96.4 wt.%,



Fisher Scientific GmbH, Schwerte, Germany), which was diluted with milli-Q water to 3.2 wt.%. All reactants were used as provided without further purification. The sodium silicate has a molar  $\text{SiO}_2\text{:Na}_2\text{O}$  ratio of 3.3, which is typical for the production of precipitated silica and gels. The volume ratio between the sodium silicate solution and the diluted sulfuric acid solution was fixed as 1:2. As detailed below, if desired, the solution was further diluted with milli-Q water. The concentrations were chosen to adjust the gelation time in an experimentally accessible time window. Depending on the water content, the time to form a gel varied from about 20 minutes to 5 hours, long enough to prevent gelation during experiment preparation, and short enough to efficiently avoid evaporation (section 2.1.2). All samples originated from the same batch of sodium silicate to avoid batch-to-batch variations.

Silica gel without additional water was alkaline with a pH-value of  $11.0 \pm 0.1$  at room temperature  $T = 23^\circ\text{C}$ , as measured with a pH-meter (Lab 850, Schott Instruments, Mainz, Germany). The pH-value was constant during the reaction. The pH-value decreased to  $10.9 \pm 0.1$ , when the temperature was increased to  $50^\circ\text{C}$ .

The solubility of silica in water increases strongly with pH.<sup>34</sup> At pH-values above 9 the silica bond can dissolve and the silica gel is in a reaction equilibrium. Therefore, the precipitated silica gel studied here is called reactive silica gel. The chemical reactions involved have been described in detail in the literature<sup>26,27,123</sup> and can be written as<sup>123</sup>:



with  $x=3.3$  in this work. The appearance of the sample changed from a transparent and colorless solution after preparation to a slightly turbid solid at the gel point to a white gel after some hours. The gel consisted of aggregates of primary particles, which were visible in SEM images (Fig. 3.1). The image illustrates the typical size of aggregates with diameters of 60 to 130 nm. The sample for SEM was prepared 1 hour after mixing the reactants and kept at  $T = 100^\circ\text{C}$  for 3 days in a vacuum oven, to remove the water from the sample.

In order to investigate the influence of the reactant concentration, extra water was added to the reaction mixture. I denoted the amount of extra water by the ratio

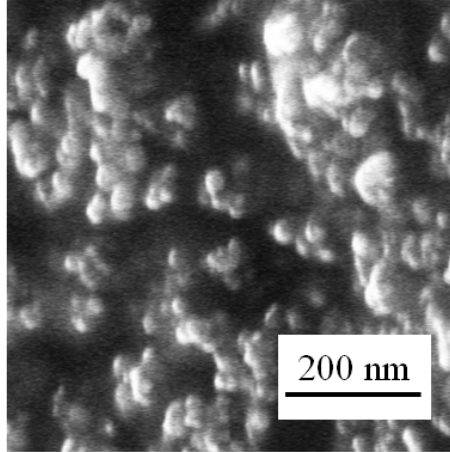


**Figure 3.1:** SEM image of the precipitated silica gel at pH=11.0. The sample was prepared 1 h after mixing of the reactants and kept at  $T = 100^\circ\text{C}$  for 3 days in a vacuum oven for complete drying.

$R$ , defined as the additional water volume divided by the total solution volume (including the additional water).

$$R = \frac{V_{\text{additional } H_2O}}{V_{\text{solution}}} \quad (3.1)$$

$R$  was varied from 0 to 20%. The silica volume fraction in the samples with  $R = 0$ , 10 and 20% were 8.6, 7.3 and 6.3%, respectively. The pH-value at  $T = 23^\circ\text{C}$  decreased from  $11.0 \pm 0.1$  for  $R = 0$  to  $10.9 \pm 0.1$  for  $R = 20\%$ . By slightly decreasing the pH value, additional water shifts the reaction equilibrium in the direction of undissolved silica bond since silica solubility decreases. Furthermore, the temperature controls the rate at which bonds form and dissolve. So the life time of the silica bonds can be adjusted by these parameters.

#### 3.1.1.2 Experimental method

The rheological experiments were performed in a strain controlled rheometer equipped with a Couette cell (Fig. 2.4 A) and the piezo-rheometer (Fig. 2.4 D), which was introduced in section 2.1.2 and 2.1.3. The experiments were performed in the

strain-controlled oscillatory mode to obtain the frequency dependent storage modulus  $G'$  and loss modulus  $G''$ . To avoid strain-induced changes in the sample, a strain of  $\gamma = 0.0005$  was chosen (details see section 3.1.2). Due to this low strain the resolution limit of the transducer ( $0.02 \text{ g} \cdot \text{cm}$ ) corresponded to a lowest measurable complex modulus  $G^*$  of 115 Pa.

After mixing for 30 seconds, the reactants were filled into the rheometer cup. It was checked by visual inspection that no air bubbles were in the system. Immiscible oil was placed as an evaporation barrier on the exposed top surface of the sample (Fig. 2.4 A). With this method, no evaporation effects were observed during the measurements.

Other rheological measurements were performed with the piezo-rheometer, detailed in section 2.1.3. I used a gap distance of  $100 \text{ } \mu\text{m}$  and  $15 \text{ } \mu\text{L}$  sample was placed between the two parallel plates. As an evaporation blockage layer, PDMS (molecular weight approx.  $8000 \text{ g/mol}$ ) was filled around the sample. I checked that the evaporation barrier had no measurable contribution to the results reported in this work (section 2.1.3).

The preparation of the sample: mixing, inserting into the rheometer, adding the evaporation blockage layer, starting the data acquisition, lasted typically 3 minutes. Slight differences, i.e., less than 10 minutes, of experiment preparation time and composition of the samples could not be excluded for each individual measurement. Since acquisition times were at least several thousands of seconds, these time differences were negligible. To prevent any shear history effects all samples were filled into the rheometer cell when they are still in their sol state. For this reason no sample was used with gelation times shorter than 5 minutes.

### 3.1.2 Results

In the following I present results as a function of time, frequency, composition, temperature, and reaction time. First I determined the linear response regime. Under oscillatory shear, a strain sweep of the reactive silica gel with  $R = 0$  was performed at a frequency  $\omega = 10 \text{ rad/s}$  and a temperature  $T = 23^\circ\text{C}$ . The storage modulus  $G'$  was constant for strains up to 0.0035 (Fig. 3.2 A). Therefore, a strain

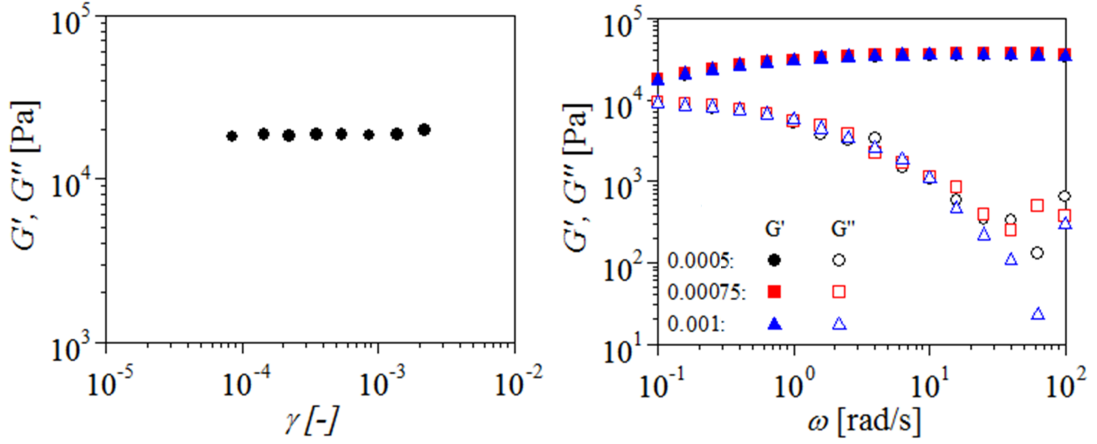


**Figure 3.2:** (A): The strain dependence of the storage modulus  $G'$  of the reactive silica gel without additional water ( $R = 0$ ) at a temperature  $T = 23^\circ\text{C}$  and frequency  $\omega = 1$  rad/s. (B): The frequency dependence of the storage and loss modulus  $G'$  and  $G''$  of the reactive silica gel without additional water ( $R = 0$ ) at a temperature  $T = 23^\circ\text{C}$  with strains  $\gamma = 0.0005$ ,  $0.00075$ , and  $0.001$ , measured 3 hours after mixing. Below the frequency  $\omega = 30$  rad/s,  $G'$  and  $G''$  were independent of the strain.

$\gamma = 0.0005$  was chosen for all measurements to ensure that all data was collected in the linear regime. The identical results from frequency sweeps at strains  $\gamma = 0.0005$ ,  $0.00075$ , and  $0.001$  gave additional justification for assuming that the data was taken in the linear response regime (Fig. 3.2 B). At high frequencies (above 30 rad/s) I observed scatter of the data for the loss modulus  $G''$ , which I attribute to resolution limit of rheometer at low amplitudes. Therefore, only data with frequencies up to 30 rad/s is presented in the rest of this work.

The gelation process was then followed by either measuring at a fixed frequency of  $\omega = 10$  rad/s (time sweep) or by repeatedly taking frequency spectra in the frequency range of  $\omega = 0.1$  to 30 rad/s (continuous frequency sweep). The time sweep data showed the time dependence up to  $10^4$  s. From the continuous frequency sweep data I could analyze the evolution of the frequency dependence.

### 3.1.2.1 Time dependence

All experiments showed a number of common features in the gelation behavior

that I first describe on the example of the silica gel with  $R = 0$  and at  $T = 23^\circ\text{C}$ . Moduli of the gel were measured with time sweep and continuous frequency sweeps. With the help of time-resolved rheometry<sup>124</sup>, the temporal evolution of the storage modulus  $G'$  and the loss modulus  $G''$  were obtained from the continuous frequency sweeps.

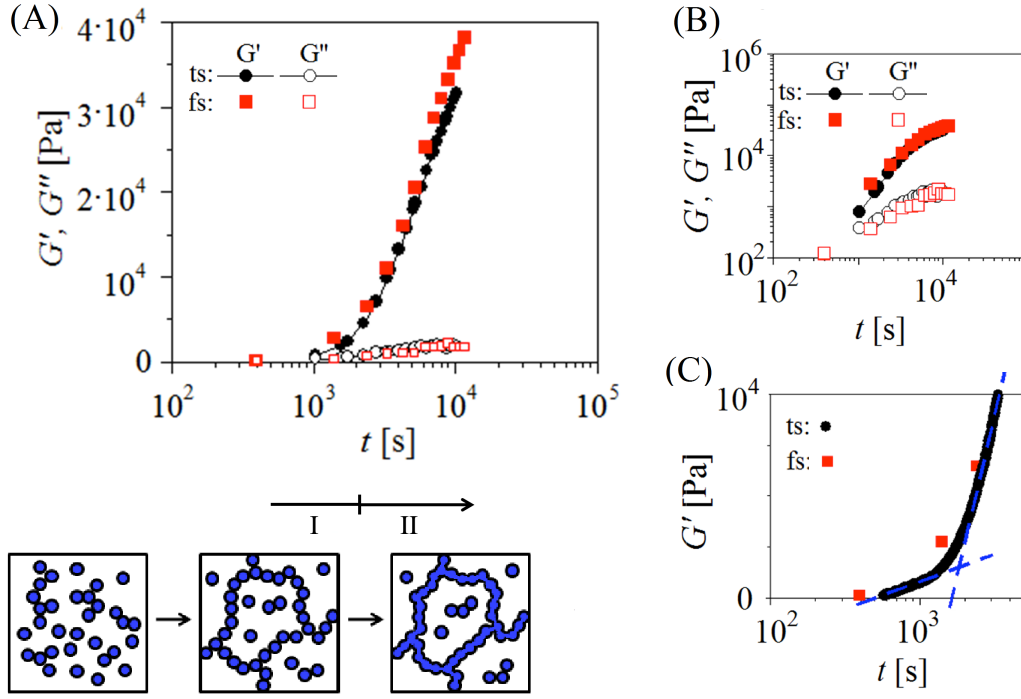


**Figure 3.3:** The growth of the moduli for a gel with  $R = 0$  at  $\gamma = 0.0005$ ,  $T = 23^\circ\text{C}$ , and  $\omega = 10$  rad/s in linear-log (A) and log-log representation (B). In the time sweep (ts, circles) only one out of 50 data points is shown. With a continuous frequency sweeps (fs, squares), moduli were also measured. Only points for  $\omega = 10$  rad/s are shown. (C): Zoom of the data at low storage modulus range ( $G' < 10^4$  Pa). All data points of the time sweep are shown. The fit lines (dashed) show the linear relation between  $G'$  and  $\log(t)$ . The intersection of both fits gives the separation between regime (I) and (II), which are discussed in detail in section 3.1.3.1. Fig. 3.1 corresponds to the last stage in the sketch. The sol state and the percolation process is not observable in this experiment.

From the continuous frequency sweep, the data points measured at  $\omega = 10$  rad/s were extracted and plotted as a function of time (Fig. 3.3 squares). Then they are compared with time sweep results (Fig. 3.3 circles). The good agreement of both curves demonstrated the compatibility of these two experimental methods.

A linear relation between the storage modulus  $G'$  and the logarithm of the reaction time  $t$  was measured (Fig. 3.3 C). This feature is also typical for physical gels<sup>23,68</sup>, see also section 1.2.2.

In Fig. 3.4, the storage modulus  $G'$  and loss modulus  $G''$  are plotted as function of time  $t$  for different compositions. An increase of  $R$ , i.e., the amount of additional water, from 0 to 20% shifted the modulus growth curve to longer times by about one decade. This demonstrates the sensitivity of the gelation process to the gel composition. Such a strong influence of the concentration on the gelation time is expected, since the experiments were carried out at concentrations close to the percolation threshold.

At the chosen strain, the response of the sol and the early gel were below the resolution limit of the rheometer (section 2.1.2) and could not be measured. Consequently, the gel point was not directly observable in the measurements.

The overall shape of the time evolution was more or less independent of composition (Fig. 3.4 A). To account for the change in time scale, I introduced a characteristic time of the gel formation (Fig. 3.4 B). It turned out to be helpful to fit the storage modulus in the range below 600 Pa with a logarithmic time dependence.

$$G' = A \cdot \log \left( \frac{t}{t_{char}} \right) \quad (3.2)$$

where  $A$  and  $t_{char}$  were used as fit parameters. The x-axis intercept of the fitted line (the extrapolation of the fit is set to 0) is defined as the characteristic time  $t_{char}$ . This characteristic time is also connected with, but not identical to, the gelation time, as defined through rheological data taken while passing the gel point (details see section 1.2.2). I assume that  $t_{char}$  and the gelation time show the same dependencies (Fig. 3.4 C).

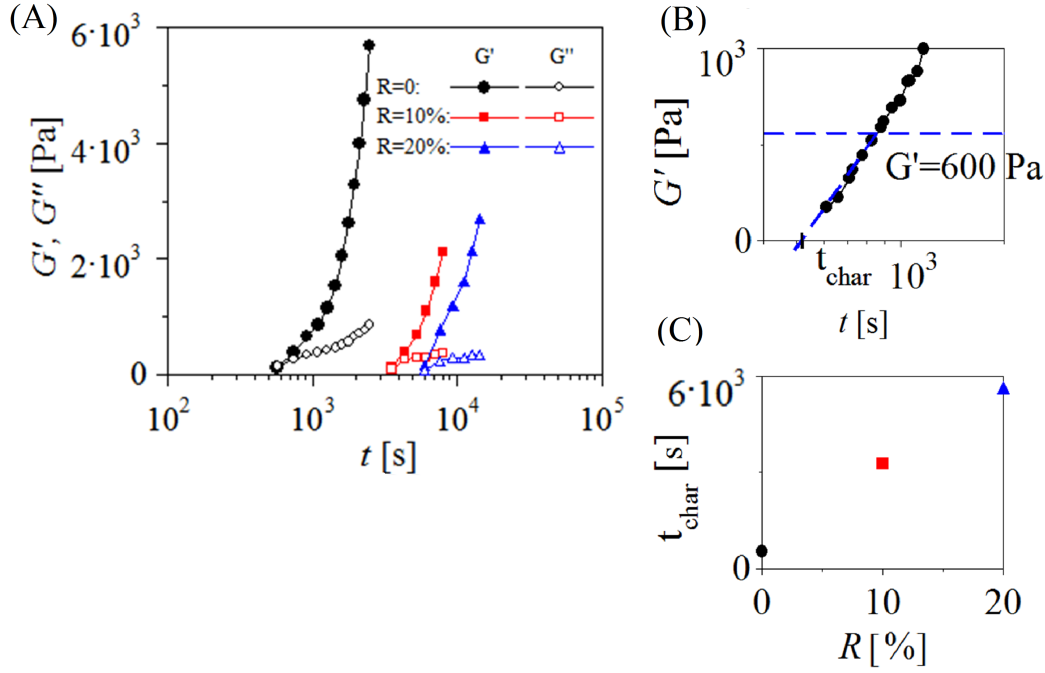


**Figure 3.4:** (A): The evolution of the moduli with time for gels with increasing  $R$ , i.e., amount of additional water. The data was measured with time sweeps at  $\gamma = 0.0005$ , at  $T = 23^\circ\text{C}$  and  $\omega = 10$  rad/s. (B): The characteristic time  $t_{char}$  was defined as the x-axis intercept of a logarithmic time dependence, which was fitted for the data  $G' < 600$  Pa. (C): The characteristic time  $t_{char}$  increased with  $R$ .

Next, the time dependence of gel development was studied at temperatures  $T = 23, 30, 40$ , and  $50^\circ\text{C}$  (Fig. 3.5). For temperatures up to  $40^\circ\text{C}$ , the characteristic time increased with temperature. However at  $T = 50^\circ\text{C}$  the characteristic time decreased again to a value between that for  $23$  and  $30^\circ\text{C}$ . The development of the gel at long times ( $t > 3 \times 10^3$  s, as measured from the slope in the semi-log plots) continuously decreases with increasing temperature. At about  $t = 5000$  s I observed a crossing of  $G'$  ( $T = 50^\circ\text{C}$ ) with  $G'$  ( $T = 30^\circ\text{C}$ ). This will be further discussed in section 3.1.3.1.

### 3.1.2.2 Frequency dependence

The frequency sweeps revealed (Fig. 3.6 A) that the storage modulus  $G'$  was con-

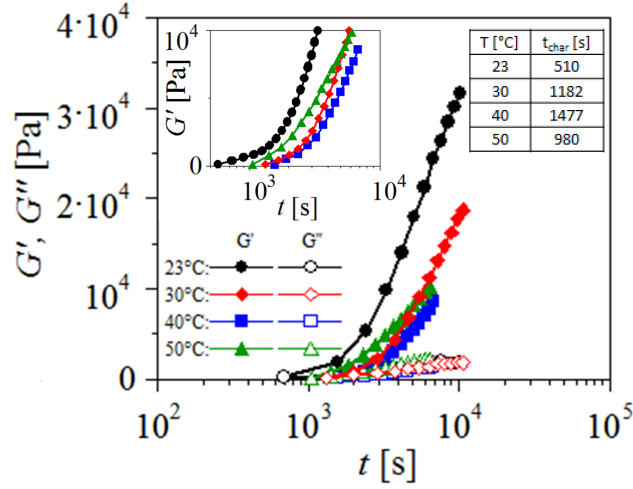


**Figure 3.5:** The time dependence of moduli at different temperatures ( $R = 0$ , measured by time sweep,  $\gamma = 0.0005$  and  $\omega = 10$  rad/s). Inset: The data at low storage modulus range ( $G' < 10^4$  Pa).

stant at high frequencies (above about  $\omega = 6$  rad/s), but frequency dependent at low frequencies. Typically the storage modulus  $G'$  changed by about a factor of 2 between 0.1 and 6 rad/s. The increase of storage modulus  $G'$  at low frequencies is at least 4.6 times larger than what would be expected from the pure ageing of the gels (compare Fig. 3.3). Therefore, the frequency dependence of the sample can clearly be separated from its time dependence. Corresponding to this behavior I also observed a weak maximum in loss modulus  $G''$  for the gel with  $R = 0$ . The resolution limit of the rheometer leads to data scatter in  $G''$  at frequencies beyond 30 rad/s (Fig. 3.2 B). For this reason I limit the frequency range of the data shown here to the frequencies below 30 rad/s.

This frequency dependence was present in all samples and also in samples from another batch of sodium silicate (data not shown). Details depended on composition, temperature and reaction time. To better visualize the deviation from the plateau value of storage modulus  $G'$ , I normalized the storage and loss moduli with the storage modulus plateau  $G'_{\text{plateau}}$  at  $\omega = 20$  rad/s. Since the storage modulus is 10 times larger than the loss modulus at high frequencies, the storage modulus is approximately equal to the absolute value of complex modulus, i.e., I normalized approximately with the absolute value of the complex modulus at high frequencies.



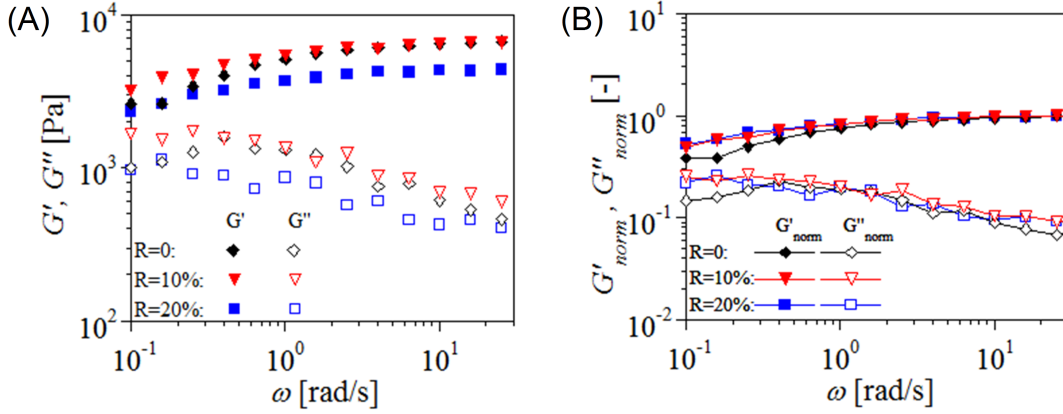


**Figure 3.6:** (A): The frequency dependence of moduli of gels with various  $R$ . The data was measured with frequency sweeps, at  $\gamma = 0.0005$ ,  $T = 23^\circ\text{C}$ , and  $t = 4 t_{char}$ . (B): The same data normalized with  $G'_{plateau} = G'(20 \text{ rad/s})$ , emphasizing the deviation from the plateau.

With this rescaling, the influence of water concentration on the frequency dependence became more easily visible (Fig. 3.6 B). The deviation of the storage modulus at low frequencies from the plateau was more pronounced at lower water concentration. The corresponding normalized loss modulus  $G''_{norm}$  showed a maximum near  $\omega = 0.4 \text{ rad/s}$ . Increasing  $R$  shifted the data curve of storage and loss moduli to lower frequency.

This frequency dependence of storage modulus  $G'$  is more significant for higher temperatures and in younger gels. The temperature dependent spectra of the gel without additional water ( $R = 0$ ) at  $t = 10 t_{char}$  are also shown in Fig. 3.7 A. With increasing temperature, the changes in storage modulus  $G'$  at low frequency became more significant. Also the maximum in loss modulus  $G''$  shifted to higher frequencies.

The time evolution of the spectra was investigated for a gel with  $R = 0$  at 5, 10 and 20 times characteristic time (Fig. 3.7 B). The frequency dependence of storage modulus  $G'$  was more pronounced for short times (younger gel) than for longer times (older gel). Additionally, the maximum of the normalized loss modulus was shifted to slightly lower frequencies.

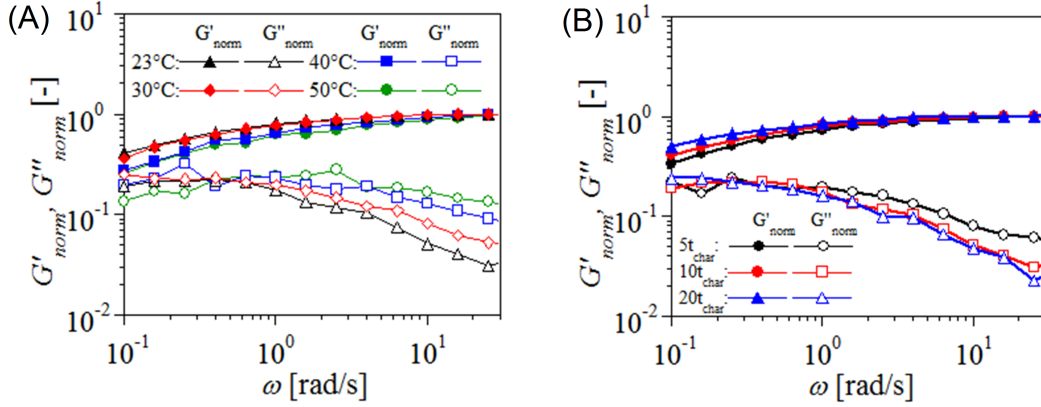


**Figure 3.7:** (A): The frequency dependence of the normalized moduli at different temperatures. The data was taken with a gel with  $R = 0$  at  $\gamma = 0.0005$  and  $t = 10 t_{\text{char}}$ . (B): The frequency dependence of the normalized moduli at different reaction times, for a gel with  $R = 0$  at  $\gamma = 0.0005$  and  $T = 23^\circ\text{C}$ .

The frequency sweep measurement was also performed in the piezo-rheometer and the results from the Couette and piezo-rheometer agreed quite well (Fig. 3.8). The curves of normalized storage and loss moduli superimpose within the measurement accuracy. The slight deviation can be either due to minor differences in the composition of the sample or differences in the contact of the sample to the surfaces of the rheometers. Due to the similarities in the chemical structure, the silica gel adheres better to the glass substrate of the piezo-rheometer than to the metal cell of the Couette rheometer. The difference in adhesion was observed during the cleaning of both cells. This is also the reason of using normalized storage and loss modulus for comparison instead of the absolute value of the storage and loss modulus.

### 3.1.3 Discussion

#### 3.1.3.1 Logarithmic time dependence of the storage modulus

The time sweep data (Fig. 3.3 to Fig. 3.5) suggests that the structure of the precipitated silica gel develops in two phases. In each of them storage modulus scaled

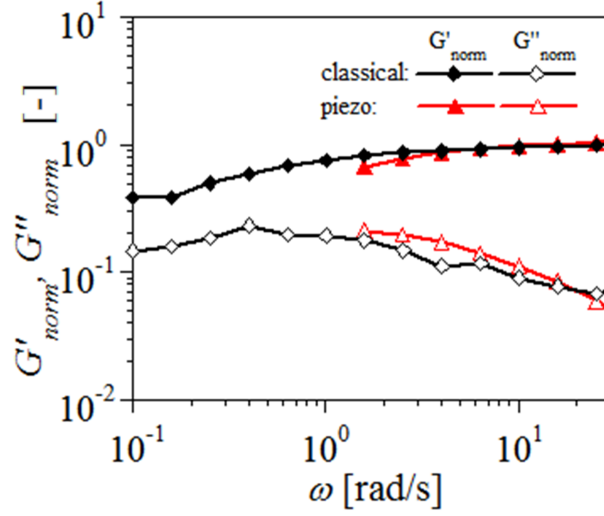


**Figure 3.8:** Comparison of the frequency dependence of the normalized moduli measured with a classical Couette rheometer and a piezo-rheometer. The gel with  $R=0$  was measured at  $\gamma = 0.0005$ ,  $T = 23^\circ\text{C}$  and  $t = 4 t_{char}$ .

with the logarithm of time. The slope of this logarithmic time dependence increased from the first to the second phase. Interestingly, such a behavior was known only for physical gels. Ronsin et al. observed the 2-stage linear behavior by gelatin gel.<sup>68</sup> Also, Nijenhuis et al. reported that the storage modulus of the physical gel (PVC plastisols) follows logarithmic time dependence after some induction period.<sup>23</sup> In the rheo-optical study of physical gelation, a similar picture was presented.<sup>125</sup> Guo et al. attribute the two different slopes in the logarithmic time dependence to the fact, that the evolution of the modulus at early time results mainly from the increase of the number of cross-links and that in the logarithmic regime, at late times, the cross-link development and internal reorganization are dominant.

A similar gelation mechanism might explain the two-stage rheological behavior of the reactive silica gel. As shown in Fig. 3.3, before regime (I) the size of aggregates and their effect on rheology are not large enough to be detected by the rheological measurement, so there is no signal at the early time range. In regime (I) the growth of aggregates and formation of bonds between aggregates contribute essentially. At the intersection of the two trend lines with different slope (Fig. 3.3 C), regime (II)

begins, in which the strengthening of bonds and reorganization of the network dominates. However, to clarify this structural development, insight in the reaction equilibrium of the chemical reaction and the growth of the aggregates are needed and will be addressed in section 3.2.

Manley et al. studied a gel of silica nano particles that were destabilized by adding the divalent salt  $\text{MgCl}_2$ .<sup>126</sup> They observed a power law like growth of storage modulus  $G'$  vs. time. Manley et al. assumed explicitly the absence of structural changes in the gel and explained the time-dependent strength of colloidal gels with the coarsening process. The local elasticity increased because of bond formation between neighboring colloidal particles. The power law of storage modulus  $G'$  vs. time is independent of the particle volume fraction. In contrast to the sample by Manley et al., the silica gel sample used in this work is a reactive system, in which the gel is in a reaction equilibrium between the formation and dissolution of chemical bonds. The different time dependence, observed in both silica gels, can be attributed to this difference in the properties of the particle-particle bonds.

The logarithmic time dependence of the modulus suggests that the reactive silica gel shares similarities with physical gels. As discussed in section 1.1.1, a major difference between physical and chemical gel is that physical gelation is a thermoreversible process, whereas chemical gelation is not. In the case of reactive silica gel, although the silica bond is formed by a chemical reaction, the bond is reversible due to the finite solubility of silica at high pH. From pH value 9 to 12, the solubility increases dramatically from 0.015 to 0.5%.<sup>127</sup> In this sample with pH = 11.0, the dissolving of silica leads to bond breakage and thus relaxations in the system are possible. This process corresponds the ageing of the gel, which is driven by the approach of the minimum of free energy, i.e., a more efficient distribution of bonds. Due to its physical-gel-like behavior, a structural relaxation in the reactive silica gel can be expected.

Quarch et al. reported a similar behavior for the temperature dependence of precipitated silica gel formation under alkaline conditions in a temperature range from 15 to 35°C.<sup>26</sup> They explained the maximum in the characteristic gelation time with the finite solubility of silica at high pH (above 10.5). With increasing temperature, both the dissolution and formation kinetics accelerate. When the acceleration of formation dominates over that of the dissolution, a decrease in the

characteristic gelation time is to be seen. In the inverse case one would expect an increase in the characteristic gelation time. For this reason, in the experimental data of the present work the observed maximum in the characteristic time  $t_{char}$  may result from the compensation of both processes.

In this study, I observed that the slope of the logarithmic time dependence at late times ( $t > 3 \times 10^3$  s) depends monotonically on temperature (Fig. 3.5). The lower the temperature, the steeper the slope. This might be due to a temperature dependent shift of the reaction equilibrium. Further studies of the temperature dependent reaction kinetics in both directions, i.e., formation and dissociation of silica is needed to get a full understanding of this behavior.

#### 3.1.3.2 Structure relaxation and fit of relaxation time

The experimental data clearly showed a frequency dependence of the storage modulus at low frequency (section 3.1.2.2). Such a behavior has already been observed for dynamically arrested colloidal systems.<sup>128,129</sup> However this latter systems also showed a minimum of  $G''$  at intermediate frequency that is not present in the reactive silica gel. This difference may be attributed to either the limited measurable frequency window or absence of polymer dynamics in the present sample system. I attribute the frequency dependence to a structural relaxation inside the sample, which results from the reversibility of silica bonds at high pH in the sample. In line with this interpretation, I found that the structural relaxation, as observed in the frequency dependence of the storage modulus, is more pronounced in the sample with lower water content, i.e., higher pH, at higher temperature and in younger gel.

To get a more quantitative description of this relaxation process, I fitted these frequency spectra with two different models, with which it was also checked whether the relaxation properties is dependent on the model. Both models were introduced in section 2.1.4.

#### Relaxation time fitted by Cole-Cole function

The modified Cole-Cole equation (Eq. 2.22 and 2.23)<sup>107,110</sup> was applied to fit the

data and to calculate the high frequency plateau of the storage modulus and the relaxation time.

The fitting was performed using Origin 8.5 and is presented in an example of a gel with  $R = 0$ , measured at  $T = 23^\circ\text{C}$  and  $t = 5 t_{char}$  (Fig. 3.9). The fit line matches with the experimental data.

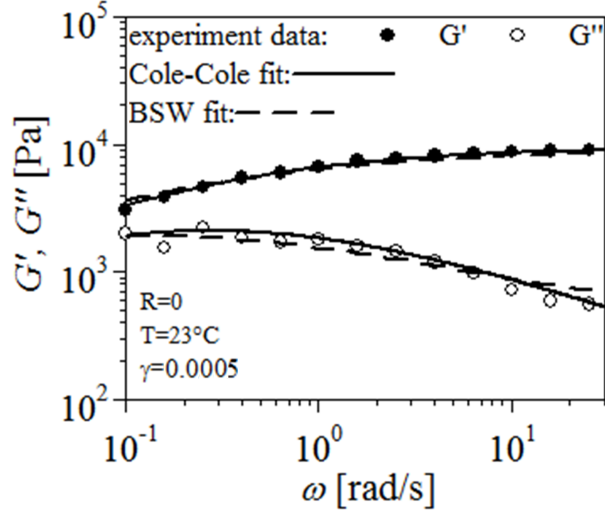


**Figure 3.9:** The moduli of a gel example ( $R = 0$  measured at  $\gamma = 0.0005$ ,  $T = 23^\circ\text{C}$  and  $t = 5 t_{char}$ ) are fitted with the modified Cole-Cole<sup>107</sup> (solid line) and BSW function (dash line).

The fitted storage modulus plateau  $G'_{plateau}$  and Cole-Cole characteristic relaxation time  $\tau_{CC}$  are plotted as a function of water concentration  $R$ , temperature  $T$  and reaction time  $t/t_{char}$  in Fig. 3.10.

With increasing  $R$  from 0 to 20%, the plateau value decreases and the relaxation time increases by more than a factor of 2 (Fig. 3.10 A). Combined with the increase of characteristic time  $t_{char}$  with increasing  $R$  (Fig. 3.4 C), it can be concluded that the gel formation and structural relaxation both decelerated with increasing amount of water. The lower reactant concentration at higher  $R$  caused the decrease of storage modulus plateau and the slow-down of gel formation. Besides, the pH-value of the solution is slightly lower at higher  $R$  and corresponding lower solubility of silica could be a reason of the slower relaxation process.

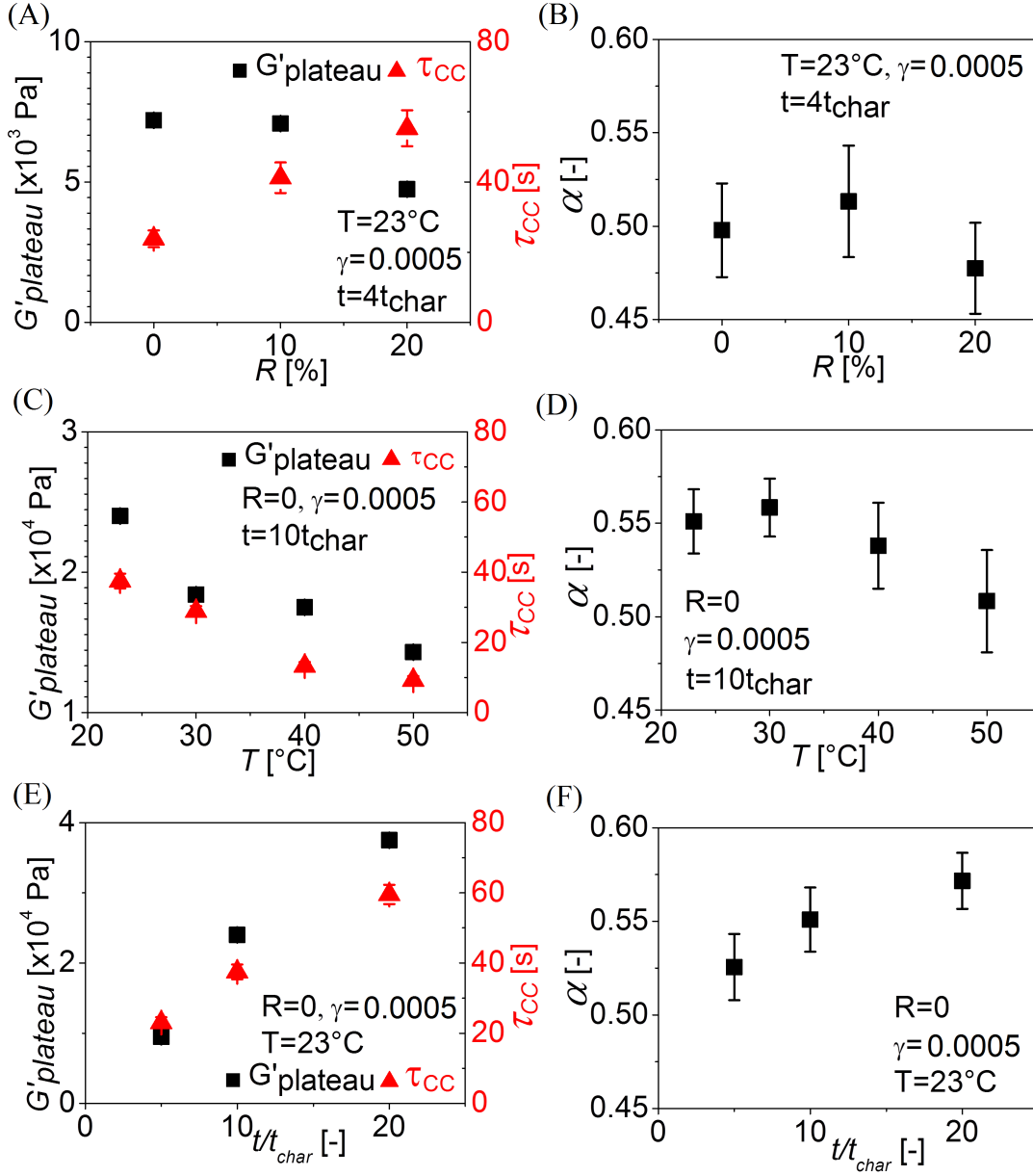


**Figure 3.10:** The results from fits with the modified Cole-Cole function. The dependence of the fitted storage modulus plateau  $G'_{plateau}$  and Cole-Cole characteristic relaxation time  $\tau_{CC}$  on water concentration  $R$  (A), temperature  $T$  (C), and reaction time  $t/t_{char}$  (E). The broadness parameter  $\alpha$  is plotted as function same parameters (B), (D) and (F).

For all investigated samples, the broadness parameter  $\alpha$  of the Cole-Cole function was on the order of 0.5, indicating a broad distribution of relaxation times. The influence of water ratio on the broadness parameter  $\alpha$  is insignificant and negligible in the range of standard deviation (Fig. 3.10 B). The relaxation spectra  $H(\tau)$  fitted with the modified Cole-Cole function and the BSW equation will be compared in the following.

The storage modulus plateau  $G'_{plateau}$ , characteristic relaxation time  $\tau_{CC}$  and broadness parameter  $\alpha$  decreased with increasing temperature (Fig. 3.10 C and D). The decrease of the characteristic relaxation time implies a shorter bond life time. This might be correlated to a shift of the reaction equilibrium with temperature (section 3.1.2.2). But complementary studies would be needed to understand the detailed correlation.

The storage modulus plateau  $G'_{plateau}$  and the relaxation time  $\tau_{CC}$  increase by more than a factor of 3 from the reaction time  $t/t_{char} = 5$  to 20 (Fig. 3.10 E). Since the pH value of the sample stayed constant during the reaction, the solubility of silica was also constant. Thus the dominating process can be assumed to be the strengthening of the network structure through reorganization of the network, leading to a better connectivity in the network and consequently slower relaxation.

#### Relaxation time calculated by BSW relaxation time spectrum

In the present work, the fit of the BSW equation was calculated by the IRIS graphics tool<sup>124</sup> with the equation 2.24 and 2.25, explained in section 2.1.4.2.

The comparison between the fit curves with modified Cole-Cole and BSW is displayed in Fig. 3.11. The characteristic relaxation time  $\tau_{CC}$  from Cole-Cole fit and the maximum relaxation time  $\tau_{max}$  from BSW fit are compared for various temperatures (Fig. 3.11 A) and reaction times (Fig. 3.11 C).

Despite differences in the absolute numbers, the general tendency is the same by the results from both models. A possible origin of these differences is the different distribution of relaxation times, explained in section 2.1.4. However, it was observed (e.g., Fig. 3.11 D) that a broader distribution of relaxation time for Cole-Cole corresponds to a smaller slope of distribution modulus  $H(\tau)$  in the BSW



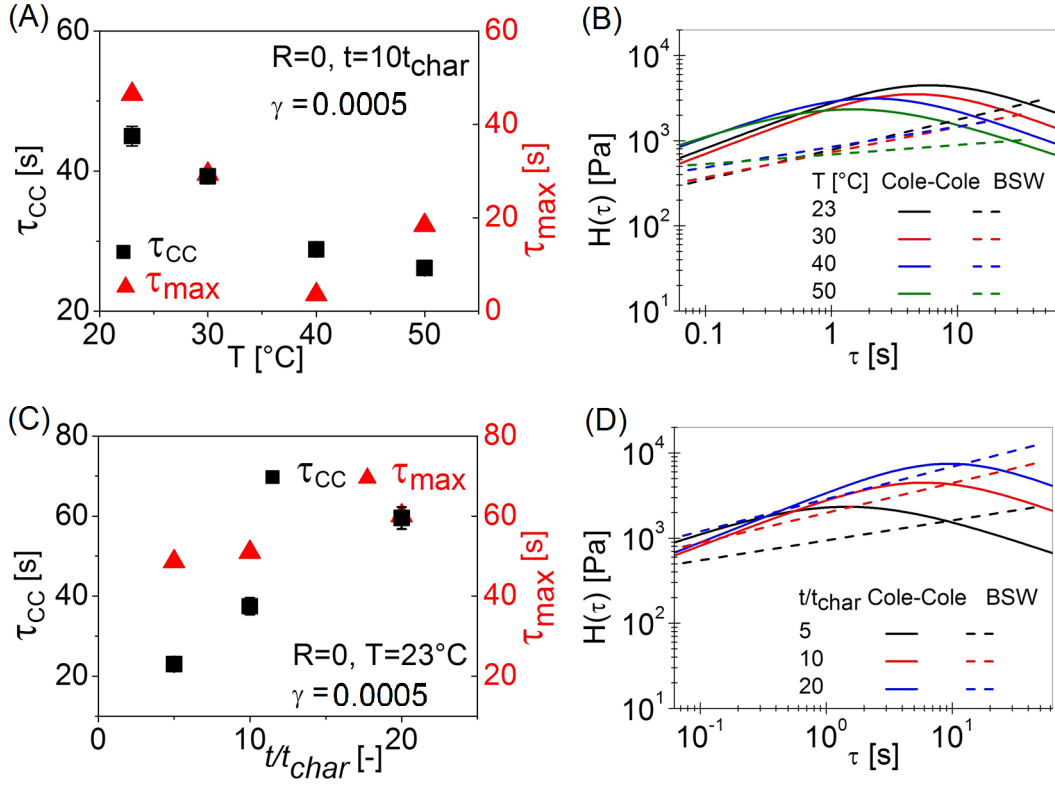


**Figure 3.11:** Comparison of the two models used: The dependence of relaxation time  $\tau_{CC}$  from the fit to the modified Cole-Cole function and maximum relaxation time  $\tau_{max}$  as calculated from the BSW function on the temperature (A) and reaction time  $t/t_{char}$  (C). The relaxation modulus  $H(\tau)$  is plotted against relaxation time  $\tau$  for the corresponding temperatures (B) and reaction times  $t/t_{char}$  (D).

fit. Thus the conclusions are independent of the actual model that was used for the analysis.

In the BSW fit data, there was a clear tendency for the relaxation modulus  $H(\tau)$  to increase with relaxation time  $\tau$ . In contrast, for a chemical (polymer) gel,  $H(\tau)$  is expected to decrease with time.<sup>130</sup> However, the relaxation properties of the reactive silica gel are similar to weak colloidal gels<sup>128,129</sup> at low frequency. For colloidal gels, the structural reorganization occurs on a large scale, which corresponds to the relaxation process at long time, i.e. low frequency. Similarly, the dissolution and formation of the silica bonds allows for the rearrangement of

the reactive silica gel on a large scale. Such processes contribute to the relaxation process at long relaxation times.

#### 3.1.4 Conclusion

Rheological material functions provided information about structural development of reactive silica gels. A particularity of the material studied in this work is the high pH value that allowed for a finite solubility of silica in the reaction mixture. Consequently, a reaction equilibrium between the bond dissolution and formation was expected. This reactive silica gel exhibited a behavior known from physical and colloidal gels: a logarithmic time dependence of the storage modulus and structural relaxation at low frequency. Two stages with different regimes were observed in the temporal evolution of the storage modulus. I attribute these two regimes to (I) the growth of aggregates and formation of bonds at short times and (II) further growth of the bonds and restructuring at longer times. Further studies of the system with NMR and DLS is presented in the following (section 3.2).

A structural relaxation was evident from the frequency dependent measurements. The storage modulus  $G'$  exhibited frequency dependence below 6 rad/s. Similar behavior was observed for colloidal gels.<sup>128</sup> The microscopic origin of the structural relaxation is assumed to be the finite solubility of silica at high pH. A more detailed analysis showed that this relaxation mode is more pronounced in concentrated samples, at higher temperatures and short times.

The experimental data of the frequency dependent mechanical moduli could be fitted with models that allow for a calculation of relaxation times and modulus. A modified Cole-Cole equation and the BSW function were used for this purpose with comparable results. Both models agree on how the properties of the low frequency relaxation depend on the experimental parameters. The extracted relaxation time is longer for higher water concentrations, lower temperatures, and older gels. The distribution of relaxation times turned out to be broader for higher temperatures and younger gels but independent of the concentration.

## 3.2 Structural analysis

To understand the rheological behavior of the reactive silica gel, a microscopic insight of the aggregation and gelation process were needed. With NMR and DLS, the structural development of the gel at high pH was analyzed on different length scales. The results revealed that the primary particles existed already in sodium silicate and aggregated after the mixing of reactants by the chemical reaction. The system was in its reaction equilibrium later on in the aggregation process.

### 3.2.1 Material and methods

#### 3.2.1.1 Material

The precipitated silica gel samples used in the experiments were prepared with the same method as introduced in section 3.1.1.1. The silica gel was formed by the chemical reaction of sodium silicate solution and sulfuric acid. The sodium silicate solution used here is from the same batch as that used for rheology sample (section 3.1). The volume ratio between the two reactants was varied for each experiment. They are listed in the Table 3.1 for the the samples for NMR, DLS measurements. The gel for NMR had a pH-value of 11.0, measured by pH-meter (Lab 850, Schott Instruments, Mainz, Germany), about 0.5% silica was soluble in the water. The chemical reaction of this silica gel was described in section 3.1.1.1 and the literature<sup>26,27</sup>.

The observed gelation time in the Table 3.1 was measured with the Couette rheometer. In the experiments, the resolution limit of the transducer ( $0.02 \text{ g} \cdot \text{cm}$ ) corresponded to a lowest measurable complex modulus of 115 Pa at strain  $\gamma = 0.0005$ . The observed gelation time in the rheological measurements was estimated from the time once the moduli were measurable. From these previous experiments I deduced the concentrations for the NMR and DLS measurement to (i) allow for a gelation time that is adapted to the measurement time and (ii) have enough signal. In all samples for DLS, the solid silica gel concentration was low enough to avoid the multiple scattering. In all samples the gelation time was much longer than sample preparation time ( $t_{\text{prep}} < 3 \text{ min}$ ). Due to slight differences in the preparation time and the sample composition, the actual gelation time of the individual

measurement did vary by maximum 10 minutes. The reaction mixtures were filled into the measurement cell in their sol state. For this reason, effects of the shear applied to sample during the filling of the measurement cells were reduced to a minimum.

	$V_{\text{Na}_2\text{O} \cdot 3.3\text{SiO}_2} :$ $V_{\text{H}_2\text{SO}_4} : V_{\text{H}_2\text{O}}$	silica concentration [wt.%]	observed gelation time [h]
NMR	4 : 2 : 3	15	0.91
DLS	2 : 1 : 75	1	> 25
	2 : 1 : 12	5	> 25
	2 : 1 : 4	10	$\approx$ 25

**Table 3.1:** Sample composition for NMR and DLS measurements.  $V_{\text{H}_2\text{O}}$  is the volume of the additional water, not including the water from the sodium silicate solution and sulfuric acid.

### 3.2.1.2 Experimental method

The presented  $^{29}\text{Si}$  MAS NMR measurements have been performed on a Bruker Avance III console operating at 139.11MHz  $^{29}\text{Si}$  Larmor frequency with a commercial double resonance MAS probe supporting MAS rotors with 4 mm outer diameter using commercial 4 mm HR-MAS rotors for the viscous samples. After mixing for 30 seconds, the mixture of the reactants was in sol state and was filled into the rotor directly. As reference sample, the untreated sodium silicate solution was measured with same procedure. It was checked by visual inspection that no air bubbles were in the sample.

For DLS measurements, freshly prepared samples were obtained by mixing the reactants in cylindrical silica glass cuvettes (Hellma, inner diameter  $\phi = 20\text{mm}$ ), which had been cleaned before with acetone in a Thurmont apparatus. The cuvettes containing the samples with concentrations of  $C = 1, 5$  and  $10 \text{ wt.}\%$  were

placed into a thermostated refractive index matching toluene bath held at a constant temperature of  $T = 23^\circ\text{C}$ . Experiments were performed on a ALV instrument (Fig. 2.9), introduced in section 2.2.1.

## 3.2.2 Results

### 3.2.2.1 Nuclear magnetic resonance spectroscopy

Quantitative  $^{29}\text{Si}$  MAS NMR spectra have been recorded in order to quantify the changes of the chemical composition of sodium silicate  $\text{Na}_2\text{O} \cdot 3.3\text{SiO}_2$  during the precipitation reaction. In the course of the chemical reaction (observed gelation time 0.91 h, Table 3.1), 24 NMR spectra have been recorded with an acquisition time of 2 h each. Remarkably, the recorded spectra did not indicate any change in chemical composition during the precipitation of the rheologically active silica particles within the experimental uncertainties.

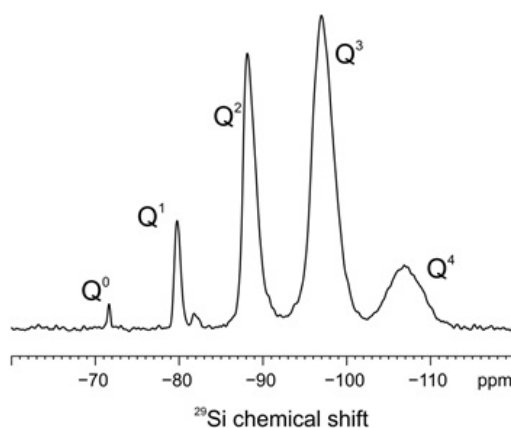


**Figure 3.12:**  $^{29}\text{Si}$  MAS spectrum of the precipitated silica gel sample recorded at 5 kHz MAS and 139.1 MHz  $^{29}\text{Si}$  Larmor frequency.

The  $^{29}\text{Si}$  MAS NMR spectra of the precipitated sample (Fig. 3.12) and an untreated sodium silicate reference sample ( $C = 40$  wt.%) were recorded with significantly longer signal averaging and thus better signal to noise ratio than the spectra recorded during the precipitation. Comparing both spectra, the following minor differences could be identified (Table 3.2). There is a small but significant

reduction of  $Q^1$  and  $Q^2$  group signal intensity, while the signal intensities of higher condensed  $Q^3$  and  $Q^4$  groups are increasing. Due to required long duration for signal averaging, it is unfortunately not possible to probe with  $^{29}\text{Si}$  MAS NMR, whether or not these changes take place right after the addition of the sulfuric acid and thus may cause the precipitation or in turn if they result from the precipitation process.

---

	$Q^0$ [%]	$Q^1$ [%]	$Q^2$ [%]	$Q^3$ [%]	$Q^4$ [%]
Sodium silicate (reference)	0.7	5.2	25.9	52.7	15.5
Reactive silica gel after 48h	0.8	2.8	19.5	59.3	17.6

---

**Table 3.2:** Comparison of  $^{29}\text{Si}$  NMR signals between sodium silicate (reference sample) and reactive silica gel sample.

(This chapter is written by Robert Graf.)

### 3.2.2.2 Dynamic light scattering

Structural analysis of aggregation processes can be performed by DLS because the contributions of the different structures to the total scattering can be separated in the time domain.<sup>131,132</sup> Therefore, time depending DLS measurements can reveal details of the aggregation mechanism. Here the essential results from DLS are presented and the background of the data analysis is introduced in appendix. Figure 3.13 shows the bimodal relaxation function  $C(q, t)$  of the initial sample at  $t = 0$  h with  $C = 10$  wt.% along with the corresponding double stretched exponential fit (Eq. A4 in appendix) and the distribution of relaxation times  $H_\tau(\ln \tau)$  (Eq. A2 in appendix) at  $q = 1.87 \times 10^{-2} \text{ nm}^{-1}$ . Similar with the structural relaxation function  $G(t)$  (Eq. 2.17) introduced in section 2.1.4, the relaxation function  $C(q, t)$  can be expressed as a superposition of exponentials. As confirmed by the  $q^2$  dependence of the relaxation rates both modes ( $k = 1$  and  $2$ ) correspond to distinct diffusing entities. The translational diffusion coefficients  $D = 5.63 \times$

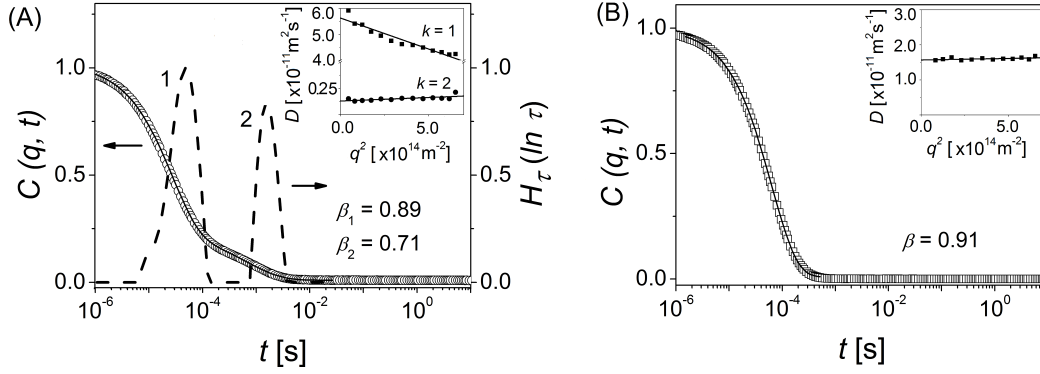


**Figure 3.13:** (A): Relaxation function  $C(q, t)$  for the concentration fluctuations (open symbols) along with the corresponding double stretched exponential fit (solid line, Eq. A4 in appendix) as well as the distribution of relaxation times  $H_\tau(\ln \tau)$  resulting from a CONTIN fit (dashed line, Eq. A2 in appendix) at  $q = 1.87 \times 10^{-2} \text{ nm}^{-1}$  of the initial sample. The peaks in  $H_\tau(\ln \tau)$  associated with relaxation modes  $k = 1$  and 2 are indicated in the plot. The diffusion coefficients  $D$  are obtained for both diffusion processes from the intercept of the linear variation of  $\Gamma/q^2$  as a function of  $q^2$ , as shown in the inset. (B) Relaxation function  $C(q, t)$  for the concentration fluctuations (open symbols) along with the corresponding KWW fit (solid line, Eq. A3 in appendix) characterized by a shape parameter  $\beta = 0.91$  for the same sample after 6 h.

$10^{-11} \text{ m}^2\text{s}^{-1}$  for the main mode ( $k = 1$ ) and  $D = 1.29 \times 10^{-12} \text{ m}^2\text{s}^{-1}$  for the slower mode ( $k = 2$ ) obtained from the intercepts of the linear variation of  $\Gamma/q^2$  versus  $q^2$  (Fig. 3.13 A inset), enabled the calculation of the effective Stokes-Einstein hydrodynamic radii (z-average) of both diffusion processes. The hydrodynamic radius of the individual structures is  $R_h = 3.8 \pm 0.4 \text{ nm}$  ( $k = 1$ ). The appearance of an additional relaxation mode ( $k = 2$ ) results from the coexistence of the freely diffusing primary particles and aggregated structures with a dimension of  $R_h = 167.0 \pm 17 \text{ nm}$  ( $k = 2$ ).

Figure 3.14 and A1 (appendix) illustrate the time dependence of  $R_h$  of the same sample determined at  $q = 1.87 \times 10^{-2} \text{ nm}^{-1}$  over a time range of  $0 \leq t \leq 25 \text{ h}$ . The dimension of the present aggregates increase significant after 3 h while at  $t < 6 \text{ h}$  the slower relaxation mode ( $k = 2$ ) disappears. Figure 3.13 B shows the single mode relaxation function along with the data evaluation by using a stretched

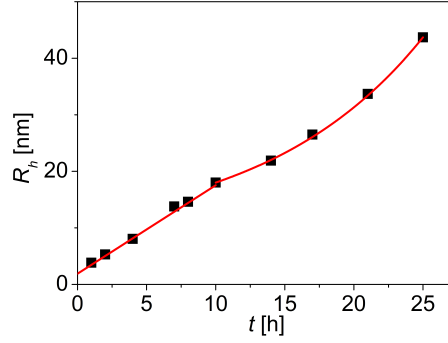


**Figure 3.14:** Time dependence of the aggregation process determined by DLS at a scattering vector of  $q = 1.87 \times 10^{-2} \text{ nm}^{-1}$  over a time range of  $0 \leq t \leq 25 \text{ h}$ .

exponential Kohlrausch Williams Watts (KWW) function (appendix) at  $t = 6 \text{ h}$ . The moderate width of  $C(q, t)$  is described by a shape parameter of  $\beta = 0.91$ . Apparently sedimentation of the aggregated structures occurs.

In the same time range  $0 \leq t \leq 6 \text{ h}$  the dimension of the formed primary particles increase significant from  $R_h = 3.8 \text{ nm}$  to  $13.8 \text{ nm}$  as shown in Figure A1. Furthermore, a linear increase of  $R_h$  in a time range of  $0 \leq t \leq 10 \text{ h}$  was obtained as shown in Fig. 3.14. A further increase of the particle dimensions at  $t > 10 \text{ h}$  can be described by fitting  $R_h$  with a cubic equation. Remeasuring the sample after about one week showed no significant changes in the  $R_h$ . This implies that the size of the primary particles saturates after about one day.

(This chapter is written by Anja Kroeger-Brinkmann.)

### 3.2.3 Discussion

From the NMR data it can be concluded that there was no significant difference of the binding state of silicium with the time. The spectrum of the initial sodium silicate solution is very similar to the spectrum of the fully gelled sample. This is compatible with the assumption that primary nano particles were already present in the initial sodium silicate solution. The small changes in the NMR spectra imply that most of the changes in aggregation process leave the chemical environment of the Si atoms unchanged. Growth at the expense of other particles and aggregation



of particles are the dominating mechanisms throughout the gelation process. Due to the high pH value and the finite solubility of silica at this pH, the system was in the reaction equilibrium between formation of new silica bonds and its dissolution. The reversibility of the bonds is also one of the key differences to other systems that show a clear growths of the  $Q^3$  and  $Q^4$  peak with the time.<sup>119,133</sup>

Small angle X-ray scattering (SAXS) studies of the precipitation of silica gel at pH from 7 to 10 and at temperature from 60 to 90°C showed a similar behavior.<sup>134</sup> They showed that at least 1 h after adding sulfuric acid in the sodium silicate, no new particle is formed and all silica in newly dosed sodium silicate deposited on the already existing particles. In addition, the existence of primary particles in nm range in sodium silicate solution was proved with SAXS measurements.<sup>135</sup> These observations confirm the interpretations that the primary silica particles exist already in the sodium silicate solution. The addition of sulfuric acid essentially initiates the aggregation process.

The DLS results allow a further detailed analysis of the aggregation mechanism. DLS and NMR agree that primary particles were present from the very beginning of the experiment. Additionally, there are two separate species measured by DLS. The small species is identified as the primary particles or small aggregates of the particles and the large species is interpreted as larger aggregates. The change in the growth law of the small species might indicate a change in the diffusional behavior of the primary particles and small aggregates. However the origin of this cannot be identified but might be hint to a hinderance of the free diffusion. The vanishing of the large species in the DLS experiments is probably due to sedimentation, which also influences the concentration of the sample. In the higher concentrations on the NMR experiments, it is assumed that these large clusters are at the origin of the system spanning network.

Based on the information from rheological (section 3.1) and structural measurements, the evolution of reactive silica gel was illustrated in Fig. 3.15. By adding sulfuric acid in the sodium silicate, the existing primary particles started to aggregate and the aggregates grew with the time (Fig. 3.15 B,C). The gel point was then reached when a volume-spanning network was formed (Fig. 3.15 D). The sample system transferred then from the sol to the gel state. At long times, the strengthening of bonds occurred (Fig. 3.15 E). Because of the high pH value of

the studied silica gel, the silica bond was reversible and the chemical reaction was in equilibrium state on the molecular level.

The time window of each experiment is also presented in Fig. 3.15. With NMR, the change of chemical composition of the whole aggregation and gelation process can be followed. DLS was applied for the analysis of particle size from the beginning of the reaction to the time point at which the formation of more aggregates lead to multiple scattering. Whether this point is before or after the gel point depends on the sample system. The size of the primary particle and aggregation kinetics can be essential factors here. Therefore the end of the time window of DLS is shown as a color gradient in the figure. Also, the start of the measurable time range of rheological measurement is related to the sample system and the rheometer. As discussed in section 1.2.2, the measurement signal can only be detected when the responding stress of the gel is large enough to reach the resolution limit of the rheometer.

#### 3.2.4 Conclusion

On the base of the rheological study (section 3.1), the temporal evolution of the system is now better understood. From the NMR experiments and studies reported in the literature I could conclude that there was only little difference in the chemical composition between the initial sample and the final gel. Also with DLS it was confirmed that the primary particles existed already before the mixing of the reactants. During the aggregation and gelation process, the system was in its reaction equilibrium. With DLS, the further growth of aggregates was characterized.

### 3.3 Modifying the gel modulus using shear strain

The NMR and DLS showed that the sol-gel process is essentially an aggregation process. Based on the comprehension of the gel evolution with the rheological measurements (section 3.1) and structural analysis (section 3.2), I demonstrate a method to modify the shear modulus by large shear strain. Various shear strains

and strain combinations were applied to the sample during the aggregation and gelation process and their effects on the mechanical properties of the sample system were studied. The storage modulus of the gel turned out to be strain-history dependent.

In the rheological investigation I focused on the following questions:

1. How does shear deformation influence the aggregation process?
2. Is the influence of shear in the ageing of the formed gel similar to the effects during the aggregation?
3. What are the induced changes in the macroscopic mechanical properties and how can they be interpreted?

#### 3.3.1 Material and methods

##### 3.3.1.1 Material

The precipitated silica gel samples with volume ratio  $V_{\text{Na}_2\text{O} \cdot 3.3\text{SiO}_2} : V_{\text{H}_2\text{SO}_4} : V_{\text{H}_2\text{O}} = 2 : 1 : 0$  were used here for the rheological experiments. Same batch of sodium silicate with samples in section 3.1 and 3.2 was applied, therefore the variation of different batches was avoided. The sample preparation method and details about the chemical reaction were introduced in section 3.1.1.1. In comparison with the sample systems for NMR and DLS measurements (Table 3.1), the sample for rheology has a silica concentration of 21 wt.% with an observed gelation time of 0.15 h. As mentioned in section 3.1.1.1, the actual gelation time of the individual samples varied (maximum 10 minutes), because of the slight differences of the sample preparation time and composition.

##### 3.3.1.2 Experimental method

The development of the shear moduli with time at room temperature  $T = 23^\circ\text{C}$  was investigated with a strain controlled rheometer (Fig. 2.4 A) equipped with Couette cell under oscillatory shear. The reactants were mixed for 30 seconds and directly filled into the rheometer cup when the mixture was still in sol state. An

immiscible oil was used as an evaporation blockage layer on surface of the sample. The preparation of sample in the Couette cell reduced shear history of the gel to a minimum. The experimental details were described in section 3.1.1.2. All measurements were performed at a fixed frequency of  $\omega = 10$  rad/s.

#### 3.3.2 Results

In section 3.1.2.1, a typical physical gel behavior: a linear relation between the storage modulus  $G'$  and the logarithm of the reaction time  $t$  was measured by the reactive silica gel (Fig. 3.3 C). Moreover the evolution of the storage modulus with the time can be divided into two regimes. In both regimes the storage modulus grew logarithmically with time. The logarithmic growth rate in the first regime was lower than that in the second regime.

The influence of the shear deformation was investigated by following the development of the silica gel under different strains and strain combinations with the Couette rheometer. The effect of small strain (far within the linear regime) on the gel evolution was studied by comparing (i) a gel sheared continuously under strain  $\gamma = 0.0005$  starting from the filling with (ii) a gel that was not sheared for the first 4000 s and then measured under strain  $\gamma = 0.0005$  (Fig. 3.16). Only a small difference in the mechanical response is visible. The good agreement of both curves of storage and loss modulus  $G'$  and  $G''$  in the time range from 4000 to 8000 s proved that the shear strain  $\gamma = 0.0005$  has only a minor effect on the gelation process.

A small time offset of about 500 s between the data points from both measurements can either be attributed to minor shear-induced alternation of the sample or to slight difference in the sample preparation and composition, discussed in section 3.3.1.1. This offset is within the uncertainty of the sample composition.

In a next step I increased the strain used for the measurements beyond the linear regime of the materials ( $\gamma > 0.0035$ ) to  $\gamma = 0.002, 0.004$  and  $0.01$  (Fig. 3.17). For long times ( $t > 1.5 \times 10^3$  s), the logarithmic time dependence of the storage modulus was also preserved. As shown in section 3.1.2.1, the slope of the logarithmic time dependence increased from the first to the second regimes. The two regimes

with different increasing rate of storage modulus, discussed in section 3.1.3.1., were seen clearly under all strain conditions. The cross-over between these two regimes occurred around  $t = 1.5 \times 10^3$  s for all measurements.

To better visualize small storage moduli and short times, the data of Fig. 3.17 is also plotted in log-log scaling (Fig. 3.17 inset). For the same reaction time, the storage modulus at short times ( $t < 1.5 \times 10^3$  s) is much lower under higher strain. With time the moduli grow faster at higher applied strain. After about 1500 s, the storage modulus measured at higher strains ( $\gamma = 0.002, 0.004$  and  $0.01$ ) exceeded that measured at strain  $\gamma = 0.0005$ . In the linear-log plot, the long-time behavior is emphasized (Fig. 3.17). The slope of the time dependence remains large under higher strain and storage modulus is also higher at long times ( $t > 1.5 \times 10^3$  s).

However, the rheometer didn't keep the strain constant after typically  $2.5 \times 10^3$  s. For longer times the strain decreased in an uncontrolled way. The automatic decrease of strain from the set value in the rheometer is presented in Fig. 3.18. From 3000 s, the strain fell outside the range of 10% deviation of set value. With the growth of gel network, the moduli increased. Although the maximum torque, which the transducer can measure, was not reached, the applied strain from rheometer was decreased from a certain time. This automatic switch of the rheometer was observed by all measurements, even by  $\gamma = 0.0005$ . When the strain was changed from one value to the other after 4000 s, the decrease of the strain continued in the same way as the the measurements which were done only under one strain. Therefore, the history effect (Fig. 3.19) can be analyzed, although at long times the strain was already lower than the 10% deviation of set value.

Therefore in Fig. 3.17 I only show data that was collected for actual strains within less than 10% deviation from the given strain value. It was assumed that these small variations of the actual strain had only negligible influence on the moduli and their time dependence.

To study the influence of the shear history, the applied strain was changed during the measurement either from high to low value or the opposite (Fig. 3.19). For the strain combination labelled "0.0005+0.004" the strain  $\gamma = 0.0005$  was applied for 4000 s, then directly switched to  $\gamma = 0.004$ . Also an experiment was performed in the inverse order "0.004+0.0005".

The data for experiments with different shear history but the same actual strain are parallel in the semi-log plot (Figure 3.19). This shows that the growth rate of the storage modulus, i.e., slope of the curve, depends only on the applied strain, but not on the shear history. In contrast, the absolute value of the measured modulus at a given time depends on the history and the current shear strain. When the applied strain was increased from 0.05 to 0.004, the measured storage modulus doubled. Similarly, as the applied strain was reduced from 0.004 to 0.0005, the storage modulus was halved.

#### 3.3.3 Discussion

As discussed in section 3.2.3, NMR and DLS results support the argument that the primary particles exist already at the beginning of the chemical reaction. With the time, aggregates are formed from the primary particles and the size of aggregates determines the diffusion and relaxation process. When the aggregates are large enough to span the whole volume of the cell (at the gel point), a macroscopic gel is observed. To distinguish the processes before and after the gel point I refer to them as aggregation and gelation, as discussed in section 1.2.

The mechanical properties of the reactive silica gel could be modified by applying shear during the aggregation and gelation process. When applying large strain during the aggregation and gelation, the storage modulus decreased at short times and increased at long times. Furthermore, the shear history measurement (Fig. 3.19) demonstrated that the slope of storage modulus vs. time, i.e., the growth rate of the modulus, was dependent on the current strain and independent on the shear history. However the absolute value of the storage modulus depends on both the current strain and shear history.

The strain dependence can be explained with the compaction of the aggregates under large strain, which was discussed in experimental studies<sup>17,18,54,78,136</sup> and simulation work<sup>56</sup>. Through the mechanical stresses acting on the aggregates and the gel, the initial open and mechanically weak aggregates become more compact and mechanically robust (Fig. 3.20 B,C). In the studied reactive silica gel, there were two simultaneous processes going under large strain. One is the breakage of the bond under shear strain (Fig. 3.20 D,E). Parts of the gel network was destroyed

and did not contribute to the modulus any more. This leads to a decrease of the shear modulus. The other is the formation of new bond amongst the compacted aggregates, which results from the chemical reaction (Fig. 3.20 F). It causes the increase of the shear modulus. Therefore, the change of the storage modulus is determined by the competition between these two processes.

In young gels the storage modulus decreased with increasing strain. This can be interpreted the following way. Under applied shear deformation, the energetically unfavorable bonds were broken and new bond could be formed amongst more compact aggregates. However, breakage of the bonds was dominant at short time (Fig. 3.17 inset). As gelation proceeded with time, the formation of new bonds became dominant. Higher strain enhanced this reorganization of the gel structure in the way that only the energetically favorable bonds remained and other bonds were broken. The more compact aggregates network leads to higher modulus at long time. Experimental results showed in Fig. 3.17 confirms this tentative argument.

Comparable results were reported by Wu et al. in a study on fumed silica dispersed in dodecane.<sup>137</sup> In this solvent, fumed silica formed gels and the gels experienced disorganization and reorganization under shear. Strong structural recovery abilities after oscillatory shear at strain from  $\gamma = 0.001$  to 0.01 and higher storage modulus were demonstrated by these silica gels. The recovery abilities were explained with the aggregation of the broken parts, driven by the high surface energy. At higher strains up to 1, the network was completely disrupted, which led to a lower modulus of the gel. The difference between the fumed silica gel and the reactive silica gel is that the fumed silica gel showed no time dependence. In the reactive silica gel, the strains could be applied during the entire aggregation and gelation process, since the sample was still in its sol state when filled into the rheometer. While the fumed silica gel was deformed when the network was already formed. The reversibility of the bonds resulted from the chemical equilibrium in the reactive gel and from a physical process in the fumed silica gel. However, an increase of gel modulus induced by shear was observed in both studies.

The flow history dependence was also discussed in other studies.<sup>77,138</sup> For the reversibly aggregated suspensions and depletion flocculated colloidal dispersion, a strong influence of the shear history on the rheological properties were concluded

from experimental data. But a comparable model of history dependence for the silica gel is lacking at present.

#### 3.3.4 Conclusion

At higher strains, the storage modulus reached higher values at long times (after 2000 s) compared to gel that was not exposed to shear during aggregation and gelation. I explain this behavior with shear-induced compaction during aggregation and gelation. Shear led to the destruction of existing energetically unfavorable bonds and the formation of new more favorable bonds with compacted aggregates. Furthermore, the growth rate of the storage modulus is only dependent on the current shear rate and independent of the shear history. I expect that the approach of modifying gel modulus under shear can be applied in the gel production for controlling the mechanical properties of end product.



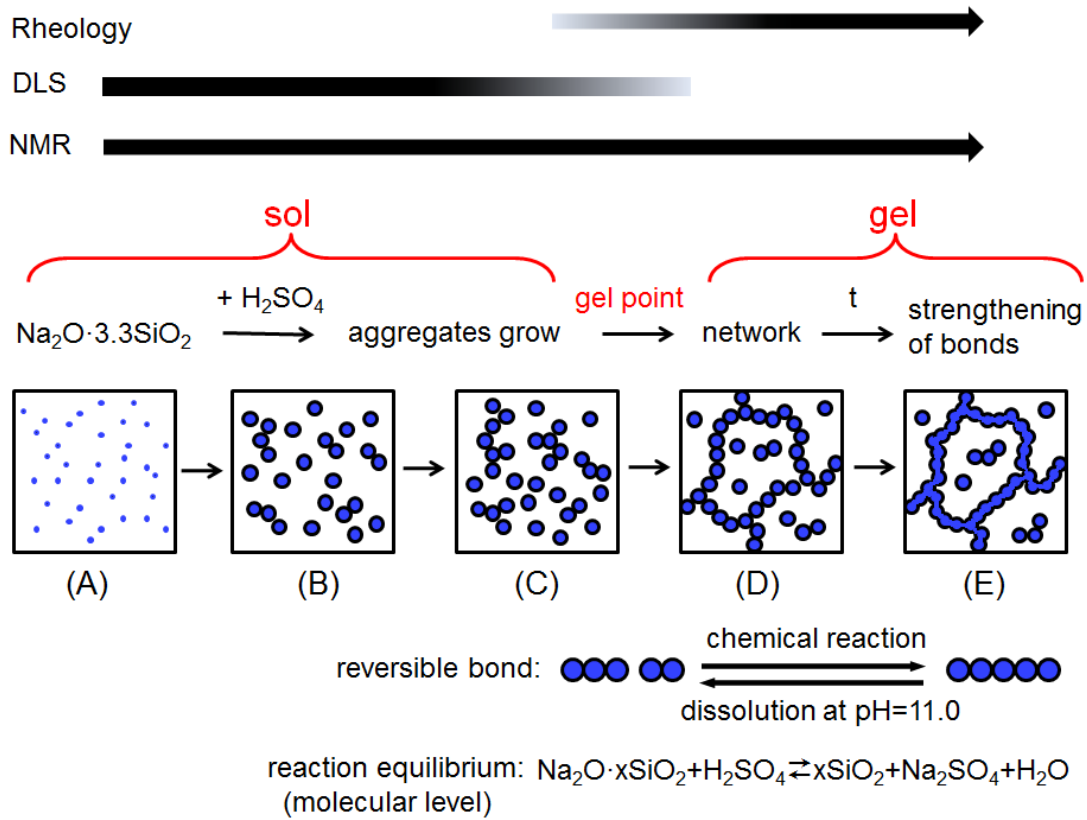


**Figure 3.15:** Illustration of the structural development of the reactive silica gel with time, which is covered to a varying extend by NMR, DLS and rheological measurements.

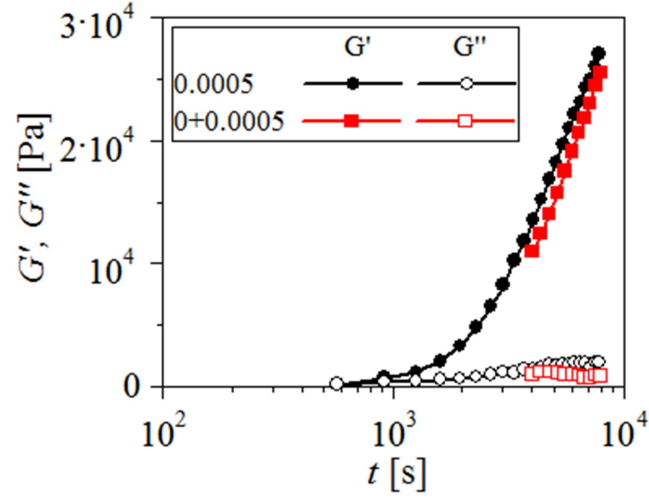


**Figure 3.16:** The time dependence of storage modulus  $G'$  (filled symbols) and loss modulus  $G''$  (open symbols) for the silica gel at temperature  $T = 23^\circ\text{C}$ , frequency  $\omega = 10$  rad/s, with a strain of  $\gamma = 0.0005$  (circles) compared with the gel without shear deformation for the first 4000 s and then sheared with a strain of  $\gamma = 0.0005$  (squares).

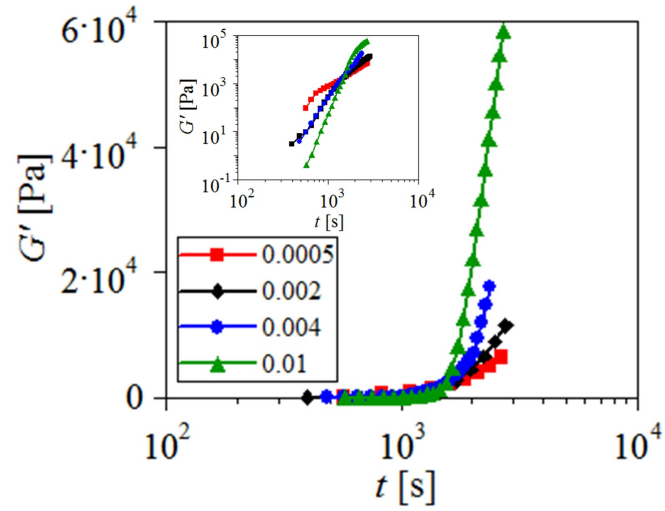


**Figure 3.17:** The growth of storage modulus  $G'$  in linear-log scale at temperature  $T = 23^\circ\text{C}$ , frequency  $\omega = 10$  rad/s and under strain  $\gamma = 0.0005$  (red squares), 0.002 (black rhombi), 0.004 (blue circles) and 0.01 (green triangles). Inset: the same data in log-log scale.

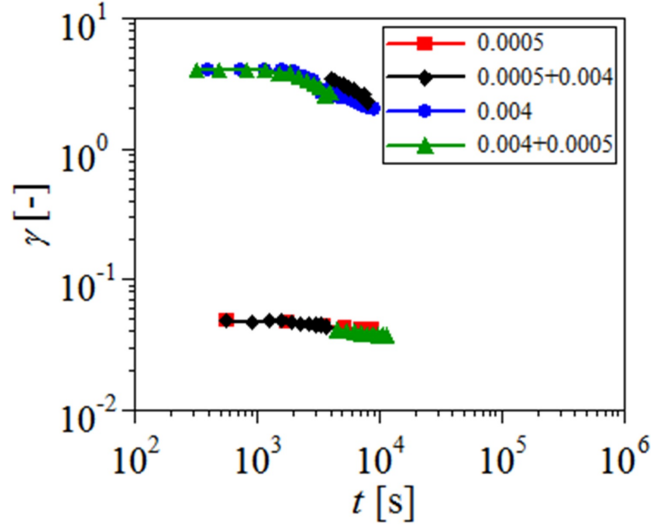


**Figure 3.18:** The decrease of strain in the Couette rheometer with the time by the measurements under strain  $\gamma = 0.0005$ ,  $0.004$ ,  $0.0005 + 0.004$  and  $0.004 + 0.0005$  at temperature  $T = 23^\circ\text{C}$  and frequency  $\omega = 10 \text{ rad/s}$ .

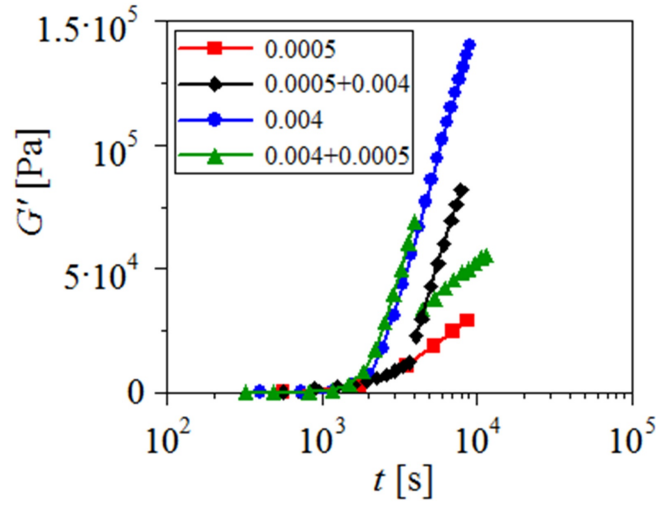


**Figure 3.19:** The growth of storage modulus  $G'$  at temperature  $T = 23^\circ\text{C}$ , frequency  $\omega = 10 \text{ rad/s}$  and under strain  $\gamma = 0.0005$  and  $0.004$  compared with that under strain combination of  $\gamma = 0.0005$  and  $\gamma = 0.0004$ . In the combined measurements each strain was applied for 4000 s. “0.0005 + 0.004” denotes the experiment starting at strain  $\gamma = 0.0005$  and then 0.004 and “0.004 + 0.0005” the experiment starting at strain  $\gamma = 0.0004$  and then 0.0005.

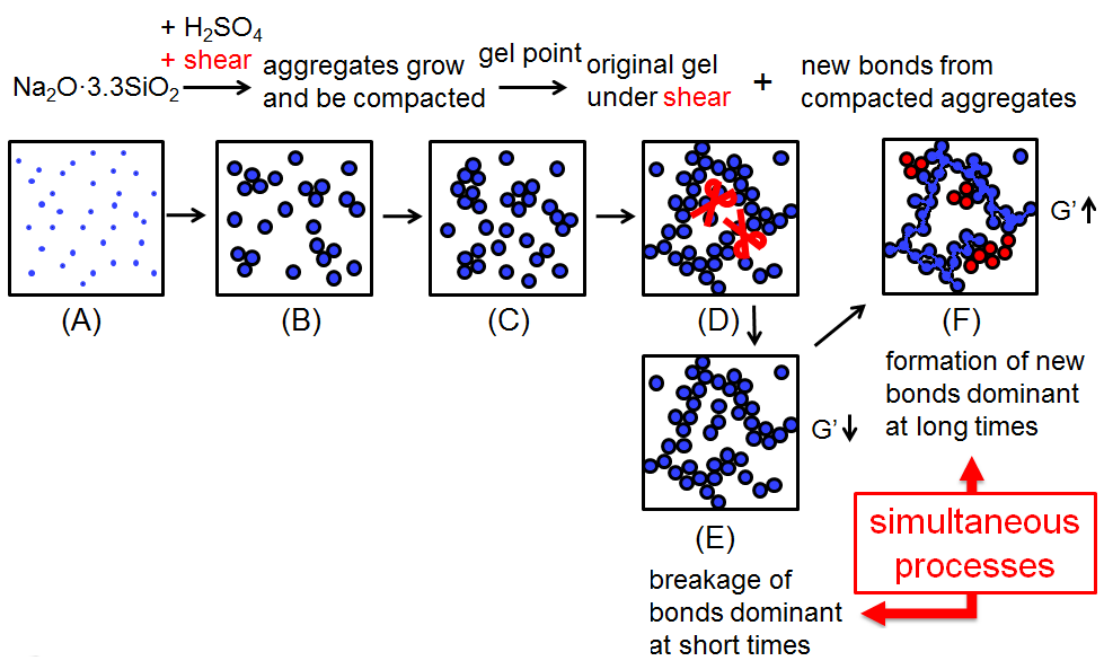


**Figure 3.20:** Illustration of the structural development of the reactive silica gel with time under large shear strain. In the sol state, aggregates become more compact under shear. In the gel state, the energetically unfavorable bonds is broken under external deformation and the new bonds can be formed amongst compacted aggregates.

## 4 Gelation of various systems

Using the piezo-rheometer, the gelation kinetics and mechanical properties of various systems were investigated. The study of antibacterial Cl-dopamine gel<sup>139</sup>, light-triggered alginate gel<sup>140</sup> and self-healing supramolecular gel<sup>141</sup> were published and introduced in the following sections. As discussed in section 2.1.3, only a small sample volume, down to 1.2 mm<sup>3</sup>, is needed for the measurement with the piezo-rheometer. Therefore, the rheological analysis on these specific gel samples with limited amounts can be performed.

Here, I cooperated with different groups, who work on the synthesis of new gel materials. The influence of chemical structural modification on the gel mechanical properties was studied. In antibacterial Cl-dopamine gel, Cl-dopamine functional group is attached to the polymer gel-precursor. A chemical reaction of this polymer and solution of NaIO<sub>4</sub> leads to the gel formation (section 4.1). In light-triggered alginate gel, the Ca<sup>2+</sup> can be released from photo-triggerable cages via irradiation with ultraviolet (UV)-light. With ionic cross-linking with Ca<sup>2+</sup>, the gelation of alginate solution is mediated (section 4.2). By self-healing supramolecular gel, the association of molecules into the gel network results from the host-guest interaction between polymers bearing crown ether and secondary amino groups. The gelation is induced by high temperature (section 4.3). The details about these gel systems are presented below.

Different from the reactive silica gel discussed above (chapter 3), all three gels studied in this chapter exhibited the typical chemical hydrogel behavior: the storage modulus is independent of the frequency, as discussed in section 1.2.2. The bonds with infinite life time are formed in the chemical gelation reactions and no reorganization occurs.

Here, more attention is paid to the gelation kinetics and its conditions. The questions addressed include:

1. How does the chemical structural modification affect the gelation process?
2. Does the absolute value of the storage modulus vary from the gel without the modification to the one with modification?
3. Can the gelation be controlled with external stimuli, e.g., light irradiation and internal reactant concentration?

### 4.1 Antibacterial Cl-dopamine gel

Various coating materials have been developed, using natural strategies, for preventing the bacterial biofilms, which are a significant cause of disease in biomedical devices. Depending on the working principle, the materials can be sorted into passive and active coatings. In passive coatings, bacterial attachment is hindered by functional polymers, e.g., ammonium functionalized polymers, polyethylene glycol (PEG) and zwitterionic polymers. In active coatings, the coating layer releases an active compound, e.g., silver or antibiotics, which kill the bacteria. Because of the effectiveness of active coating, many techniques have been applied, from which antibacterial peptides, antibiotics, quorum sensing inhibitors, essential oils and bacteriolytic enzymes can be released.<sup>142</sup> Since the substrate rigidity influences bacterial attachment considerably, the mechanical properties of the biofilm, i.e., shear modulus, are essential for its application.<sup>143</sup>

Inspired by the studies on the sand castle worm *Phragmatopoma californica*<sup>144</sup>, a new strategy was developed to confer antifouling properties on polymer surfaces by functionalizing the surface with biocide, using 2-chloro-4,5-dihydroxyphenylalanine (Cl-DOPA) from the proteinaceous glue of the sandcastle.<sup>139</sup>

Concerning the antimicrobial properties of chlorocatechols (Cl-catechol)<sup>145,146</sup>, a flexible and effective biocompatible antifouling strategy using a polymer bound Cl-catechol group is presented. In this work, a piezo-rheometer was applied to study the mechanical properties of gels with a Cl-dopamine group and their gelation kinetics. This study was published in “Antibacterial strategies from the sea: polymer bound Cl-catechols for prevention of biofilm formation”<sup>139</sup>.

## 4.1.1 Materials and methods

Poly(ethylene glycol) O,O', O'', O''' -tetra (acetic acid chloro-dopamine) amide (PEG-ClDOP<sub>4</sub>) and Poly(ethylene glycol) O,O', O'', O''' -tetra (acetic acid dopamine) amide (PEG-DOP<sub>4</sub>), used as a reference, were synthesized by the del Campo group at MPIP.<sup>139</sup> To study the antibacterial effect of Cl-dopamine, the functional group was incorporated into star-PEG gel-precursors, which gel under oxidative conditions.

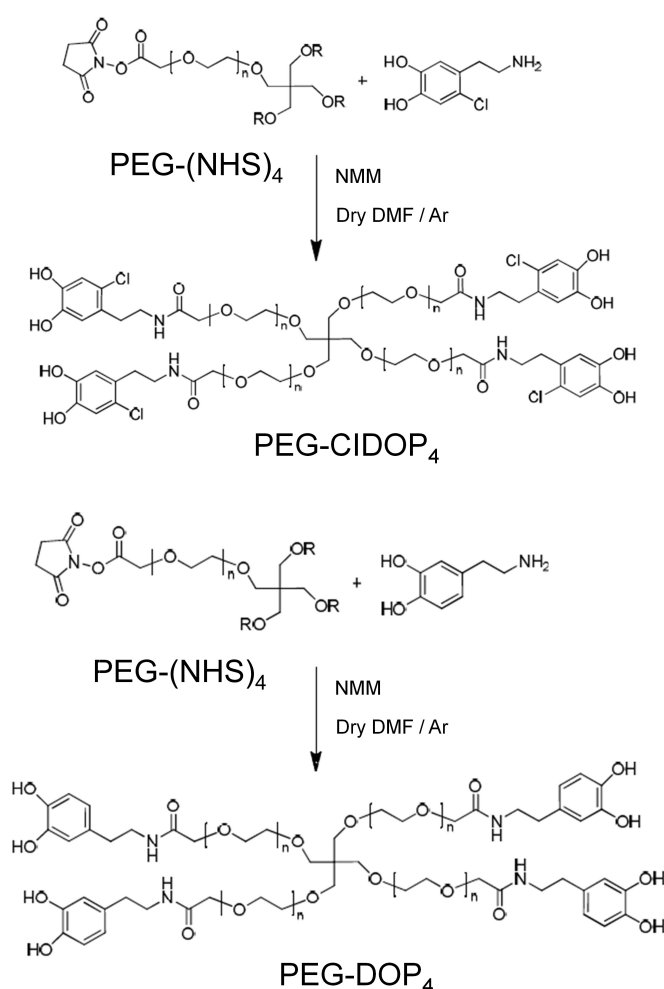


**Figure 4.1:** Synthesis of PEG-ClDOP<sub>4</sub> and PEG-DOP<sub>4</sub>.<sup>139</sup>

The detailed chemical reactions are described by Garcia et al.<sup>139</sup> and introduced briefly here (Fig. 4.1). First, the chlorodopamine (Cl-Dop) was produced by adding N-Chloro-succinimide (NCS) to a solution of dopamine hydrochloride in trifluoroacetic acid (TFA). Cl-Dop was reacted with N-methylmorpholine in dry dimethylformamide (DMF) under an argon atmosphere for 15 minutes. PEG-N-hydroxysuccinimide<sub>4</sub> (PEG-NHS<sub>4</sub>) was added in DMF. After dialysis, the PEG-ClDOP<sub>4</sub> was obtained. In an alternative route, dopamine was reacted with N-methylmorpholine (NMM) in dry DMF under an argon atmosphere. After 15 minutes, PEG-NHS<sub>4</sub> was added. The dialyzed end product was PEG-DOP<sub>4</sub>.

With the piezo-rheometer, the mechanical properties of the gels were investigated. A mixture of 8  $\mu$ l of a 200 mg/ml solution of PEG-ClDOP<sub>4</sub>, or PEG-DOP<sub>4</sub>, in H<sub>2</sub>O and 8  $\mu$ l of a 10 mM solution of NaIO<sub>4</sub> in H<sub>2</sub>O was placed in the rheometer cell. The gap between the substrates was set to 100  $\mu$ m. The sample was filled into the cell in its fluid state. To prevent the evaporation of the solution in the system, PDMS (molecular weight approx. 8000 g/mol) was applied as an evaporation barrier (see section 2.1.3 for details). Continuous frequency sweeps were performed at  $T = 23^\circ\text{C}$  and under strain  $\gamma=0.0032$ . Usually the maximum strain amplitude, beyond which the sample is outside the linear range, of polymer gels is at least one order of magnitude higher than the applied strain here. For example, the maximum strain amplitude is about 0.5 for strong polymer gels and 0.05 for weak polymer gels.<sup>147</sup> For this reason, it can be assumed that the sample was in its linear range under strain  $\gamma=0.0032$  and the gel structure was not destroyed by the shear during the measurement in the piezo-rheometer. The same experimental condition was applied for the systems in section 4.2 and 4.3. The frequency ranged from 0.63 to 6300 rad/s. The time evolution of the mechanical properties was studied until the cross-linking process was completed, i.e., a plateau of the storage modulus as function of time was reached, as discussed in section 1.2.2.

#### 4.1.2 Gelation kinetics and mechanical properties

To understand the mechanical properties and compare the rigidity of the gel with and without Cl-dopamine functionalization, the evolution of their shear modulus at a constant frequency of  $\omega = 63$  rad/s at  $T = 23^\circ\text{C}$  was studied. Both storage



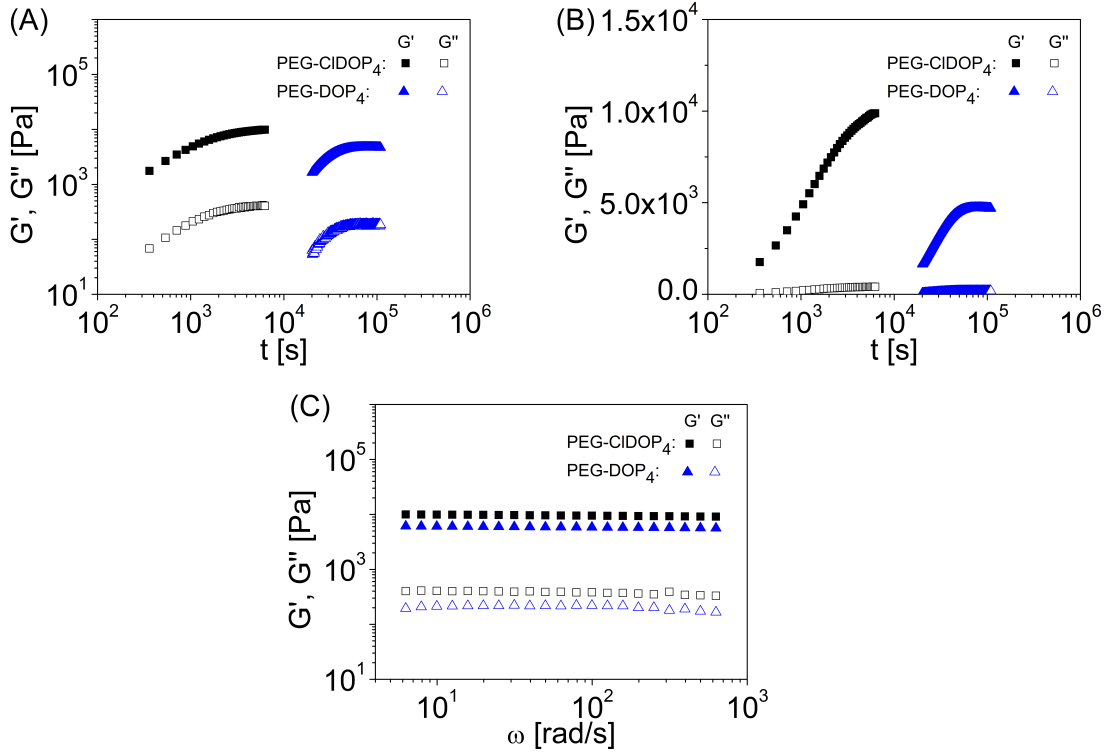


**Figure 4.2:** Evolution of the shear and loss modulus  $G'$  and  $G''$  during the gelation of PEG-DOP<sub>4</sub> and PEG-ClDOP<sub>4</sub> at  $T = 23^\circ\text{C}$  and frequency  $\omega = 63 \text{ rad/s}$  in log-log (A) and linear-log representation (B). (C): The frequency spectra of crosslinked PEG-DOP<sub>4</sub> and PEG-ClDOP<sub>4</sub> gels at  $T = 23^\circ\text{C}$ .

and loss modulus increased with time until they reached a plateau in the log-log representation (Fig. 4.2 A), indicating that the gelation was completed. A significant difference in the gelation kinetics of both samples was observed. The plateau of PEG-ClDOP<sub>4</sub> was achieved after  $5 \times 10^3 \text{ s}$ . The time to reach the plateau of PEG-DOP<sub>4</sub> was about  $5 \times 10^4 \text{ s}$ , 10 times longer. This clearly indicates that the incorporation of Cl-dopamine group accelerated the gelation process. Further studies for understanding the influence of chloro functionalization on gelation kinetics, e.g., NMR, are in progress.

In order to compare with the reactive silica gel (Fig. 3.3 A), the development of the storage and loss modulus with time was also plotted in linear-log scale (Fig. 4.2 B). In the reactive silica gel, a typical physical gel behavior was observed. The

development of the storage modulus with the time can be separated to two regimes with different growth rates. The growth rate of the second regime, i.e., at long time, is larger than that of the first regime. This means that the storage modulus increases further with the time at long time. The explanation was discussed in section 3.1.3.1. Furthermore, the similarity between reactive silica gel and physical gels can be explained with the dissolution of the bonds at high pH-value, which corresponds to the gel reorganization.

On the contrary, the growth of storage modulus of PEG-DOP<sub>4</sub> gel does not show two regimes. The storage modulus reaches a plateau at time over  $5 \times 10^5$  s, which is a characteristic behavior of chemical gel. For the PEG-ClDOP<sub>4</sub> gel, the growth rate decreases with the time significantly. A plateau of the storage modulus can be expected in the linear-log representation. Because of the limited measurement time window, it cannot be observed here. This plateau of the storage modulus as function of time results from the chemical bonds with infinite life time, formed in the gelation reaction. Therefore, no aging effect is seen in chemical gels.

After cross-linking, the storage modulus of PEG-ClDOP<sub>4</sub> and PEG-DOP<sub>4</sub> gel were independent of the frequency (Fig. 4.2 C). Both gels showed similar rigidity after complete conversion with storage moduli of 6 and 10 kPa for the crosslinked PEG-ClDOP<sub>4</sub> and PEG-DOP<sub>4</sub> respectively. Therefore, possible differences in bacterial assays between Cl-dopamine and dopamine functionalized coatings cannot be attributed to the variation in the substrate rigidity.

With rheological methods, the antibacterial properties of Cl-dopamine was proved to be independent of the substrate modulus. By evaluating attachment of the gram negative bacterium *E. coli*, a clear decrease of up to 80% in bacteria density at the surface was seen with increasing Cl-dopamine concentration in the PEG-ClDOP<sub>4</sub> gel, indicating an inhibitory effect on bacterial attachment of the Cl-dopamine functionalized coating.<sup>139</sup> In addition, the same effect was also showed with Cl-dopamine modified alginate, hyaluronic acid and gelatin, where the functional group was incorporated through one-pot method, as described by Kang et al..<sup>146</sup>

### 4.1.3 Conclusion

The time-dependence of the storage and loss modulus demonstrated that the addition of Cl-dopamine functional group accelerated the gelation process. In a linear-log representation of the moduli and time, typical chemical gel behavior, i.e., a storage modulus plateau as function of time at long time and the frequency independence of storage modulus, was observed in PEG-DOP<sub>4</sub> gel. This results from the chemical bonds of the gel network, which have infinite life time. In addition, the storage modulus was compared between PEG-ClDOP<sub>4</sub> and PEG-DOP<sub>4</sub> gel after complete cross-linking. No significant difference was noted. Therefore, the antibacterial properties of Cl-dopamine gel are not related with the substrate rigidity.

## 4.2 Light-triggered gelation of alginates with caged $\text{Ca}^{2+}$

By incorporating photo-triggerable  $\text{Ca}^{2+}$  cages, a new method of modulating the cross-linking of alginate with UV-irradiation was presented by Cui et al..<sup>140</sup> Recently, the release of photo labile protected groups through irradiation has been used as an advanced method in various bio-systems, to modify the chemical and physical properties of the materials.<sup>148,149</sup> The functional groups released from the photo cleavage reaction activates further chemical reaction, so that the whole process can be controlled by irradiation. This strategy has been applied in many systems, like tuning mechanical properties in 3D scaffolds for cell growth<sup>150,151</sup>, delivering drugs or biochemicals<sup>152</sup>, or controlling the cell properties on bio-surfaces<sup>153,154</sup>.

Alginates are natural polysaccharides, which are widely used in the form of gels as impressing-making materials in dentistry. The gelation of alginate solution is mediated by ionic cross-linking with divalent cations, typically  $\text{Ca}^{2+}$ . The mechanism was described in detail in the literature<sup>155</sup>. With the addition of  $\text{Ca}^{2+}$  solution (usually  $\text{CaCl}_2$ ), the gelation occurs instantly and the rapid gelation kinetics leads to a poor distribution of  $\text{Ca}^{2+}$  cations, resulting in inhomogeneous gels.<sup>156</sup> Caged  $\text{Ca}^{2+}$  has been applied for achieving localized  $\text{Ca}^{2+}$  jumps in neurobiological mate-

rial.<sup>157,158</sup> In these materials, the  $\text{Ca}^{2+}$  bounded water-soluble chelators release the  $\text{Ca}^{2+}$  cations upon light irradiation. The dissociation constant  $K_d$  increases from nanomol to millimol range after the irradiation and the process is irreversible.<sup>158</sup>

In this joint work, the gelation of alginate with light-triggered caged  $\text{Ca}^{2+}$  was investigated with rheological measurements in a piezo-rheometer. The moduli of light-induced cross-linked alginate gel were compared to the moduli of mixtures of alginate and soluble  $\text{Ca}^{2+}$  in analogous concentration. An increase of storage modulus shown by light-induced gelation demonstrated the improvement of the system homogeneity and its mechanical properties. The work was recorded in paper “Light-triggered crosslinking of alginates with caged  $\text{Ca}^{2+}$ ”<sup>140</sup>.

### 4.2.1 Materials and methods

The photo labile  $\text{Ca}^{2+}$  chelator nitr-T ( $\text{nitr-T-Ca}^{2+}$ ) and a 15 wt.% sodium alginate (ALG) (Acros organics, Geel, Belgium) were used as reactants for the gelation reaction. The synthesis of  $\text{Ca}^{2+}$  chelator nitr-T is detailed by Cui et al.<sup>140</sup>. In short, a 1,2-bis(o-aminophenoxy)ethane- $\text{N,N,N',N'}$ -tetraacetic acid (BAPTA) chelating unit was substituted by two photosensitive o-nitrobenzhydryl groups at the para-positions (Fig. 4.3 A).<sup>140</sup> Upon light irradiation, a nitrosobenzophenone photoproduct was formed by an intramolecular redox reaction and the  $\text{Ca}^{2+}$  is released. The gelation under irradiation was observed macroscopically (Fig. 4.3 B). A opalescent yellow ALG/ $\text{nitr-T-Ca}^{2+}$  solution containing 10 wt.% ALG and 40 mM  $\text{nitr-T-Ca}^{2+}$  (Fig. 4.3 B-I) became a gel after light exposure (Fig. 4.3 B-II), suggesting the ionic cross-linking process of free  $\text{Ca}^{2+}$  and alginate. After addition of sodium ethylenediaminetetraacetate (EDTA), a strong  $\text{Ca}^{2+}$  chelator, the gel destabilized (Fig. 4.3 B-III). The reference sample ALG/ $\text{nitr-T}$  solution (without  $\text{Ca}^{2+}$ ) of the same concentration did not show gel behavior. All samples were prepared by the del Campo group (MPIP).

To study the mechanical properties of the light-triggered gelation process, the piezo-rheometer was equipped with a UV lamp with 360 nm wavelength (Polychrome V lamp, TILL Photonics GmbH, Grafelfing, Germany). A sketch of the setup is showed in Fig. 4.4. After mixing of ALG/ $\text{nitr-T-Ca}^{2+}$  (10 wt.% ALG and 40 mM  $\text{nitr-T-Ca}^{2+}$ ), 2  $\mu\text{L}$  of the sample was placed in the piezo-rheometer cell

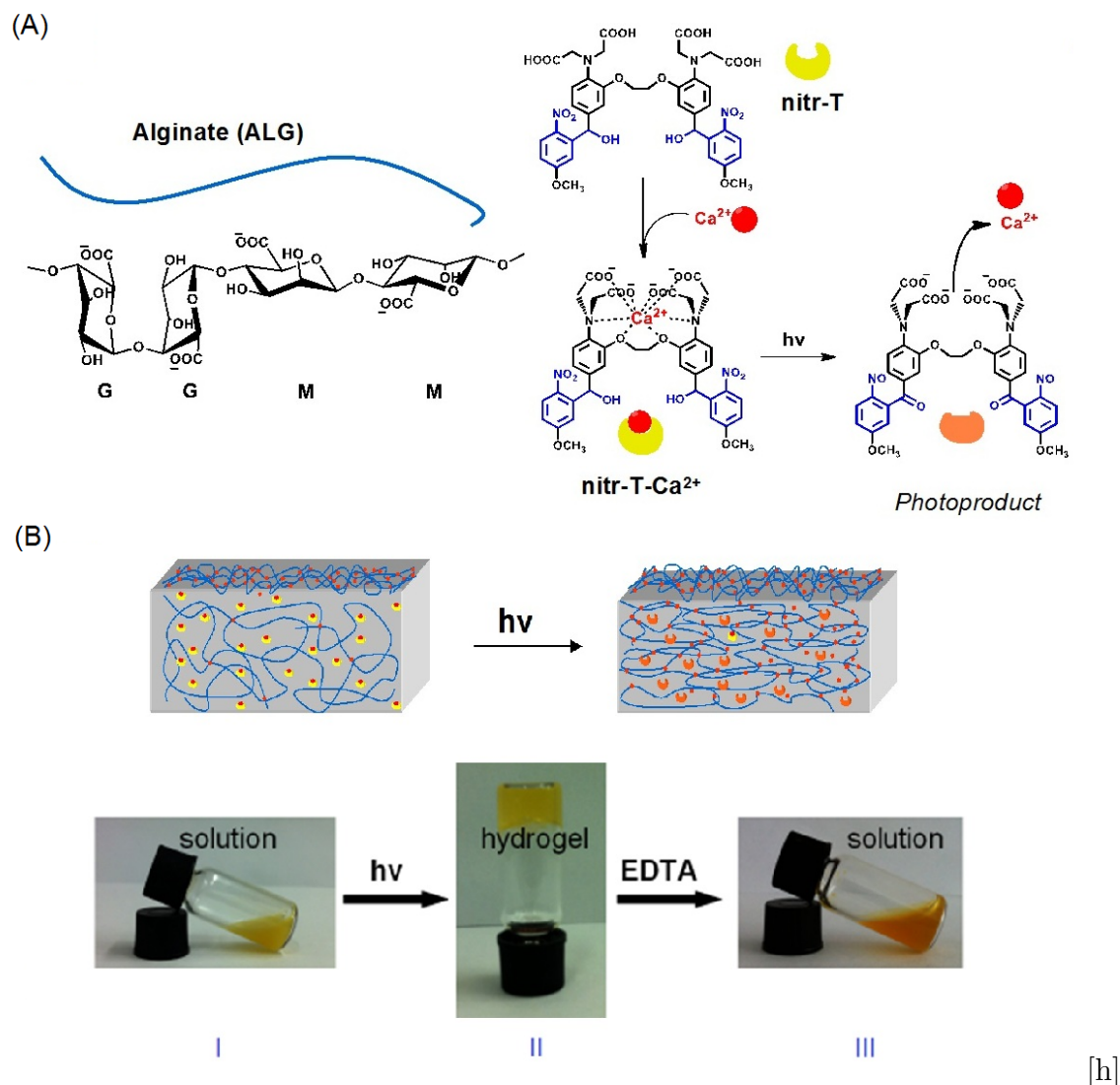


**Figure 4.3:** (A) Components of the photo-triggerable alginate gel including nitr-T- $\text{Ca}^{2+}$  and its light-induced cross-linking.<sup>140</sup> (B) Photographs of 300  $\mu\text{L}$  of ALG/nitr-T- $\text{Ca}^{2+}$  solution (10 wt.% ALG and 40 mM nitr-T- $\text{Ca}^{2+}$ ) before irradiation (I) and after irradiation (II) followed by addition of 50  $\mu\text{L}$  of 1 wt.% EDTA solution (III), adapted from the study<sup>140</sup>.

with a gap of 50  $\mu\text{m}$ . PDMS was filled around the sample, to avoid the evaporation of water (see section 2.1.3 for details). The transparent glass plates allowed in-situ irradiation of the sample. The possible influence of UV-light on the piezo element was excluded by performing the rheological measurements when the UV lamp was switched off after irradiation. This combination of rheometer and in-situ irradiation offered the opportunity to follow the gelation of the sample continuously. Each hour, a frequency spectrum from 1.58 to 2495.68 rad/s at  $T = 23^\circ\text{C}$  and under a strain of  $\gamma=0.0032$  was measured. It was assumed that under this strain amplitude the system was in its linear range, as discussed in section 3.4.1.1. The mechanical properties of reference ALG/nitr-T and immiscible oil PDMS were studied under the same conditions. Also, the  $\text{Ca}^{2+}$ /alginate mixture with comparable soluble  $\text{Ca}^{2+}$  concentrations were tested. Thus, the moduli of the gel produced by photo triggerable  $\text{Ca}^{2+}$  (ALG/nitr-T- $\text{Ca}^{2+}$ ) could be compared with the moduli of the gels induced by direct addition of soluble  $\text{Ca}^{2+}$ .

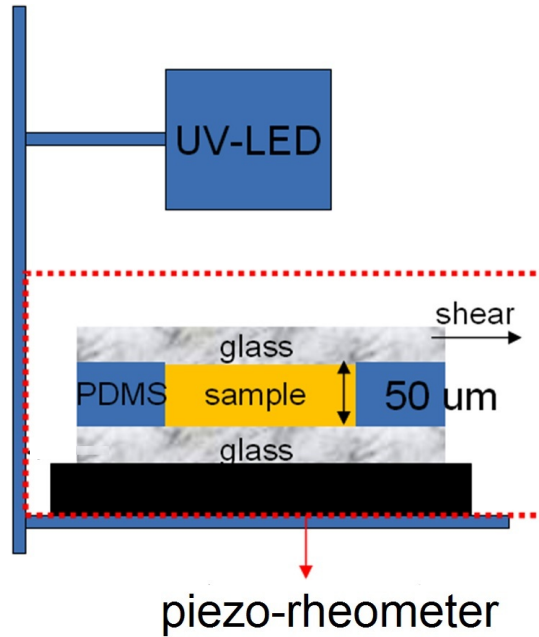


**Figure 4.4:** Setup of the combination of piezo-rheometer and UV lamp.<sup>140</sup>

### 4.2.2 Gel behavior of ALG/nitr-T- $\text{Ca}^{2+}$

Fig. 4.5 A shows the frequency dependence of the storage modulus  $G'$  of the mixture after exposure to increasing doses. Before irradiation, the mixture was fluid, which was confirmed by the increase of storage modulus with frequency. The increase of the storage modulus in logarithmic scale can be described by a power law with a slope of 0.5. Therefore the terminal range, in which a power law with a slope of 2 is expected (section 1.2.2), is not reached. Upon exposure with UV light, the storage modulus at a constant frequency increased, especially in the low frequency range. The slope of the curve  $G'-\omega$  decreased, indicating that cross-linking occurs as a consequence of the released  $\text{Ca}^{2+}$ . This change is more visible at conversions smaller than 75%. At full conversion, the storage modulus curve presents a plateau up to a frequency of 20 rad/s, demonstrating the formation of a gel network. This behavior was discussed with the sketch of Fig. 1.3 (section 1.2.2). The inset in Fig. 4.5 A shows the growth of the storage modulus with increasing exposure dose, i.e., increasing concentration of released  $\text{Ca}^{2+}$ , at  $\omega=1.58$  rad/s.

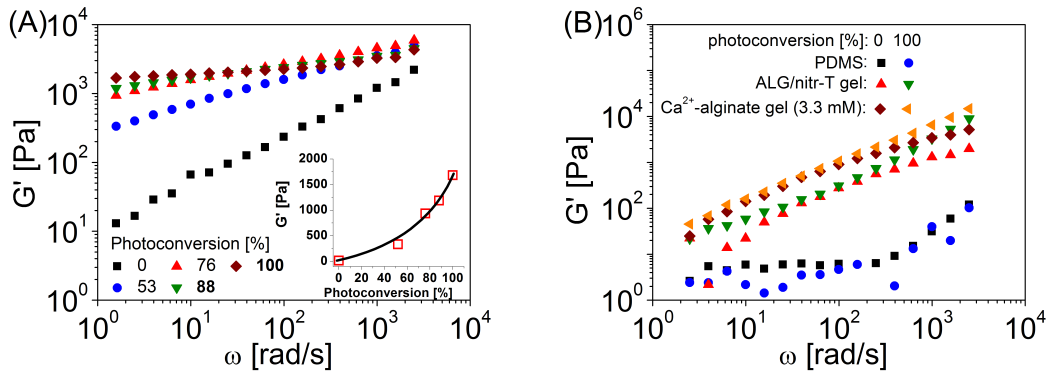


**Figure 4.5:** (A) The frequency dependence of the storage modulus  $G'$  of ALG/nitr-T- $\text{Ca}^{2+}$  solution (10 wt.% ALG and 40 mM nitr-T- $\text{Ca}^{2+}$ ) after different exposure doses. The inset represents  $G'$  against photoconversion at  $\omega=1.58$  rad/s. (B) The frequency dependence of storage modulus of evaporation barrier PDMS, ALG/Nitr-T solution (10 wt.% ALG and 40 mM nitr-T), and  $\text{Ca}^{2+}$ -alginate gel in water. No significant difference can be observed between the storage modulus before and after the irradiation. All the measurements in diagrams (A) and (B) were performed at temperature  $T = 23^\circ\text{C}$  and under strain  $\gamma = 0.0032$ .

Here the sample with photo conversion rate of 0% corresponds to the sample at short gelation time and photo conversion of 100% is related to the longer time. Therefore, the development of frequency spectrum for samples with increasing conversion rate can be compared with that for samples with increasing reaction time. And the illustration of time-dependence of the frequency spectrum in the gel state (Fig. 1.4 B) can be used to describe the experimental data (Fig. 4.5 A). At short reaction time, which corresponds to the low conversion rate in the measurement, the plateau of storage modulus as function of frequency happens at low frequencies. With the increase of the reaction time, the frequency spectrum is shifted to high frequency and the plateau happens at higher frequencies. Also, the plateau value of the storage modulus increases. Both phenomena were exhibited by the frequency spectrum of the samples. The plateau for sample at low conversion rate was not observed in the experiment, because the frequencies, at which the plateau happened, is expected to be below the measurable frequency range.

As a control experiment, the frequency spectrum of evaporation barrier PDMS, ALG/nitr-T (in the absence of  $\text{Ca}^{2+}$ ) and  $\text{Ca}^{2+}$ -alginate gel (3.3 mM) under the same conditions were also measured (Fig. 4.5 B). No change in the moduli upon exposure with UV light was observed. This data proves that the light-induced

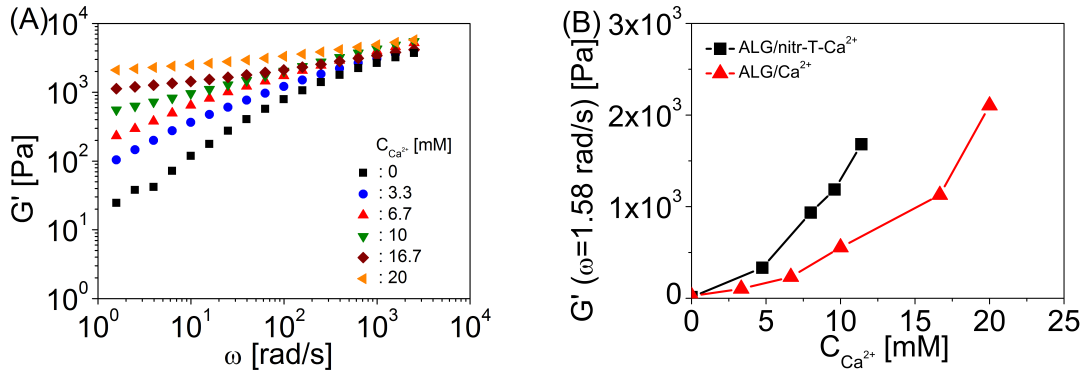


**Figure 4.6:** (A) The frequency dependence of  $G'$  of  $\text{Ca}^{2+}$ /alginate mixtures with different concentrations of soluble  $\text{Ca}^{2+}$ , measured at temperature  $T = 23^\circ\text{C}$  and under strain  $\gamma = 0.0032$ . (B) The dependence of  $G'$  with the available  $\text{Ca}^{2+}$  concentration for cross-linking in ALG gels with caged or soluble  $\text{Ca}^{2+}$ . Data were taken from the curves in Fig. 4.5 A and 4.6 A.  $G'$  values were measured at  $\omega = 1.58$  rad/s. At higher frequencies  $G'$  becomes less sensitive to cross-linking degree.



modulation of the mechanical properties of alginate gels is caused by the exploitation of caged  $\text{Ca}^{2+}$  photo release.

A direct comparison of the mechanical properties of the light-induced  $\text{Ca}^{2+}$  cross-linked alginate gels with ALG cross-linked gels with analogous concentrations of soluble  $\text{Ca}^{2+}$  was then performed. A similar change in the frequency dependence of the storage modulus was observed (Fig. 4.6 A). The storage modulus at a constant frequency increased with increasing  $\text{Ca}^{2+}$  concentration, which results from the ionic cross-linking of alginate with  $\text{Ca}^{2+}$ . For the concentration  $C_{\text{Ca}^{2+}}=20$  mM, a plateau of storage modulus at low frequencies  $\omega < 20$  rad/s can be seen.

The released  $\text{Ca}^{2+}$  amount in ALG/nitr-T- $\text{Ca}^{2+}$  was then calculated from the photo conversion rate. The storage moduli (at  $\omega=1.58$  rad/s) of the gels with various  $\text{Ca}^{2+}$  concentrations are listed in Table 4.1.

Photo-conversion <sup>a</sup> (%)	Photo-product <sup>b</sup> (mM)	$C_{\text{free } \text{Ca}^{2+}}$ (mM)	$C_{\text{bonded } \text{Ca}^{2+}}$ (mM)	$G'$ (at $\omega=1.58$ rad/s) (Pa)
0	0	0	0	10...20*
53	9.6	1.65	3.1	$3.3 \times 10^2$
76	22	2.8	5.2	$9.4 \times 10^2$
88	30	3.4	6.2	$1.2 \times 10^3$
100	40	4	7.4	$1.7 \times 10^3$

**Table 4.1:** The rheological properties of ALG/nitr-T- $\text{Ca}^{2+}$  gel under different exposure doses. (<sup>a</sup> Calculated from the photolysis kinetic measured with UV-Vis spectra, details is presented by Cui et al.<sup>140</sup>, <sup>b</sup> Obtained from the photo-conversion vs. composition curve from the literature<sup>148</sup>) \*: The measured value is at the resolution limit of Couette rheometer (Fig. 2.5), therefore the absolute value is imprecise and a range from 10 to 20 Pa is given here.

Furthermore, the storage modulus of the crosslinked ALG is plotted as a function of the available  $\text{Ca}^{2+}$  concentrations for cross-linking, either after light exposure or by addition of soluble  $\text{Ca}^{2+}$  (Fig. 4.6 B). For the same  $\text{Ca}^{2+}$  concentration, alginates with caged  $\text{Ca}^{2+}$  showed significantly higher storage modulus ( $1.2 \times 10^3$  Pa for 9.6 mM  $[\text{Ca}^{2+}]$ ) than alginate with soluble  $\text{Ca}^{2+}$  ( $5.5 \times 10^2$  Pa for 10 mM  $[\text{Ca}^{2+}]$ ). This result is attributed to a more homogeneous distribution of  $\text{Ca}^{2+}$  cation at the molecular level when caged  $\text{Ca}^{2+}$  is used for gelation. In the case of soluble  $\text{Ca}^{2+}$ , the diffusion and homogeneous distribution of the  $\text{Ca}^{2+}$  cation is blocked by fast ionic exchange during mixing with the alginate solution.

### 4.2.3 Conclusion

The release of photo labile  $\text{Ca}^{2+}$  in the nitr-T- $\text{Ca}^{2+}$  was applied in the gelation process of alginate gel. The nitr-T- $\text{Ca}^{2+}$  works as a photo triggerable source of  $\text{Ca}^{2+}$  and upon irradiation, the uncaged  $\text{Ca}^{2+}$  activates the gelation process. The cross-linking process was confirmed by the growth of the shear modulus with increasing exposure dose and the extension of the frequency range, in which the plateau of storage modulus was observed. With comparable  $\text{Ca}^{2+}$  concentration, the light-triggered ALG/nitr-T- $\text{Ca}^{2+}$  gel exhibited a much larger storage modulus than the ALG/ $\text{Ca}^{2+}$  gel, which is the mixture of alginate and soluble  $\text{Ca}^{2+}$ . Therefore, a significant improvement of system homogeneity by the light-mediated alginate gel was confirmed. This method of incorporating photo-triggerable  $\text{Ca}^{2+}$  cages offers the possibility to actively modify the swelling and the mechanical properties of the polymer scaffold with external reaction parameters, e.g., irradiation time, and can be applied in drug delivery and tissue engineering.

Furthermore, the piezo-rheometer set up was extended by combining with a UV lamp, which allows in-situ irradiation in the rheometer cell. It is possible to measure a sample after different exposure times by repeating the procedure of irradiation and rheological measurement continuously. Therefore, this combination opens a new way to study the mechanical properties of photo sensitive systems under various irradiation conditions.

## 4.3 Supramolecular gel via host-guest complexation

In recent years, supramolecular gels, which are sensitive to external stimuli, such as temperature, light and chemical entities, have attracted considerable attention as smart materials. The spontaneous association of molecules into stable, structurally well-defined aggregates by non-covalent bonds can be induced and modified by external stimuli.<sup>159–161</sup> Here, a self-healing supramolecular gel was developed by Liu et al., using the host-guest interaction between polymers bearing crown ether and secondary amino groups.<sup>141</sup> The motivations of the studies of supramolecular gels are the understanding of not only the gel structure, but also the mechanical properties for potential technological applications in many fields, like catalysis and separation.<sup>162</sup> Furthermore, the self-healing ability of this sample system can also extend the functionality of the material.<sup>163</sup>

In the present study, a functionalized polymer with crown ether side chain, which is well known as a supramolecular host, was synthesized. According to the host-guest interaction of crown ether and organic ammonium salts, a supramolecular gel can be formed. Because of the stronger covalent-bonds in the gel through the polymer scaffold, advantages in the mechanical properties and thermal stability are gained in comparison with the gel with low molecular organic gelators.<sup>159,160,164</sup> Besides stimuli-responsive as well as the self-healing behavior, the shear moduli and the influence of the host-guest ratio on the moduli were investigated. This work was presented in “Supramolecular Gel based on Glycidyl 4-Functionalized-1,2,3-Triazole Polymer via Host-Guest Complexation”<sup>141</sup>.

### 4.3.1 Materials and methods

The host and guest polymers used in this work are Glycidyl 4-functionalized-1,2,3-triazole (GTP) containing Dibenzo-24-crown-8 (DB24C8) unit: GTP-DB24C8-t-Bu and Dibenzylideneacetone (DBA) unit: GTP-DBA-t-Bu (Fig. 4.7). They are abbreviated as GTP-Host and -Guest here. Both were prepared at the Ikeda group in MPIP. The gel was formed by the complexation of crown ether and secondary ammonium salt (Fig. 4.7). The synthesis was described by Liu et al.<sup>141</sup>. Since the

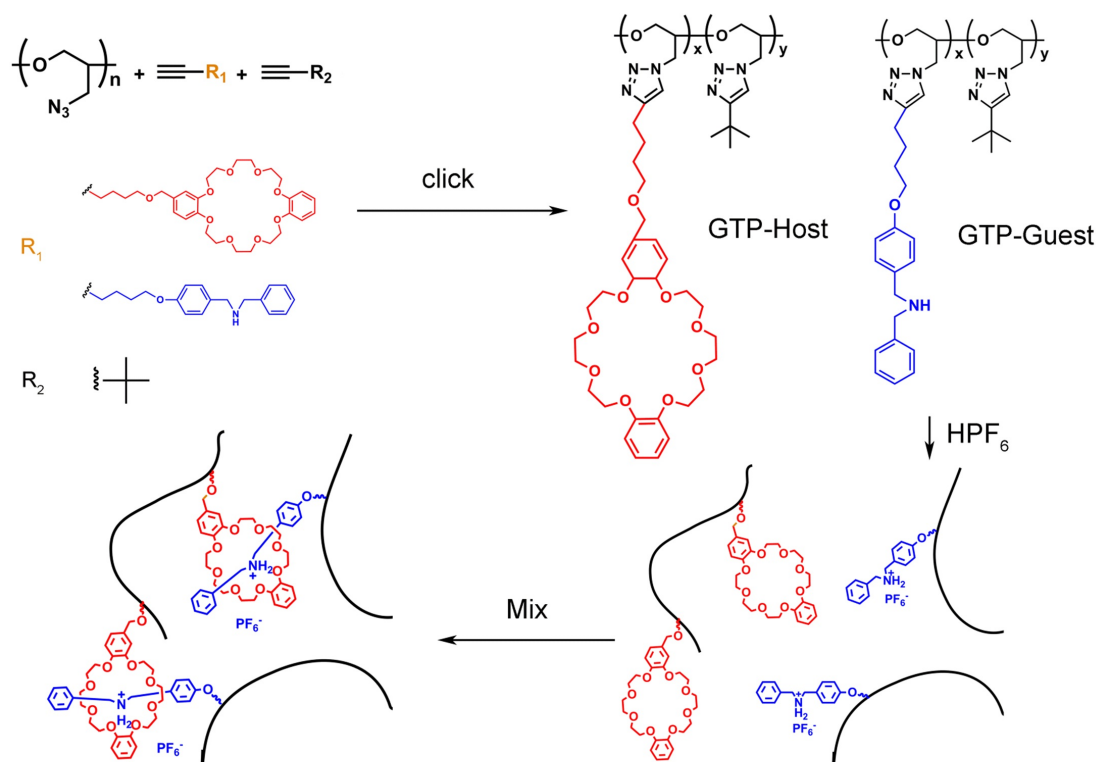


**Figure 4.7:** The synthesis of the functionalized GTP-Host and -Guest for gel and the formation of supramolecular gel.<sup>141</sup>

functionalized GTPs tend to aggregate in the solution, the molecules are likely to interact and entangle with each other. Therefore, a small amount of cross-linking points formed by host-guest interaction is enough to induce the gelation. Because of the temperature sensitivity of the host-guest interaction, the mixture of GTP-Host and -Guest gels at the room temperature and becomes fluid above 50°C. The self-healing effect comes from the reversibility of the host-guest interaction.

In the gel samples, certain amount of GTP-DB24C8-t-Bu and GTP-DBA-t-Bu was added into the solvent 1,1,2,2-Tetrachloroethane (TEC) and their concentrations vary from 2 to 5.5%. The polymers were totally dissolved by heating the mixture to about 80°C. When it was cooled down to the room temperature, a gel was formed. The mechanical properties of the samples were investigated with the piezo-rheometer. A small amount (between 15-25  $\mu\text{g}$ ) of the gelled sample was placed in the piezo-rheometer cell with a gap size of 100  $\mu\text{m}$ . The volume of the sample was

calculated from the weight using the density  $\rho = 1.59 \text{ gcm}^{-3}$ . A structure change during the filling of the sample into the cell was not seen in the rheological data. The small standard deviations in Fig. 4.8 B indicated that the measurements were well reproducible. It was assumed that the good reproducibility, i.e., no structure change after the filling, resulted from the self-healing of the system. The evaporation of the solvent TEC is slow at room temperature (boiling temperature:  $147^\circ\text{C}$ , vapor pressure: 8 mmHg at  $T = 20^\circ\text{C}$ ) and therefore negligible in the time window of the experiment, typically 10 minutes. Frequency sweeps were performed at  $T = 23^\circ\text{C}$ , under strain  $\gamma=0.0032$  and from frequency 1.58 to 2000 rad/s. It was assumed that the small amplitudes ensured that the sample was measured in the linear response regime.

### 4.3.2 Influence of host guest concentration on the moduli

The shear moduli of the gels with different polymer contents from 4 to 11 wt.% are presented in Fig. 4.8 A. The ratio between GTP-Host and -Guest was kept as 1:1. In all of the curves, the storage modulus  $G'$  is independent of the frequency for frequency below 100 rad/s. With an increasing polymer content, more host-guest complexation resulted in a higher density of cross-linking, which led to a higher storage modulus.

Furthermore, the frequency range of the storage modulus plateau is also related to the density of cross-linking. In the case of a 4 wt.% gel, it can be observed that the storage modulus was constant at low frequencies up to 100 rad/s. Above 100 rad/s, the storage modulus increased slightly with the frequency, which can be an indication of the transition to either the rubber plateau or dynamic glass at higher frequency range. The relatively low cross-linking density of the 4 wt.% gel was assumed to be the reason for frequency dependent behavior at frequencies above 100 rad/s. Less cross-linking points led to more mobility of polymer chains and therefore stronger influence of polymer dynamics on the gel modulus was seen. Once the polymer content was increased to 11 wt.%, a stable plateau was observed over a wide frequency range.

Furthermore, the ratio between GTP-Host and -Guest was varied and its influence on the plateau of storage modulus is presented in Fig. 4.8 B. The  $^1\text{H}$  and  $^{13}\text{C}$  NMR

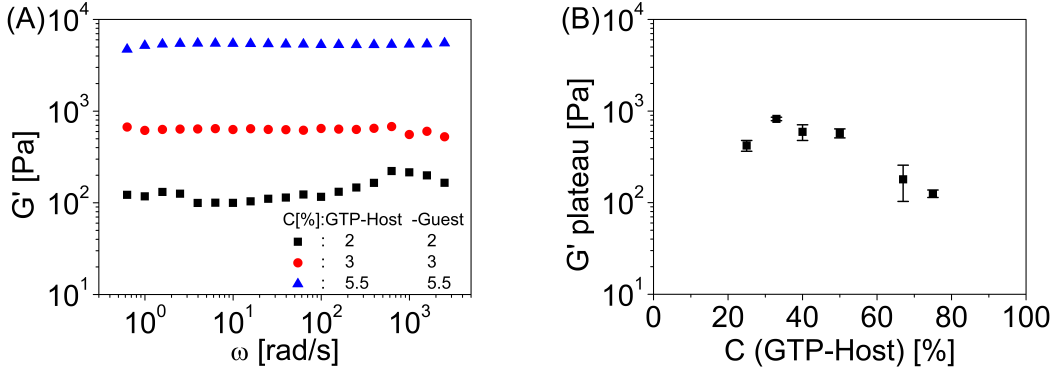


**Figure 4.8:** (A) The frequency dependence of storage modulus  $G'$  of the gels with different GTP-Host and -Guest content, measured at the temperature of  $T = 25^\circ\text{C}$  and under strain  $\gamma=0.0032$ . (B) The plateau value of storage modulus  $G'$  with different mixing ratio of GTP-Host and -Guest. The plateau value was obtained as an average value of the storage modulus  $G'$  in the frequency range from 1.58 to 100 rad/s. Total polymer concentration: 6 wt.%.

measurements showed that GTP-Host and -Guest have almost the same binding units for inclusion complexation. Considering this, it can be predicted that the best mixing ratio for obtaining a tough gel would be 1 : 1, because this ratio should give highest crosslink density in the gel. The ratio 1 : 1 corresponds to  $C(\text{GTP-Host})=50\%$  in Fig. 4.8 B. And the total concentration of the polymers was fixed to be 6 wt.%. As expected, the highest  $G'$  plateau value was obtained at a mixing ratio of 1 : 1.

Ideally, the  $G'$  plateau value should decrease symmetrically with enriching one component against another (GTP-Host or -Guest). However, the rheological data presents an asymmetric peak when the modulus is plotted as a function of the GTP-Host concentration. The modulus decreases slightly with decreasing of GTP-Host concentration in the GTP-Host poor range ( $C(\text{GTP-Host}) < 50\%$ ), while it decreases significantly with increasing of GTP-Host in the GTP-Host rich range ( $C(\text{GTP-Host}) > 50\%$ ). Since the gel forms not only by the host-guest interaction but also by the interaction between the polymer molecules, the different intensity of the interaction within the polymers has a strong influence on the gel modulus.

The interaction within the polymers can be studied with the viscosity. Since the viscosity presents the resistance of a system to the deformation, stronger interac-

tion within the system leads to higher viscosity. For this reason, the viscosity of GTP-Host and -Guest solution in TCE were checked macroscopically. The GTP-Guest solution showed a much higher viscosity than a GTP-Host solution with the same polymer content (in mol). This demonstrates a stronger interaction between the GTP-Guest molecules themselves. As the molecular interaction in the GTP-Guest solution also contributes to the modulus, GTP-Guest rich gels has higher storage modulus than GTP-Host rich gels when the cross-linking concentration is the same.

#### 4.3.3 Conclusion

The cross-linking of host-guest complexation and the interaction between the polymer molecules lead to the reversible gelation of the self-healing supramolecular gels. With the rheological measurements in the piezo-rheometer, the mechanical behavior of the sample systems with various GTP-Host and -Guest concentrations was studied. When the amount of functional groups, i.e., cross-linking points, increases, the storage modulus rises and the frequency range of the storage modulus plateau extends to higher frequency. By the variation of the polymer ratio between GTP-Host and -Guest, the degree of cross-linking and the corresponded storage modulus can be modified. Also, the interaction within the polymers influences the viscosity and has then significant influence on the gel modulus. Because of the higher viscosity of GTP-Guest solution, the GTP-Guest rich gels have higher storage modulus when compared to the GTP-Host rich gels in comparable cross-linking concentration. This strategy offers a new approach to the self-healing gel material. Also, the gelation of this super molecular gel can be easily controlled with temperature and the mechanical properties can be tuned with the concentration of functional groups.





## 5 Conclusion

In the present work, the structural evolution of various gel systems and the influence of internal and external parameters on their mechanical properties were investigated. With the rheological measurements in Couette and piezo-rheometer and structural analysis, an insight into the sol-gel process was obtained.

As model system, the reactive silica gel at high pH demonstrated a physical gel behavior in time and frequency dependent experiments. The finite solubility of silica at high pH value resulted in a reaction equilibrium and reversible silica bond of the gel network. The reversible bond was then interpreted as the origin of its rheological properties. The structural relaxation of the system deduced from the frequency dependence of the shear modulus was analyzed with modified Cole-Cole and BSW models. Comparable results on the effect of reactant concentration, temperature and reaction time on the gelation were presented.

The structural study (NMR and DLS) of the aggregation in the reactive silica gel confirmed that the primary particles existed already in the initial sodium silicate solution. Aggregates were formed after adding sulfuric acid and the growth of the aggregates was analyzed. Based on the understanding of the gelation, a method was developed to tune the final storage modulus with the external shear and shear history. A higher modulus at long times can be reached by applying high strain. In the sol state, the aggregates were compacted under shear. In the gel state, there is a competition between two simultaneous processes: (i) breakage of energetically unfavorable bonds and (ii) formation of new bonds with compacted aggregates.

In comparison, other gel systems (antibacterial Cl-dopamine gel, light-triggered alginate gel and self-healing supramolecular gel) demonstrated a typical chemical gel behavior, which results from the bonds with infinite life time. The piezo-rheometer was utilized to investigate the gelation kinetics and frequency dependence of the

storage modulus of the samples with different chemical modifications. Furthermore, success was achieved by combining the piezo-rheometer set up with a UV lamp, which allows rheological measurement of photo sensitive systems under in-situ irradiation.

# Appendix

The datas of DLS were analyzed by the group of Anja Kroege-Brinkmann in MPIP. For better understanding of the experimental data, presented in section 3.2.2.2, the theory background is introduced here shortly.

In DLS, the experimental normalized autocorrelation function  $K(q, t)$  of the photon correlation spectroscopy intensity  $I(q)$  at a scattering vector  $q$  (details see section 2.2.1) is related to the normalized time correlation function  $g(q, t) = \langle E^*(q, 0)E(q, t) \rangle / \langle |E(q, 0)|^2 \rangle$  of the scattered electric field  $E(q, t)$  by the Siegert relation:

$$K(q, t) = 1 + f^* |aK(q, t)|^2 = 1 + f^* |C(q, t)|^2 \quad (\text{A1})$$

where  $f^*$  is a coherence instrumental factor and  $a$  is the fraction of the total scattered intensity  $I(q)$  associated with fluctuations relaxing with times longer than 0.1  $\mu\text{s}$ . To analyze the computed relaxation functions  $C(q, t)$ , an inverse Laplace transformation using the constraint regularized CONTIN method was applied<sup>113</sup>. This method assumes that  $C(q, t)$  can be written by a superposition of exponentials, similar with the relaxation modulus  $G(t)$  (Eq. 2.17).

$$C(q, t) = \int_{-\infty}^{\infty} H_{\tau}(\ln \tau) \exp[-t/\tau] d(\ln \tau) \quad (\text{A2})$$

where  $H_{\tau}(\ln \tau)$  is the distribution of relaxation times. The characteristic relaxation times correspond to the peak positions of  $H_{\tau}(\ln \tau)$  which are numbered by  $k = 1, 2$  and so on. Furthermore, the area under the peak defines the value  $a$  (Eq. A1) and hence the intensity  $aI(q)$  associated with the particular dynamic process. For single but nonexponential decay,  $C(q, t)$  can be represented by the stretched exponential KWW function<sup>165</sup>,

$$C(q, t) = a \exp[-(t/\tau^*(q))^{\beta}] \quad (\text{A3})$$

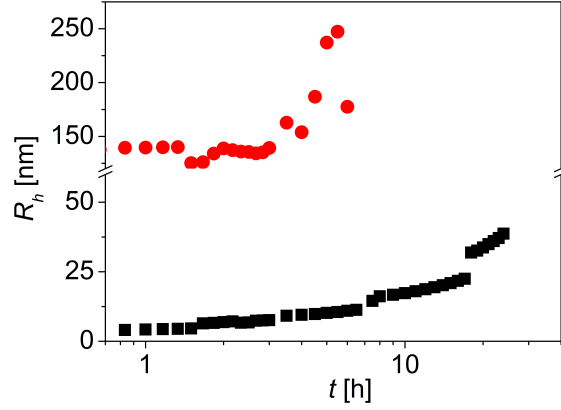


Figure A1: Time dependence of the aggregation process determined by DLS at a scattering vector of  $q = 1.87 \times 10^{-2} \text{ nm}^{-1}$  over a time range of  $0 \leq t \leq 25 \text{ h}$ .

where the shape parameter  $0 < \beta \leq 1$  characterizes the distribution of relaxation times. The closer this value is to 0 the stronger the relaxation function deviates from a single exponential. In such cases of double but nonexponential decay,  $C(q, t)$  can be represented by a double stretched exponential function.

$$C(q, t) = a_1 \exp[-(t/\tau_1^*(q))^{\beta_1}] + a_2 \exp[-(t/\tau_2^*(q))^{\beta_2}] \quad (\text{A4})$$

where  $\tau_1$  and  $\tau_2$  are the characteristic relaxation times.

(This chapter is written by Anja Kroeger-Brinkmann.)

# List of abbreviations

$A$ :	contact area
$a$ :	fraction of the total scattered intensity
$C$ :	concentration
$C(q, t)$ :	computed relaxation functions in dynamic light scattering
$D$ :	diffusion coefficient
$d$ :	diameter
$E(q, t)$ :	scattered electric field strength
$F$ :	force
$f^*$ :	coherence instrumental factor
$I(q, t)$ :	scattered light intensity
$K_d$ :	dissociation constant
$K(q, t)$ :	auto-correlation function
$k$ :	number of peak in distribution of relaxation times
$G_0$ :	equilibrium modulus
$G_N^0$ :	plateau modulus in BSW function
$G^*$ :	complex modulus
$G'$ :	storage modulus
$G'_{plateau}$ :	plateau value of the storage modulus
$G''$ :	loss modulus
$G_e$ :	equilibrium modulus
$G_i$ :	relaxation strength of one element
$g(q, t)$ :	normalized time correlation function in dynamic light scattering
$H(\tau)$ :	relaxation time spectrum
$i$ :	imaginary unit

$k_B$ :	Boltzmann's constant
$l$ :	length
$n$ :	number
$n_e$ :	slope of the spectrum for the $\alpha$ -relaxation region in BSW function
$n_g$ :	slope of the spectrum for the $\beta$ -relaxation region in BSW function
$n_{solv}$ :	refractive index of the solvent
$P$ :	Cauchy principal value
$Q^n$ :	quantification of $^{29}\text{Si}$ NMR signals, $n$ denotes the number of Si atoms attached to the oxygen atoms of a $\text{SiO}_4$ tetrahedron
$q$ :	scattering vector
$R$ :	ratio of extra water
$R_g$ :	gas constant
$r$ :	radius
$r_H$ :	hydrodynamic radius
$T$ :	temperature
$T_A$ :	absolute temperature
$t$ :	time
$t_{char}$ :	characteristic time
$v$ :	number of moles of network strand per unit volume
$y$ :	thickness
$\alpha$ :	parameter in the modified Cole-Cole function, describing the broadness of the distribution of relaxation times
$\beta$ :	shape parameter
$\gamma$ :	shear strain
$\hat{\gamma}$ :	strain-amplitude
$\gamma^*$ :	complex strain
$\dot{\gamma}$ :	shear rate
$\Delta$ :	deflection
$\Delta x$ :	displacement
$\delta$ :	phase angle

---

$\eta$ :	viscosity
$\eta_0$ :	steady shear viscosity
$\theta$ :	scattering angle
$\theta_m$ :	magic angle
$\lambda_0$ :	wavelength of the incident laser beam
$\rho$ :	density
$\sigma$ :	shear stress
$\tau$ :	shear stress
$\hat{\tau}$ :	stress-amplitude
$\tau^*$ :	complex stress
$\tau_0$ :	relaxation time for $\beta$ -relaxation region in BSW function
$\tau_{CC}$ :	characteristic relaxation time by modified Cole-Cole function
$\tau_i$ :	relaxation time of one element
$\tau_{max}$ :	longest relaxation time in BSW function
$\tau_r$ :	relaxation time
$\tau_T$ :	torque
$\phi$ :	volume fraction
$\omega$ :	angular frequency
$\omega_C$ :	cross-over frequency
ALG:	sodium alginate
BAPTA:	1,2-bis(o-aminophenoxy)ethane-N,N,N',N'-tetraacetic acid
BSW:	Baumgaertel-Schausberger-Winter model
Cl-catechol:	chlorocatechols
Cl-Dop:	chlorodopamine
Cl-DOPA:	2-chloro-4,5-dihydroxyphenylalanin
DB24C8:	Dibenzo-24-crown-8
DBA:	Dibenzylideneacetone
DLS:	dynamic light scattering
DMF:	dimethylformamide
DWS:	diffusing wave spectroscopy
EDTA:	ethylenediaminetetraacetate

GTP:	Glycidyl 4-functionalized-1,2,3-triazole
GTP-DB24C8-t-Bu:	Glycidyl 4-functionalized-1,2,3-triazole containing Di-benzo-24-crown-8
GTP-DBA-t-Bu:	Glycidyl 4-functionalized-1,2,3-triazole containing Di-benzylideneacetone
GTP-Guest:	Glycidyl 4-functionalized-1,2,3-triazole containing Di-benzylideneacetone
GTP-Host:	Glycidyl 4-functionalized-1,2,3-triazole containing Di-benzo- 24-crown-8
KWW:	Kohlrausch Williams Watts
LDPT:	laser deflection particle tracking
MAS:	magic angle spinning
MPIP:	Max Plank Institute for Polymer Research
NCS:	N-Chloro-succinimide
NMM:	N-methylmorpholine
NMR:	nuclear magnetic resonance spectroscopy
nitr-T-Ca <sup>2+</sup> :	Ca <sup>2+</sup> chelator nitr-T
PEG:	polyethylene glycol
PEG-ClDOP <sub>4</sub> :	Poly(ethylene glycol) O,O', O'', O''' -tetra (acetic acid chloro-dopamine) amide
PEG-DOP <sub>4</sub> :	Poly(ethylene glycol) O,O', O'', O''' -tetra (acetic acid dopamine) amide
PEG-NHS <sub>4</sub> :	PEG succinimidyl carboxymethyl ester
PDMS:	Polydimethylsiloxan
SAXS:	small angle X-ray scattering
Si:	silicium
TEC:	1,1,2,2-Tetrachloroethane
TFA:	trifluoroacetic acid
UV:	ultraviolet



# Bibliography

- [1] R. G. Larson. *The structure and rheology of complex fluids*. Oxford university press, 1999. 1, 2, 3
- [2] P.-G. de Gennes. *Scaling Concepts in Polymer Physics*. Cornell University Press, 1979. 1, 3
- [3] V. Trappe and P. Sandkuhler. Colloidal gels - low-density disordered solid-like states. *Current Opinion in Colloid & Interface Science*, 8(6):494–500, 2004. 1
- [4] A. H. Krall and D. A. Weitz. Internal dynamics and elasticity of fractal colloidal gels. *Physical Review Letters*, 80(4):778–781, 1998. 1
- [5] H. H. Winter and F. Chambon. Analysis of linear viscoelasticity of a cross-linking polymer at the gel point. *Journal of Rheology*, 30(2):367–382, 1986. 1, 8
- [6] F. T. Wall. Statistical thermodynamics of rubber. iii. *Journal of Chemical Physics*, 11(11):527–530, 1943. 2
- [7] L. R. G. Treloar. *The physics of rubber elasticity*. Clarendon Press, 1975. 2
- [8] R.J. Hunter. *Foundations of Colloid Science*. Oxford University Press, 2001. 2
- [9] E. Zaccarelli. Colloidal gels: equilibrium and non-equilibrium routes. *Journal of Physics-Condensed Matter*, 19(32), 2007. 2
- [10] K. A. Dawson. The glass paradigm for colloidal glasses, gels, and other arrested states driven by attractive interactions. *Current Opinion in Colloid & Interface Science*, 7(3-4): 218–227, 2002.
- [11] F. Sciortino and P. Tartaglia. Glassy colloidal systems. *Advances in Physics*, 54(6-7): 471–524, 2005.
- [12] P. A. Smith, G. Petekidis, S. U. Egelhaaf, and W. C. K. Poon. Yielding and crystallization of colloidal gels under oscillatory shear. *Physical Review E*, 76(4):041402, 2007. 6, 10
- [13] S. B. Lindstrom, T. E. Kodger, J. Sprakel, and D. A. Weitz. Structures, stresses, and fluctuations in the delayed failure of colloidal gels. *Soft Matter*, 8(13):3657–3664, 2012. 2

- [14] J. E. Martin and D. Adolf. The sol-gel transition in chemical gels. *Annual Review of Physical Chemistry*, 42:311–339, 1991. 3
- [15] P. J. Flory. *Principles of polymer chemistry*. Cornell University Press., 1953. 3
- [16] P. N. Segre, V. Prasad, A. B. Schofield, and D. A. Weitz. Glasslike kinetic arrest at the colloidal-gelation transition. *Physical Review Letters*, 86(26):6042–6045, 2001. 3
- [17] C. J. Rueb and C. F. Zukoski. Viscoelastic properties of colloidal gels. *Journal of Rheology*, 41(2):197–218, 1997. 10, 67
- [18] M. J. Solomon and P. Varadan. Dynamic structure of thermoreversible colloidal gels of adhesive spheres. *Physical Review E*, 63(5):051402, 2001. 3, 67
- [19] L. Yu and J. Ding. Injectable hydrogels as unique biomedical materials. *Chemical Society Reviews*, 37(8):1473–1481, 2008. 3
- [20] D. Stauffer. Gelation in concentrated critically branched polymer-solutions - percolation scaling theory of intramolecular bond cycles. *Journal of the Chemical Society-Faraday Transactions II*, 72:1354–1364, 1976. 3
- [21] F. Chambon and H. H. Winter. Linear viscoelasticity at the gel point of a cross-linking PDMS with imbalanced stoichiometry. *Journal of Rheology*, 31(8):683–697, 1987. 3, 9
- [22] P. Matricardi, M. Dentini, V. Crescenzi, and S. B. Ross-Murphy. Gelation of chemically cross-linked polygalacturonic acid derivatives. *Carbohydrate Polymers*, 27(3):215–220, 1995. 3, 9
- [23] K. T. Nijenhuis and H. H. Winter. Mechanical-properties at the gel point of a crystallizing polyvinyl-chloride solution. *Macromolecules*, 22(1):411–414, 1989. 3, 9, 10, 34, 40, 45
- [24] D. F. Hodgson and E. J. Amis. Dynamic viscoelasticity during sol-gel reactions. *Journal of Non-Crystalline Solids*, 131:913–920, 1991. 9, 10
- [25] K. T. Nijenhuis. Thermoreversible networks - viscoelastic properties and structure of gels - introduction. *Thermoreversible Networks*, 130:1–12, 1997. 3
- [26] K. Quarch and M. Kind. Inorganic precipitated silica gel. part 1: Gelation kinetics and gel properties. *Chemical Engineering & Technology*, 33(6):1034–1039, 2010. 4, 35, 46, 53
- [27] R. K. Iler. *The chemistry of silica*. John Wiley & Sons, Inc., 1979. 4, 35, 53
- [28] O. Ruff and P. Mautner. Die aktiven formen der kieselsäure (das Silicagel) und deren adsorptionsvermögen. *Angewandte Chemie*, 40(15):428–434, 1927. 4
- [29] C. B. Hurd, C. L. Raymond, and P. S. Miller. Studies on silicic acid gels. iv. the effect of the hydrogen-ion concentration upon the time of set. *Journal of Physical Chemistry*, 38(5):663–674, 1934. 4

- 
- [30] C. B. Hurd and A. J. Marotta. Studies on silicic acid gels. xii. the time of set of acidic and basic mixtures containing phosphoric acid. *Journal of the American Chemical Society*, 62: 2767–2770, 1940. 4
- [31] C. B. Hurd, R. C. Pomatti, J. H. Spittle, and F. J. Alois. Studies on silicic acid gels. xv. the effect of temperature upon the tune of set of alkaline gel mixtures. *Journal of the American Chemical Society*, 66:388–390, 1944. 4
- [32] C. J. Brinker and G. W. Scherer. *Sol-Gel Science*. Elsevier Science, 1989. 4, 5, 6
- [33] P. C. Carman. Constitution of colloidal silica. *Transactions of the Faraday Society*, 36: 0964–0972, 1940. 4
- [34] M. Prasad, S. M. Mehta, and J. B. Desai. Viscosity of the silicic acid gel-forming mixtures. *Journal of Physical Chemistry*, 36(5):1384–1390, 1932. 4, 10, 35
- [35] G. W. Scherer. Relaxation of a viscoelastic gel bar: I. Theory. *Journal of Sol-Gel Science and Technology*, 1(2):169–175, 1994. 4
- [36] G. W. Scherer. Relaxation of a viscoelastic gel bar: II. Silica gel. *Journal of Sol-Gel Science and Technology*, 2(1):199–204, 1994. 4, 5
- [37] G. W. Scherer. Influence of viscoelasticity and permeability on the stress response of silica gel. *Langmuir*, 12(5):1109–1116, 1996. 4
- [38] G. W. Scherer. Bending of gel beams: method for characterizing elastic properties and permeability. *Journal of Non-Crystalline Solids*, 142(0):18–35, 1992. 4, 5
- [39] J. Vermant. Large-scale structures in sheared colloidal dispersions. *Current Opinion in Colloid & Interface Science*, 6(5-6):489–495, 2001. 6
- [40] J. Vermant and M. J. Solomon. Flow-induced structure in colloidal suspensions. *Journal of Physics-Condensed Matter*, 17(4):R187–R216, 2005. 6
- [41] J. Mewis and N. J. Wagner. Current trends in suspension rheology. *Journal of Non-Newtonian Fluid Mechanics*, 157(3):147–150, 2009. 6
- [42] L. C. Hsiao, R. S. Newmana, S. C. Glotzera, and M. J. Solomon. Role of isostaticity and load-bearing microstructure in the elasticity of yielded colloidal gels. *Proceedings of the National Academy of Sciences*, 2012. 6, 10
- [43] M. Laurati, K. J. Mutch, N. Koumakis, J. Zausch, C. P. Amann, A. B. Schofield, G. Petekidis, J. F. Brady, J. Horbach, M. Fuchs, and S. U. Egelhaaf. Transient dynamics in dense colloidal suspensions under shear: shear rate dependence. *Journal of Physics-Condensed Matter*, 24:464104, 2012.
- [44] D. Derks, H. Wisman, A. van Blaaderen, and A. Imhof. Confocal microscopy of colloidal dispersions in shear flow using a counter-rotating cone-plate shear cell. *Journal of Physics-Condensed Matter*, 16(38):S3917–S3927, 2004.

- [45] R. Besseling, L. Isa, E. R. Weeks, and W. C. K. Poon. Quantitative imaging of colloidal flows. *Advances in Colloid and Interface Science*, 146(1-2):1–17, 2009.
- [46] X. Cheng, J. H. McCoy, J. N. Israelachvili, and I. Cohen. Imaging the microscopic structure of shear thinning and thickening colloidal suspensions. *Science*, 333(6047):1276–1279, 2011. 6
- [47] P. Varadan and M. J. Solomon. Direct visualization of flow-induced microstructure in dense colloidal gels by confocal laser scanning microscopy. *Journal of Rheology*, 47(4):943–968, 2003. 6
- [48] G. Petekidis, D. Vlassopoulos, and P. N. Pusey. Yielding and flow of colloidal glasses. *Faraday Discussions*, 123:287–302, 2003. 6
- [49] A. Mohraz and M. J. Solomon. Orientation and rupture of fractal colloidal gels during start-up of steady shear flow. *Journal of Rheology*, 49(3):657–681, 2005. 6, 10
- [50] D. Denisov, M. T. Dang, B. Struth, G. Wegdam, and P. Schall. Resolving structural modifications of colloidal glasses by combining x-ray scattering and rheology. *Scientific reports*, 3(1631), 2013. 6
- [51] J. Bender and N. J. Wagner. Reversible shear thickening in monodisperse and bidisperse colloidal dispersions. *Journal of Rheology*, 40(5):899–916, 1996. 6
- [52] J. P. Pantina and E. M. Furst. Directed assembly and rupture mechanics of colloidal aggregates. *Langmuir*, 20(10):3940–3946, 2004. 6
- [53] N. J. Wagner and J. F. Brady. Shear thickening in colloidal dispersions. *Physics Today*, 62(10):27–32, 2009. 6
- [54] C. D. Muzny, G. C. Straty, and H. J. M. Hanley. Small-angle neutron-scattering study of dense sheared silica-gels. *Physical Review E*, 50(2):R675–R678, 1994. 6, 67
- [55] C. D. Muzny, D. Hansen, G. C. Straty, D. J. Evans, and H. J. M. Hanley. Simulation and SANS studies of gelation under shear. *International Journal of Thermophysics*, 16(2):337–346, 1995. 6
- [56] R. Seto, R. Botet, G. K. Auernhammer, and H. Briesen. Restructuring of colloidal aggregates in shear flow: Coupling interparticle contact models with stokesian dynamics. *The European physical journal. E, Soft matter*, 35(12):9805–9805, 2012. 6, 67
- [57] H. J. M. Hanley, C. D. Muzny, B. D. Butler, G. C. Straty, J. Bartlett, and E. Drabarek. Shear-induced restructuring of concentrated colloidal silica gels. *Journal of Physics-Condensed Matter*, 11(6):1369–1380, 1999. 6
- [58] H. Tanaka, S. Jabbari-Farouji, J. Meunier, and D. Bonn. Kinetics of ergodic-to-nonergodic transitions in charged colloidal suspensions: Aging and gelation. *Physical Review E*, 71(2), 2005. 7

- 
- [59] P. J. Flory. Molecular size distribution in three dimensional polymers. i. Gelation. *Journal of the American Chemical Society*, 63(11):3083–3090, 1941. 7
- [60] P. J. Flory. Constitution of three-dimensional polymers and the theory of gelation. *The Journal of Physical Chemistry*, 46(1):132–140, 1942.
- [61] W. H. Stockmayer. Theory of molecular size distribution and gel formation in branched polymers ii general cross linking. *Journal of Chemical Physics*, 12(4):125–131, 1944. 7
- [62] W. Burchard and S.B. Ross-Murphy. *Physical networks: Polymers and gels*. Elsevier science publishers, 1988. 7
- [63] S. Corezzi, D. Fioretto, D. Puglia, and J. M. Kenny. Light scattering study of vitrification during the polymerization of model epoxy resins. *Macromolecules*, 36(14):5271–5278, 2003. 7, 34
- [64] P. D. Patel and W. B. Russel. An experimental study of aqueous colloidal suspensions containing dissolved polymer: B. Rheology. *Journal of Colloid and Interface Science*, 131(1):201–210, 1989. 7, 34
- [65] F. Chambon and H. H. Winter. Stopping of crosslinking reaction in a PDMS polymer at the gel point. *Polymer Bulletin*, 13(6):499–503, 1985. 9
- [66] C. Y. M. Tung and P. J. Dynes. Relationship between viscoelastic properties and gelation in thermosetting systems. *Journal of Applied Polymer Science*, 27(2):569–574, 1982. 9
- [67] H. H. Winter. Can the gel point of a cross-linking polymer be detected by the  $G'$  -  $G''$  crossover. *Polymer Engineering and Science*, 27(22):1698–1702, 1987. 9
- [68] O. Ronsin, C. Caroli, and T. Baumberger. Interplay between shear loading and structural aging in a physical gelatin gel. *Physical Review Letters*, 103(13):138302, 2009. 10, 34, 40, 45
- [69] A. Chenite, M. Buschmann, D. Wang, C. Chaput, and N. Kandani. Rheological characterisation of thermogelling chitosan/glycerol-phosphate solutions. *Carbohydrate Polymers*, 46(1):39–47, 2001. 10
- [70] Y. G. Lin, D. T. Mallin, J. C. W. Chien, and H. H. Winter. Dynamic mechanical measurement of crystallization-induced gelation in thermoplastic elastomeric poly(propylene). *Macromolecules*, 24(4):850–854, 1991.
- [71] K. Kobayashi, C. I. Huang, and T. P. Lodge. Thermoreversible gelation of aqueous methyl-cellulose solutions. *Macromolecules*, 32(21):7070–7077, 1999. 10
- [72] S. Kesavan and R. K. Prudhomme. Rheology of Guar and HPG cross-linked by Borate. *Macromolecules*, 25(7):2026–2032, 1992. 10

- [73] M. Verheul and S. P. F. M. Roefs. Structure of particulate whey protein gels: Effect of NaCl concentration, pH, heating temperature, and protein composition. *Journal of Agricultural and Food Chemistry*, 46(12):4909–4916, 1998. 10
- [74] O. Mueller, H. E. Gaub, M. Baermann, and E. Sackmann. Viscoelastic moduli of sterically and chemically cross-linked actin networks in the dilute to semidilute regime: measurements by oscillating disk rheometer. *Macromolecules*, 24(11):3111–3120, 1991. 10
- [75] J. A. Yanez, E. Laarz, and L. Bergström. Viscoelastic properties of particle gels. *Journal of Colloid and Interface Science*, 209(1):162–172, 1999. 10
- [76] D. Bonn and M. M. Denn. Yield stress fluids slowly yield to analysis. *Science*, 324(5933):1401–1402, 2009. 10
- [77] K. Masschaele, J. Fransaer, and J. Vermant. Flow-induced structure in colloidal gels: direct visualization of model 2d suspensions. *Soft Matter*, 7(17):7717–7726, 2011. 10, 69
- [78] K. Masschaele, J. Fransaer, and J. Vermant. Direct visualization of yielding in model two-dimensional colloidal gels subjected to shear flow. *Journal of Rheology*, 53(6):1437–1460, 2009. 10, 67
- [79] T. G. Mason and D. A. Weitz. Optical measurements of frequency-dependent linear viscoelastic moduli of complex fluids. *Physical Review Letters*, 74(7):1250–1253, 1995. 11
- [80] A. Palmer, T. G. Mason, J. Y. Xu, S. C. Kuo, and D. Wirtz. Diffusing wave spectroscopy microrheology of actin filament networks. *Biophysical Journal*, 76(2):1063–1071, 1999. 11
- [81] F. Ziemann, J. Rädler, and E. Sackmann. Local measurements of viscoelastic moduli of entangled actin networks using an oscillating magnetic bead micro-rheometer. *Biophysical Journal*, 66(6):2210–2216, 1994. 11
- [82] F. Amblard, A. C. Maggs, B. Yurke, A. N. Pargellis, and S. Leibler. Subdiffusion and anomalous local viscoelasticity in actin networks. *Physical Review Letters*, 77(21):4470–4473, 1996. 11
- [83] Y. Tseng and D. Wirtz. Mechanics and multiple-particle tracking microheterogeneity of alpha-actinin-cross-linked actin filament networks. *Biophysical Journal*, 81(3):1643–1656, 2001. 11
- [84] Y. Tseng, T. P. Kole, S. J. Lee, and D. Wirtz. Local dynamics and viscoelastic properties of cell biological systems. *Current Opinion in Colloid & Interface Science*, 7(3-4), 2002. 11
- [85] B. Schnurr, F. Gittes, F. C. MacKintosh, and C. F. Schmidt. Determining microscopic viscoelasticity in flexible and semiflexible polymer networks from thermal fluctuations. *Macromolecules*, 30(25):7781–7792, 1997. 11

- 
- [86] R. Bartolino and G. Durand. Plasticity in a smectic-A liquid crystal. *Physical Review Letters*, 39(21):1346–1349, 1977. 11, 20
- [87] K. Okano and J. Yamamoto. Mechanical transfer-function of thin smectic-A slab having homeotropic structure. *Japanese Journal of Applied Physics Part 1-Regular Papers Short Notes & Review Papers*, 29(6):1149–1150, 1990.
- [88] P. Martinoty, J. L. Gallani, and D. Collin. Hydrodynamic and nonhydrodynamic behavior of layer-compression modulus B at the nematic-smectic- A phase transition in 8 OCB. *Physical Review Letters*, 81(1):144–147, 1998. 11, 20
- [89] J. L. Gallani, L. Hilliou, P. Martinoty, F. Doublet, and M. Mauzac. Mechanical behavior of side-chain liquid crystalline networks. *Journal De Physique II*, 6(3):443–452, 1996. 11
- [90] L. Kirschenmann and W. Pechhold. Piezoelectric rotary vibrator (PRV) - a new oscillating rheometer for linear viscoelasticity. *Rheologica Acta*, 41(4):362–368, 2002. 11
- [91] J. J. Crassous, R. Regisser, M. Ballauff, and N. Willenbacher. Characterization of the viscoelastic behavior of complex fluids using the piezoelectric axial vibrator. *Journal of Rheology*, 49(4):851–863, 2005.
- [92] C. Clasen, B. P. Gearing, and G. H. McKinley. The flexure-based microgap rheometer (FMR). *Journal of Rheology*, 50(6):883–905, 2006.
- [93] D. C. Vadillo, T. R. Tuladhar, A. C. Mulji, and M. R. Mackley. The rheological characterization of linear viscoelasticity for ink jet fluids using piezo axial vibrator and torsion resonator rheometers. *Journal of Rheology*, 54(4):781–795, 2010.
- [94] M. Roth, M. D’Acunzi, D. Vollmer, and G. K. Auernhammer. Viscoelastic rheology of colloid-liquid crystal composites. *Journal of Chemical Physics*, 132(12), 2010. 11, 20
- [95] J. D. Ferry. *Viscoelastic properties of Polymers*. John Wiley & Sons, 1980. 13, 23
- [96] H. Münstedt. Lecture script: Rheology of polymers Friedrich-Alexander Universität Erlangen-Nürnberg. 2007. 15
- [97] G. Strobl. *The Physics of Polymers*. Springer-Verlag, 2007. 16, 22
- [98] G. A. Carri and H. H. Winter. Mapping of the relaxation patterns of polymer melts with linear flexible molecules of uniform length. *Rheologica Acta*, 36(3):330–344, 1997. 16, 25, 27
- [99] C. W. Macosko. *Rheology principles, measurements, and applications*. John Wiley & Sons, 1994. 18
- [100] M. Couette. Etudes sur le frottement des liquides. *Annales de Chimie et de Physique serie VII*, 21:433–510, 1890. 18

- [101] K. Okano and J. Yamamoto. Mechanical transfer-function of thin smectic-A slab having homeotropic structure. *Japanese Journal of Applied Physics Part 1-Regular Papers Short Notes & Review Papers*, 29(6):1149–1150, 1990. 20
- [102] M. Roth. Rheology of arrested colloids: a parameter study using novel experimental methods. *Ph.D. thesis, Johannes Gutenberg-University Mainz*, 2011. 20
- [103] T. Gisler and D. A. Weitz. Tracer microrheology in complex fluids. *Current Opinion in Colloid & Interface Science*, 3(6):586–592, 1998. 22
- [104] F. C. MacKintosh and C. F. Schmidt. Microrheology. *Current Opinion in Colloid & Interface Science*, 4(4):300–307, 1999. 22
- [105] P. J. Lu, J. C. Conrad, H. M. Wyss, A. B. Schofield, and D. A. Weitz. Fluids of clusters in attractive colloids. *Physical Review Letters*, 96(2):028306, 2006. 22
- [106] M. Baumgaertel and H. H. Winter. Determination of discrete relaxation and retardation time spectra from dynamic mechanical data. *Rheologica Acta*, 28(6):511–519, 1989. 23, 24, 25
- [107] C. Friedrich and H. Braun. Generalized cole-cole behavior and its rheological relevance. *Rheologica Acta*, 31(4):309–322, 1992. 24, 25, 26, 27, 47, 48
- [108] M. Baumgaertel, A. Schausberger, and H. H. Winter. The relaxation of polymers with linear flexible chains of uniform length. *Rheologica Acta*, 29(5):400–408, 1990. 24, 27
- [109] C. Friedrich, W. Waizenegger, and H. H. Winter. Relaxation patterns of long, linear, flexible, monodisperse polymers: BSW spectrum revisited. *Rheologica Acta*, 47(8):909–916, 2008. 25, 27
- [110] N. W. Tschoegl. *The Phenomenological Theory of Linear Viscoelastic Behavior: An Introduction*. Springer-Verlag, 1989. 27, 47
- [111] H. H. Winter, M. Siebenbuerger, D. Hajnal, O. Henrich, M. Fuchs, and M. Ballauff. An empirical constitutive law for concentrated colloidal suspensions in the approach of the glass transition. *Rheologica Acta*, 48(7):747–753, 2009. 27
- [112] P.A. Kralchevsky, K.D. Danov, and N.D. Denkov. *Handbook of surface and colloid chemistry*. CRC Press, 1997. 29
- [113] S. W. Provencher. Contin - a general-purpose constrained regularization program for inverting noisy linear algebraic and integral-equations. *Computer Physics Communications*, 27(3):229–242, 1982. 29, 30, 93
- [114] W. Brown. *Dynamic light scattering: the method and some applications*, volume 49. Oxford University Press, 1993. 30



- 
- [115] A. Kroegeer, J. Belack, A. Larsen, G. Fytas, and G. Wegner. Supramolecular structures in aqueous solutions of rigid polyelectrolytes with monovalent and divalent counterions. *Macromolecules*, 39(20):7098–7106, 2006.
- [116] K. Jaskiewicz, A. Larsen, I. Lieberwirth, K. Koynov, W. Meier, G. Fytas, A. Kroegeer, and K. Landfester. Probing bioinspired transport of nanoparticles into polymersomes. *Angewandte Chemie*, 124(19):4691–4695, 2012. 30
- [117] P.W. Atkins. *Physical Chemistry*. Oxford University Press, 1998. 30
- [118] G. Engelhardt and D. Michel. *High-resolution solid-state NMR of silicates and zeolites*. John Wiley & Sons, 1987. 31
- [119] L. Zhang, M. D’Acunzi, M. Kappl, A. Imhof, A. van Blaaderen, H. Butt, R. Graf, and D. Vollmer. Tuning the mechanical properties of silica microcapsules. *Physical Chemistry Chemical Physics*, 12(47):15392–15398, 2010. 31, 59
- [120] T. Cosgrove. *Colloid Science Principles, Methods and Applications*. WILEY, 2010. 32
- [121] M. Wang, H. H. Winter, and G. K. Auernhammer. Time and frequency dependent rheology of reactive silica gels. close to submission, . 33
- [122] M. Wang, A. Kroegeer, R. Graf, H. H. Winter, and G. K. Auernhammer. Reactive silica gels: formation and strain-history dependence. in preparation, . 33
- [123] S. R. Kamath and A. Proctor. Silica gel from rice hull ash: Preparation and characterization. *Cereal Chemistry*, 75(4):484–487, 1998. 35
- [124] M. Mours and H. H. Winter. Time-resolved rheometry. *Rheologica Acta*, 33(5):385–397, 1994. 39, 50
- [125] L. Guo, R. H. Colby, C. P. Lusignan, and A. M. Howe. Physical gelation of gelatin studied with rheo-optics. *Macromolecules*, 36(26):10009–10020, 2003. 45
- [126] S. Manley, B. Davidovitch, N. R. Davies, L. Cipelletti, A. E. Bailey, R. J. Christianson, U. Gasser, V. Prasad, P. N. Segre, M. P. Doherty, S. Sankaran, A. L. Jankovsky, B. Shiley, J. Bowen, J. Eggers, C. Kurta, T. Lorik, and D. A. Weitz. Time-dependent strength of colloidal gels. *Physical Review Letters*, 95(4), 2005. 46
- [127] G. B. Alexander, W. M. Heston, and R. K. Iler. The solubility of amorphous silica in water. *Journal of Physical Chemistry*, 58(6):453–455, 1954. 46
- [128] M. Laurati, G. Petekidis, N. Koumakis, F. Cardinaux, A. B. Schofield, J. M. Brader, M. Fuchs, and S. U. Egelhaaf. Structure, dynamics, and rheology of colloid-polymer mixtures: From liquids to gels. *Journal of Chemical Physics*, 130(13), 2009. 47, 51, 52
- [129] K. N. Pham, G. Petekidis, D. Vlassopoulos, S. U. Egelhaaf, W. C. K. Poon, and P. N. Pusey. Yielding behavior of repulsion- and attraction-dominated colloidal glasses. *Journal of Rheology*, 52(2):649–676, 2008. 47, 51

- [130] H. H. Winter and M. Mours. *Rheology of Polymers Near Liquid-Solid Transitions Neutron Spin Echo Spectroscopy Viscoelasticity Rheology*, volume 134 of *Advances in Polymer Science*. Springer-Verlag, 1997. 51
- [131] B.J. Berne and R. Pecora. *Dynamic light scattering: with applications to chemistry, biology, and physics*. Dover Publications, 2000. 56
- [132] Si Wu, Long Wang, Anja Kroeger, Yeping Wu, Qijin Zhang, and Christoph Bubeck. Block copolymers of PS-b-PEO co-assembled with azobenzene-containing homopolymers and their photoresponsive properties. *Soft Matter*, 7(24):11535–11545, 2011. 56
- [133] A. J. Vega and G. W. Scherer. Study of structural evolution of silica-gel using  $^1\text{H}$  and  $^{29}\text{Si}$  nmr. *Journal of Non-Crystalline Solids*, 111(2-3):153–166, 1989. 59
- [134] P. H. Bolt, T. P. M. Beelen, and R. A. van Santen. A small angle x-ray scattering study on high pH silica precipitations. *Colloids and Surfaces a-Physicochemical and Engineering Aspects*, 122(1-3):183–187, 1997. 59
- [135] T. Gerber, B. Himmel, and C. Hubert. WAXS and SAXS investigation of structure formation of gels from sodium-water glass. *Journal of Non-Crystalline Solids*, 175(2-3):160–168, 1994. 59
- [136] R. C. Sonntag and W. B. Russel. Structure and breakup of flocs subjected to fluid stresses: i. Shear experiments. *Journal of Colloid and Interface Science*, 113(2):399–413, 1986. 67
- [137] X. Wu, Y. Wang, M. Wang, W. Yang, B. Xie, and M. Yang. Structure of fumed silica gels in dodecane: enhanced network by oscillatory shear. *Colloid and Polymer Science*, 290(2):151–161, 2012. 68
- [138] W. Wolthers, M. H. G. Duits, D. van den Ende, and J. Mellema. Shear history dependence of the viscosity of aggregated colloidal dispersions. *Journal of Rheology*, 40(5):799–811, 1996. 69
- [139] L. Garcia-Fernandez, J. Cui, C. Serrano, Z. Shafiq, R. A. Gropeanu, V. S. Miguel, J. I. Ramos, M. Wang, G. K. Auernhammer, S. Ritz, A. A. Golriz, R. Berger, M. Wagner, and A. Del Campo. Antibacterial strategies from the sea: polymer-bound Cl-catechols for prevention of biofilm formation. *Advanced materials*, 25(4):529–33, 2013. 71, 72, 73, 74, 76
- [140] J. Cui, M. Wang, Y. Zheng, Rodríguez M., Gemma M., and A. del Campo. Light-triggered cross-linking of alginates with caged  $\text{Ca}^{2+}$ . *Biomacromolecules*, 14(5):1251–1256, 2013. 71, 77, 78, 79, 80, 83
- [141] D. Liu, D. Wang, M. Wang, Y. Zheng, K. Koynov, G. K. Auernhammer, H. Butt, and T. Ikeda. Supramolecular organogel based on crown ether and secondary ammonium functionalized glycidyl triazole polymers. *Macromolecules*, accepted, 2013. 71, 85, 86

- 
- [142] K. Glinel, P. Thebault, V. Humblot, C. M. Pradier, and T. Jouenne. Antibacterial surfaces developed from bio-inspired approaches. *Acta Biomaterialia*, 8(5):1670–1684, 2012. 72
- [143] J. A. Lichter, M. T. Thompson, M. Delgadillo, T. Nishikawa, M. F. Rubner, and K. J. Van Vliet. Substrata mechanical stiffness can regulate adhesion of viable bacteria. *Biomacromolecules*, 9(6):1571–1578, 2008. 72
- [144] C. J. Sun, A. Srivastava, J. R. Reifert, and J. H. Waite. Halogenated DOPA in a marine adhesive protein. *Journal of Adhesion*, 85(2-3):126–138, 2009. 72
- [145] H. Lee, S. M. Dellatore, W. M. Miller, and P. B. Messersmith. Mussel-inspired surface chemistry for multifunctional coatings. *Science*, 318(5849):426–430, 2007. 72
- [146] S. M. Kang, N. S. Hwang, J. Yeom, S. Y. Park, P. B. Messersmith, I. S. Choi, R. Langer, D. G. Anderson, and H. Lee. One-step multipurpose surface functionalization by adhesive catecholamine. *Advanced Functional Materials*, 22(14):2949–2955, 2012. 72, 76
- [147] G. M. Kavanagh and S. B. Ross-Murphy. Rheological characterisation of polymer gels. *Progress in Polymer Science*, 23(3):533–562, 1998. 74
- [148] H. Zhao, E. S. Sterner, E. B. Coughlin, and P. Theato. o-Nitrobenzyl alcohol derivatives: Opportunities in polymer and materials science. *Macromolecules*, 45(4):1723–1736, 2012. 77, 83
- [149] J. Cui, V. S. Miguel, and A. del Campo. Light-triggered multifunctionality at surfaces mediated by photolabile protecting groups. *Macromolecular Rapid Communications*, 2012. 77
- [150] A. M. Kloxin, A. M. Kasko, C. N. Salinas, and K. S. Anseth. Photodegradable hydrogels for dynamic tuning of physical and chemical properties. *Science*, 324(5923):59–63, 2009. 77
- [151] A. M. Kloxin, M. W. Tibbitt, A. M. Kasko, J. A. Fairbairn, and K. S. Anseth. Tunable hydrogels for external manipulation of cellular microenvironments through controlled photodegradation. *Advanced Materials*, 22(1):61, 2010. 77
- [152] V. Yesilyurt, R. Ramireddy, and S. Thayumanavan. Photoregulated release of noncovalent guests from dendritic amphiphilic nanocontainers. *Angewandte Chemie-International Edition*, 50(13):3038–3042, 2011. 77
- [153] S. Petersen, J. M. Alonso, A. Specht, P. Duodu, M. Goeldner, and A. del Campo. Phototriggering of cell adhesion by caged cyclic RGD peptides. *Angewandte Chemie-International Edition*, 47(17):3192–3195, 2008. 77
- [154] M. Wirkner, J. M. Alonso, V. Maus, M. Salierno, T. T. Lee, A. J. Garcia, and A. del Campo. Triggered cell release from materials using bioadhesive photocleavable linkers. *Advanced Materials*, 23(34):3907–3910, 2011. 77

- [155] B. T. Stokke, K. I. Draget, O. Smidsrod, Y. Yuguchi, H. Urakawa, and K. Kajiwarra. Small-angle X-ray scattering and rheological characterization of alginate gels. 1. Ca-alginate gels. *Macromolecules*, 33(5):1853–1863, 2000. 77
- [156] C. K. Kuo and P. X. Ma. Maintaining dimensions and mechanical properties of ionically crosslinked alginate hydrogel scaffolds in vitro. *Journal of Biomedical Materials Research Part A*, 84A(4):899–907, 2008. 77
- [157] G. C. R. Ellis-Davies. Caged compounds: photorelease technology for control of cellular chemistry and physiology. *Nature Methods*, 4(8):619–628, 2007. 78
- [158] G. C. R. Ellis-Davies. Neurobiology with caged calcium. *Chemical Reviews*, 108(5):1603–1613, 2008. 78
- [159] S. Dong, Y. Luo, X. Yan, B. Zheng, X. Ding, Y. Yu, Z. Ma, Q. Zhao, and F. Huang. A dual-responsive supramolecular polymer gel formed by crown ether based molecular recognition. *Angewandte Chemie-International Edition*, 50(8):1905–1909, 2011. 85
- [160] T. Oku, Y. Furusho, and T. Takata. A concept for recyclable cross-linked polymers: Topologically networked polyrotaxane capable of undergoing reversible assembly and disassembly. *Angewandte Chemie-International Edition*, 43(8):966–969, 2004. 85
- [161] Y. Zheng, A. Hashidzume, Y. Takashima, H. Yamaguchi, and A. Harada. Temperature-sensitive macroscopic assembly based on molecular recognition. *Acs Macro Letters*, 1(8):1083–1085, 2012. 85
- [162] N. M. Sangeetha and U. Maitra. Supramolecular gels: Functions and uses. *Chemical Society Reviews*, 34(10):821–836, 2005. 85
- [163] S. D. Bergman and F. Wudl. Mendable polymers. *Journal of Materials Chemistry*, 18(1):41–62, 2008. 85
- [164] S. J. Langford, M. J. Latter, V. Lau, L. L. Martin, and A. Mechler. Organogels derived from tetranitrated crown ethers. *Organic Letters*, 8(7):1371–1373, 2006. 85
- [165] M. N. Berberan-Santos, E. N. Bodunov, and B. Valeur. Mathematical functions for the analysis of luminescence decays with underlying distributions: 2. Becquerel (compressed hyperbola) and related decay functions. *Chemical Physics*, 317(1):57–62, 2005. 93

# Acknowledgments

Pursuing a Ph.D. is a hard but enjoyable process accompanied by hardships, frustrations, inspiration and the help of many kind people. From them, I have received support and encouragement over the past three years. Though words alone are not enough to express my gratitude to everyone who has helped me, I would still like to give my thanks to all these people.

First, I would like to thank Prof. Hans-Jürgen Butt for the opportunity to be part of his group. I appreciate his contributions throughout our discussions, as well as the freedom to research under his supervision.

I would like to thank my direct supervisor Dr. Günter K. Auernhammer, who introduced me to the research topics, gave me constructive feedback on the scientific projects and suggestions on my papers and presentations. I am extremely grateful for the opportunity of the exchange at the University of Massachusetts (UMASS) and the support he gave me, from the application process to when I was in Amherst. Thank you for spending so many Friday nights on Skype discussing with me about my research while I was there. I am also thankful to have learnt to be more optimistic and patient from him, though I still have to work on it.

I appreciate the help of my supervisor in UMASS Prof. H. Henning Winter for the valuable chance of working in his lab for 7 months and for sharing his ideas with me. His experience and knowledge in the field of polymer network rheology was a great help for my study.

I also want to say thank you to my second supervisor Prof. Angelika Kühnle at the University of Mainz for the interesting discussions about my work in your group seminar, which made me think about the problems from another aspect.

I am thankful to all my collaborators for our successful work together. For the project of silica gel, I want to thank Anja Kroeger-Brinkmann, Robert Graf, Gunnar Glaßer and Dr. Ingo Lieberwirth from MPIP for the structural analysis, Hussein Sahabi and Prof. Matthias Kind from Karlsruhe Institute for Technology (KIT) for the inspiring ideas, Dimitri Merger and Prof. Manfred Wilhelm for the non-linear rheological measurements. For the project of antibacterial Cl-dopamine gel and light-triggered alginate gel, I want to thank Dr. Cristina Serrano, Dr. Jiaxi Cui and Dr. Aranzazu del Campo for the idea of the cooperation and the fruitful discussions. For the project of self-healing supramolecular gel, I want to thank Dr. Dian Liu, Dr. Yijun Zheng and Dr. Taichi Ikeda for providing samples and the discussions that followed.

For the technical support, I would like to express my thanks to Gabriele Schäfer, Stefan Geiter, Maren Müller, for allowing me to concentrate more on the scientific experimentation.

My special thanks goes to my forerunner Dr. Marcel Roth for guiding me during my beginning here. He was always helpful and patient for answering my questions about the experiments and data analysis, even when he was writing his Ph.D. thesis.

I also would like to thank Jennifer Wenzl for our constructive discussions on confocal microscopy, Lena Mammen for the SEM measurements of silica gel and Brian Momani for the rheological measurements at UMASS.

For proof-reading and reviewing this thesis, I am grateful to Dr. Tassilo Kaule, Dr. Karen Johnsten, Dr. Azhar Juhari, Dr. Javed Ally, Peter Reichert, Dan King and David Wang. Thanks for all your comments and feedback which have allowed me to think about my research work from other perspectives.

When I look back, I appreciate my Master supervisor at University of Erlangen-Nürnberg Dr. Christian Triebel and Prof. Helmut Münstedt, who aroused my interest in science and encouraged me to do my Ph.D. in germany.

Furthermore, I want to say thank you to all my colleagues, who brought laughter at work and made all-day labs more fun. I hope they enjoyed working with me as much as I did with them. Especially to Veronika Beer, Xu Deng and Tomas Correlas, special thanks also to Dr. Doris Vollmer, for her invitation to the interview in MPIP and also for interesting conversations I would always leave with.

To my friends, I would like to thank you all for your support and encouragement. In particular, Maria Chiappelli, Brittany DeRonde, Dayong Cheng and Yujie Liu, for making my stay in Amherst both pleasant and enjoyable. A big thanks to Karin Winter as well, for being the best landlord and for teaching me to “play by ear”. To my previous neighbor and current roommates Roger Wenner, Miriam Dangel, Ida Dreler and Julia Breit, I want to say thank you for letting me feel like I was at home in Mainz. To my friends Jiannan Sun, Jule Gobel, Michael Dlugosch and Michael Rix, I want to thank you for all your encouragement and I’ll always remember the good times we’ve had together.

Last but certainly not least, I want to thank my parents Jianping Wang and Qinghua Jiang for all their love and support. My parents have sacrificed always been there for me every step along the way and encouraged me to pursue my Ph.D. abroad. I would not have made it this far without them.

# Curriculum Vitae and Publications

## Curriculum Vitae

### Miao Wang

Date of birth: April 14th. 1987  
Place of birth: Shanghai, China  
Nationality: China

#### Dissertation

03/2010-05/2013      Max Planck Institute for Polymer Research, Mainz, Germany  
Group of Prof. Hans-Jürgen Butt, Experimental Physics of  
Interfaces  
Project leader: Günter K. Auernhammer  
Ph.D. thesis:      Mechanical properties and structure of gel systems

07/2011-02/2012      University of Massachusetts, Amherst, MA, USA  
Cooperation exchange  
Group of Prof. H. Henning Winter, Experimental rheology

#### Educational background

04/2008-02/2010      Friedrich-Alexander University Erlangen-Nürnberg, Erlangen,  
Germany  
Major:      Materials Science (M.Sc.) (1.6)  
Focus:      Polymer Materials  
Master Thesis:      Viscose and elastic properties of nano-particle filled  
Poly(methyl methacrylate)  
Group of Prof. Helmut Münstedt  
Supervisor: Dr. Christian Triebel

02/2006-02/2008	Reutlingen University, Reutlingen, Germany Cooperation exchange
Major:	Chemistry with Marketing (B.Sc.) (1.4)
10/2005-01/2006	Tongji University, Shanghai, China German intensive course
09/2003-07/2005	Donghua University, Shanghai, China
Major:	Applied Chemical Engineering (B.Sc.)
02/2001-07/2003	Nan Yang Muster High School, Shanghai, China Qualification for university entrance

### Conferences and Workshops

09/2012	The XVith International Congress on Rheology, Lisbon, Portugal (oral presentation)
03/2012	76th Annual Meeting of the DPG, Berlin, Germany (poster presentation)
11/2011	2011 MRS Fall Meeting & Exhibit, Boston, MA, USA (oral presentation)
10/2011	83rd Annual Meeting of The Society of Rheology, Cleveland, OH, USA
03/2011	Annual Meeting of the German Rheological Society, Berlin, Germany (poster presentation)
09/2010	SFB TR6 Summer School on Soft Matter “Physics of colloidal suspensions and granular media”, Corsica, France (poster presentation)

## Publications

**M. Wang**, H. H. Winter, G. K. Auernhammer. Time and frequency dependent rheology of reactive silica gels, close to submission

**M. Wang**, A. Kroeger-Brinkmann, R. Graf, H. H. Winter, G. K. Auernhammer. Reactive silica gels: formation and strain-history dependence, in preparation

L. Garcia-Fernandez, J. Cui, C. Serrano, Z. Shafiq, R. A. Gropeanu, V. S. Miguel, J. I. Ramos, **M. Wang**, G. K. Auernhammer, S. Ritz, A. A. Golriz, R. Berger, M. Wagner, A. Del Campo. Antibacterial strategies from the sea: polymer-bound cl-catechols for prevention of biofilm for-



mation, *Advanced materials*, 25 (4): 529-33, 2013

J. Cui, **M. Wang**, Y. Zheng, M. Rodríguez, M. Gemma, A. del Campo. Light-Triggered Cross-Linking of Alginates with Caged  $\text{Ca}^{2+}$ , *Biomacromolecules*, 14 (5): 1251-1256, 2013

D. Liu, D. Wang, **M. Wang**, Y. Zheng, K. Koynov, G. K. Auernhammer, H. Butt, T. Ikeda. Supramolecular Organogel based on Crown Ether and Secondary Ammoniumion Functionalized Glycidyl Triazole Polymers, *Macromolecules*, accepted

Y. Zheng, **M. Wang**, D. Liu, J. Cui, G. Auernhammer, H.-J. Butt, T. Ikeda. Supramolecular Nanosheet Gel: Near-covalent elastic moduli and stimuli responsiveness, in preparation